Augmentation of Effective Thermal Conductivity of Metal Hydride Beds and its Effect on the Performance of Energy Conversion and Storage Devices

Ph.D. Thesis

By

YOGESH MADARIA

DISCIPLINE OF MECHANICAL ENGINEERING

INDIAN INSTITUTE OF TECHNOLOGY INDORE

April 2016

Augmentation of Effective Thermal Conductivity of Metal Hydride Beds and its Effect on the Performance of Energy Conversion and Storage Devices

A THESIS

Submitted in partial fulfillment of the

requirements for the award of the degree

of

DOCTOR OF PHILOSOPHY

by

YOGESH MADARIA

DISCIPLINE OF MECHANICAL ENGINEERING

INDIAN INSTITUTE OF TECHNOLOGY INDORE

April 2016

Acknowledgements

This PhD work is deeply influenced by the contributions of some valuable persons and hence I am pleased to have an opportunity to express my gratitude towards them and acknowledge their support and contribution.

At first I would like to express my gratitude towards my thesis supervisor, ***Dr. E. Anil Kumar****, Associate Professor, Discipline of Mechanical Engineering, for his valuable guidance and constant support during the period of this work.*

My sincere thanks are due towards my PSPC members – ***Dr. I. A. Palani*** *and* ***Dr. Antony Vijesh*** *for their comments and suggestions towards improving the PhD work. I would also like to thank* ***Prof. S. Srinivasa Murthy,*** *Visiting Professor****,*** *IISc Bangalore for guidance extended by him.*

I humbly acknowledge ***Prof. Pradeep Mathur****, Director, IIT Indore and administration of IIT Indore for providing a helpful and supportive environment to facilitate research. Also, I am grateful to SERB, DST for partially funding my research work through Project No. SERB/F/0810/2013-14.*

I would like to thank ***Dr. R. H. Shinde*** *(SOH) and* ***Mr. Senthil Kumar*** *(SOE), RRCAT, Indore for their cooperation and permission to avail ball milling facility. I am thankful to* ***Mr. Ashwin Patil****, RRCAT, Indore for contributing through his technical knowledge.*

I wish to thank ***Mr. Anand Petare*** *(AWS) and all the staff members of Discipline of Mechanical Engineering, IIT Indore especially* ***Ashwin Wagh***, ***Arun Bhagwaniya***, ***Rishiraj Chauhan***, ***Virendra Tak, Pawan Chauhan***, ***Anand Yadav***, ***Jeevan Singh***, ***Satish Kaushal, Deepak Dhepte, Deepak Rathod***, ***Pawnendra Muchhal*** *and* ***Vinay Mishra*** *for their help in different aspects of experimentation works.*

I would like to thank ***Satish Bisen***, *Manager (Library), IIT Indore, for extending support in matters related to library.*

I am extremely thankful to ***Vinod Kumar Sharma***, ***Vinod Kumar Singh***, ***Rakesh Sharma***, ***Dharmendra Panchariya***, ***Debashis Panda***, ***Dhananjay Mishra***, ***Manish Kumar Agrawal***, ***Sambhaji T. Kadam***, ***Hari Mohan Kushwaha***, ***Yogesh Singh***, ***Sandesh Chougule Patil***, ***Balmukund Dhakar***, ***Ankur Saxena, Naresh Raghuwanshi, Vikas Sharma, Kratika Pathak, Rajan Lanjekar***, ***Vishal Nirgude and Gaurav Bajpai,*** *Research Scholars IIT Indore for making my stay at IIT Indore enjoyable.*

My heartfelt thanks are due towards my friends ***Anjum Ajmeri, Monisha Nayak, Abdul Rahman Khan, Anil Verma, Varinder Sharma, Rachana Jain, Sanjay Gupta and Gaurav Mongia*** *whose love and support helped me to remain calm.*

I would like to express heartiest thanks to ***my father, brothers and sisters and my wife*** *for their love and inspiration. Finally, I thank to all who directly or indirectly rendered me help and support.*

List of Publications

List of Journal Publications based on PhD Thesis

1. Yogesh Madaria, Anil Kumar Emadabathuni, S. Srinivisa Murthy, M. Prakash Maiya, Simulation of effective thermal conductivity of metal hydride packed beds, Heat Transfer Engineering, 2016, 37 (7-8), 616-624. (I.F-1.016)

2. **Yogesh Madaria**, E. Anil Kumar, Effect of heat transfer enhancement on the performance of metal hydride based hydrogen compressor, International Journal of Hydrogen Energy, 2016, 41, 3961-3973. (I.F-3.205)

3. **Yogesh Madaria**, E. Anil Kumar, S. Srinivasa Murthy, Effective thermal conductivity of reactive packed beds of hydriding materials, Applied Thermal Engineering, 2016, 98, 976-990. (I.F-3.043)

4. **Yogesh Madaria**, E. Anil Kumar, Measurement and Augmentation of Effective Thermal Conductivity of $La_{0.8}Ce_{0.2}Ni_5$ hydride bed, Journal of Alloys and Compounds. (I.F-3.014)
   DOI: 10.1016/j.jallcom.2016.08.283

List of Papers in Conference Proceedings based on PhD Thesis

1. E. Anil Kumar, **Yogesh Madaria**, Studies on Mg + $LaNi_5$ based composites with respect to their suitability towards thermal energy storage, 21st World Hydrogen Energy Conference 2016, Zaragoza, Spain, 13th to 16th June 2016.

2. **Yogesh Madaria**, E. Anil Kumar, Augmentation of effective thermal conductivity of metal hydride beds, International Conference on Polygeneration, ICP-2015, Anna University, Chennai, India, February 2015.

3. **Yogesh Madaria**, E. Anil Kumar, S. Srinivasa Murthy, M. Prakash Maiya, Simulation of Effective thermal conductivity of metal hydride packed beds, International Symposium on Innovative Materials for Processes in Energy Systems, IMPRES-2013, Fukuoka Japan, September 2013.

Abstract

Keywords: Metal hydride beds: Effective thermal conductivity; Augmentation; Sorption kinetics; Metal hydride based hydrogen compressor, Metal hydride based thermal energy storage system

Metal hydride beds have drawn attention of researchers owing to their capability of reversible absorption and desorption of hydrogen accompanied by exothermic and endothermic reactions respectively. Applications of hydriding materials for solid state hydrogen storage, hydrogen compression, thermal energy storage and sorption heating and cooling systems have been demonstrated successfully. However, the performance of these devices significantly depends upon heat and mass transfer characteristics of the Metal Hydride (MH) beds. One of the important parameters regulating heat and mass transfer in the hydriding bed is its Effective Thermal Conductivity (ETC), which is dependent on several operating parameters, such as, thermal conductivities of solid and gas, gas pressure, bed temperature, void fraction, hydrogen concentration, etc. In general, the value of ETC for these beds is low and needs to be enhanced.

Mathematical simulation of ETC helps in understanding its dependency on different operating, geometric and material parameters. Several mathematical models are available for the estimation of effective thermal conductivity (ETC) of non-reactive packed beds. Keeping in view the salient differences between metal hydride beds in which chemisorption of hydrogen takes place and conventional non-reactive packed beds, modified models are proposed here to predict the ETC. Variation in properties, such as, solid thermal conductivity and porosity during hydrogen absorption and desorption processes are incorporated. These extended models have been applied to simulate the ETC of $MmNi_{4.5}Al_{0.5}$

hydride bed and are compared with the experimental results. Applicability of the extended models for estimation of the ETC at different operating conditions such as pressure, temperature and hydrogen concentration are discussed.

Reaction between metal alloy and hydrogen, being a complex phenomenon, causes considerable changes in bed porosity, solid thermal conductivity, etc. For accurate measurement of ETC of MH beds, the experimental set up and ETC cell need to be designed precisely. Experimental measurement of ETC of MH beds using one dimensional steady state, radial heat transfer, absolute method has been attempted in the present work.

It is well known fact that the value of ETC of MH powder beds lie in the range of 0.1 to 1.5 W m^{-1} K^{-1}. Many researchers have attempted augmentation of ETC of MH beds applying different techniques. Among the different techniques reported in literature, compaction and pelletization has resulted in the best level of ETC augmentation. The present work attempts to study the effect of combination of two augmentation techniques, such as, inclusion of high thermal conductivity metallic structure and pelletization. $La_{0.8}Ce_{0.2}Ni_5$ and Mg + 50 wt% $LaNi_{4.6}Al_{0.4}$ are considered for metal hydride based hydrogen compression (MHHC) and metal hydride based energy storage (MHTES) applications respectively. Two types of pellets are fabricated. First type is made by mixing 6 wt% graphite flakes with metal alloy/composite powder, while the second type has a three dimensional structure made with copper wire mesh, embedded to it in addition to the constituents of first type. The ETC of the three types of beds namely, loose metal powder bed (LMP), bed of pellets of metal alloy/composite powder mixed with graphite flakes (PMPGF) and bed of pellets of metal alloy/composite powder mixed with graphite flakes and embedded with copper wire mesh structure (PMPGFCu) are measured and compared at different hydrogen pressures and concentrations and average

bed temperatures. The hydrogen absorption and desorption rates of three types of beds with both the materials are tested at a wide range of pressure and temperature conditions and their performances are compared with respect to hydrogen compression and energy storage applications..

This thesis presents important data related to simulation, experimental measurement and augmentation of ETC of MH beds. Additionally, the effect of ETC augmentation on sorption characteristics of MH beds and consequently on the performance of MHHC and MHTES is also presented. The results obtained will add value to the knowledge base of ETC augmentation and its effect on sorption characteristics of MH beds.

Table of Contents

List of Figures

List of Figures (continued)

List of Figures (continued)

List of Figures (continued)

List of Tables

NOMENCLATURE

A	area; m^2
B	shape factor, in Eq. (2.13)
c	specific heat; kJ kg^{-1} K^{-1}
C_v	volumetric specific heat; J m^{-3} K^{-1}
d	diameter; m
d_c	contact length of solid particles; m
D_p	diameter of unconsolidated particles in a packed bed, in Eq. (2.10); m
f_{VE}	expansion factors of solid particles, in Eq. (2.1)
ΔH	reaction enthalpy; kJ kg^{-1}
h_{rs}	heat transfer coefficient for radiation, solid to solid, in Eq. (2.10); $Wm^{-2}K^{-1}$
h_{rv}	heat transfer coefficient for radiation, void to void, in Eq. (2.10); W m^{-2} K^{-1}
k	thermal conductivity, W m^{-1} K^{-1}
k_e^0	mean effective thermal conductivity of bed with stationary fluid in Yagi and Kunii model, in Eq. (2.10), W m^{-1} K^{-1}
Kn	Knudsen number, l_{mf}/l_v
K_0	Bessel's function of zeroth order, in Eq. (2.17)

Nomenclature (continued)

K_1	Bessel's function of first order, in Eq. (2.17)
l_{mf}	mean free path, in Eq. (2.8); m
l_v	characteristic length of void; m
l_{ff}	effective thickness of the fluid film adjacent to the surface of two solid particles in Yagi-Kunii model; m
m	mass; kg
M	Molar weight; mol g^{-1}
N_A	Avogadro's constant, 6.0221415×10^{23}; particles/mole
n	half the number of pendular rings surrounding a particle in Masamune-Smith model
P	pressure; Pa
$\dot{Q}$	heat transfer rate; W
q	heat flux; Wm^{-2}
r	radius; m
R	characteristic gas constant; kJ kg^{-1} K^{-1}
t	time; s
T	temperature; K
V	volume; m^3
W	work done; kJ
ΔV	volume expansion of the hydride; $2.9\times10^{-30}m^3$/H-atom

Nomenclature (continued)

X	weight of hydrogen absorbed per g of metal; g of H_2/g of metal
X_e	effective pore length; m

Greek Symbols

α	thermal diffusivity; m^2s^{-1}
β	ratio of the average length between the centers of two neighboring solids in the direction of heat flow to the mean diameter of packing, in Eq. (2.10)
κ	hydrogen concentration
ρ	density; kgm^{-3}
θ_0	contact angle between solid particles, in Eq. (2.17); radian
φ	porosity
γ	adiabatic compression index
η	efficiency
σ	Stefan-Boltzmann constant; $W\ m^{-1}\ K^{-4}$
Ω	volume of unit cell in Asakuma et al. [40] used in Table 1.4
λ	In Masamune and Smith Model; Fraction of total porosity considered for heat transfer by conduction and radiation through voids
ψ, ξ	accommodation coefficient for gas, solid respectively
δ	In Yagi and Kunii Model; Cross sectional area of perfect contact surfaces/Total cross sectional area

Nomenclature (continued)

	and in Masamune and Smith Model; Area fraction considered for heat transfer through a series path comprising an effective solid-path length and gas-path length
θ_2	contact angle associated with pendular rings of gas in Masamune-Smith model, in Eq. (2.19)
ε	effective thickness of fluid in void in relation to the thermal conduction/mean diameter of the solid $\left(l_{ff}/D_p\right)$
ρ_s	alloy density; kg/m^3
ϖ	k_g^*/k_s^* in Eq. (2.13)
υ	Volume expansion factor dependent on hydrogen concentration, in Eq. (2.2)

Subscripts

a	absorption
s	solid particle
b	breakaway
c	compressor
d	desorption
g	gas
e	effective

Nomenclature (continued)

f	final
g	gas
h	hollow space
H	hydrogen atom
H_2	hydrogen molecule
i	initial
L	longitudinal
max	maximum
p	probe
r	reactor
ref	reference
s	solid
w	wire
x	x direction
0	at zero pressure

Superscripts

*	in pores (for gas); dependent on hydrogen concentration (for solid)

Abbreviations

ETC	Effective Thermal Conductivity

LMP	Lose metal powder
LMHP	Lose metal hydride powder
MH	Metal hydride
PMPGF	Pellets of metal alloy powder mixed with graphite flakes
PMPGFCu	Pellets of metal alloy powder mixed with graphite flakes and embedded with copper wire mesh structure
PMHGF	Pellets of metal hydride powder mixed with graphite flakes
PMHGFCu	Pellets of metal hydride powder mixed with graphite flakes and embedded with copper wire mesh structure

Chapter 1

Introduction and Literature Review

1.1 Metal Hydrides

Efficient, reliable and safe storage of hydrogen is a key aspect in achieving hydrogen as an energy carrier of future. Owing to the difficulties and impracticalities involved in gaseous and liquefied hydrogen storage, solid state hydrogen storage had emerged as an appropriate solution. Capability of hydrogen to form a compound with many metals provided several researchers numerous dimensions for exploration of better material/method for solid state hydrogen storage. In last four decades, huge number of metals/alloys have been discovered/developed, each one comparatively better than its predecessors. Hydrogen absorption and desorption by metal hydrides is exothermic and endothermic reaction respectively. The reaction enthalpy being considerable in quantity, metal hydrides are found suitable for many non-hydrogen storage applications also. Some of non-hydrogen storage applications of metal hydrides are Metal Hydride based Hydrogen Compressor (MHHC), Metal Hydride based Thermal Energy Storage system (MHTES), Metal Hydride based Cooling System (MHCS), etc. The efficiency of any application of metal hydrides depends mainly on the capacity and rate of hydrogen absorption/desorption. The hydrogen absorption capacity is a material dependent property but the kinetics of absorption/desorption can very well be improved by material modification and better heat transfer characteristics of the MH bed. As the hydrogenation and dehydrogenation are exothermic and endothermic reactions, heat transfer characteristics of metal hydrides certainly play important role in the kinetics of hydrogen absorption and desorption. Generally metal hydride (for any application) is in the form of powder packed bed. The cyclic hydrogenation/dehydrogenation of material results

in deterioration of particles and hence the usual size of particles of metal hydride beds is in the range of 15-25 microns. The minute size of powder results in poor heat transfer characteristics of metal hydride beds.

1.2 Effective Thermal Conductivity (ETC) of Metal Hydride (MH) beds

The heat transfer in these beds is mainly through conduction in solid and hydrogen gas as convection due to the fluid motion is generally negligible. Moreover, the operating temperature ranges are not prominent enough to cause thermal radiation. Owing to these facts Effective Thermal Conductivity (ETC) becomes a crucial parameter governing the heat and mass transfer processes of these beds [1, 3-6]. ETC of reactive packed beds of hydriding materials mainly depends on the thermal conductivity of solid and gas, gas pressure, bed temperature, void fraction and hydrogen concentration [7-10]. Thus, variations in these parameters result in the variation in ETC. In general the value of ETC for these beds is low and needs to be enhanced with several augmentation techniques [1, 11-16].

In contrast to measurement of ETC for non-reactive packed beds where generally low pressure and finite particle sizes are involved, in case of MH packed beds, the following characteristics make the estimation of ETC relatively difficult:

(a) Continuous variation in concentration and particle size due to absorption and desorption of hydrogen,

(b) High reaction pressures, and;

(c) Continuously varying reaction temperature and reaction rates.

Variation in bed size due to particle expansion and contraction with hydrogen absorption and desorption leads to change in porosity of the bed and contact resistance between particles which has an obvious effect on ETC [17]. Kempf and Martin [18] in their measurement of ETC of MH bed provided a flexible terminal connection to the hot plate so that always

the heater plate remains in contact with the powder surface, thereby making the variation in particle size immaterial. Special gaskets, O-rings etc. are required to make the bed a leak proof assembly [8, 18-20]. Filter of very fine mesh size is used to prevent the passage of solid particles outside the reactor during evacuation of the reactor [8, 18-21]. Higher reaction pressure increases the difficulty in making and maintaining the system leak proof.

The ETC measurement for reactive packed beds of metal hydrides can be done by several arrangements as discussed in following sections.

1.2.1 Methods based on temperature profile measurement - Steady and transient techniques

In *steady state method*, the test material is filled in to a simple geometry, either cylindrical or rectangular enclosure. The boundary conditions are maintained constant to achieve one dimensional heat flux and the bed is allowed to reach steady state and the temperature profile is measured. Thermal conductivity can be calculated by comparing the experimental results with Fourier or Laplace equation [22].The steady state methods [8, 9, 18, 20, 22-25] are time consuming. Also some loss in accuracy is seen due to non-fulfillment of assumption of homogeneous beds caused by the presence of thermocouples within the bed [26].

In *transient method* of measurement [19, 26-37] thermal response due to a sudden heat pulse is recorded. The ETC of the bed is then obtained by fitting the solution of the Fourier equation to the measured temperature-time curve. Most commonly used transient techniques are hot wire method, thermal probe method and transient plane source method.

1.2.2 Methods based on heat flow direction- Radial and Axial heat transfer

In case of radial and axial methods the aspect ratio of the hydriding packed bed should be kept appropriate so that the temperature gradient in the lateral direction (other than direction of heat flux) can be assumed negligible without loss in accuracy. Several researchers have adopted *Radial* [9, 19, 20, 23, 27, 28] and *Axial* [8, 18, 21, 24, 25, 33] heat transfer methods for ETC measurements.

1.2.3 Absolute and comparative methods

In absolute heat flux measurement technique, ETC can be calculated from the measurements only on the test material. In comparative method, a second reference material with known thermal conductivity is placed in series with the test material. From the experiment the ratio between the unknown thermal conductivity of the metal hydride and the known one of the reference material is obtained. *Absolute* technique is not widely used [18] whereas the *Comparative* method is adopted by most of the researchers [8, 9, 20, 22-25].

1.3 Measurement of ETC of Metal Hydride Beds

Generally a combination of above classifications is used for measurement of ETC of hydriding packed beds. The experimental techniques mainly based on the methods of temperature profile measurement are briefly described here.

1.3.1 Steady state method

Anil Kumar et al. [8] used steady state, axial heat transfer, comparative method based on ASTM standard E1225 for the measurement of ETC of $MmNi_{4.5}Al_{0.5}$ hydride bed. Fig. 1.1 shows the schematic of the ETC cell. As shown in the figure, the upper plate was used as the constant higher

temperature source and the lower plate with the arrangement of cooling fluid circulation was used as the heat sink. Guard heaters and heavy insulation were used to assure no heat transfer in radial direction. The ETC cell was made of SS 316. Seven thermocouples, each of 1 mm size, were silver brazed to the cell to measure the temperature profile in axial and radial directions. PTFE disc with calibrated value of thermal conductivity was used as reference material to calculate the heat transfer rate. Table 1.1 gives the experimental details of ETC measurement, using steady state method, reported by different authors.

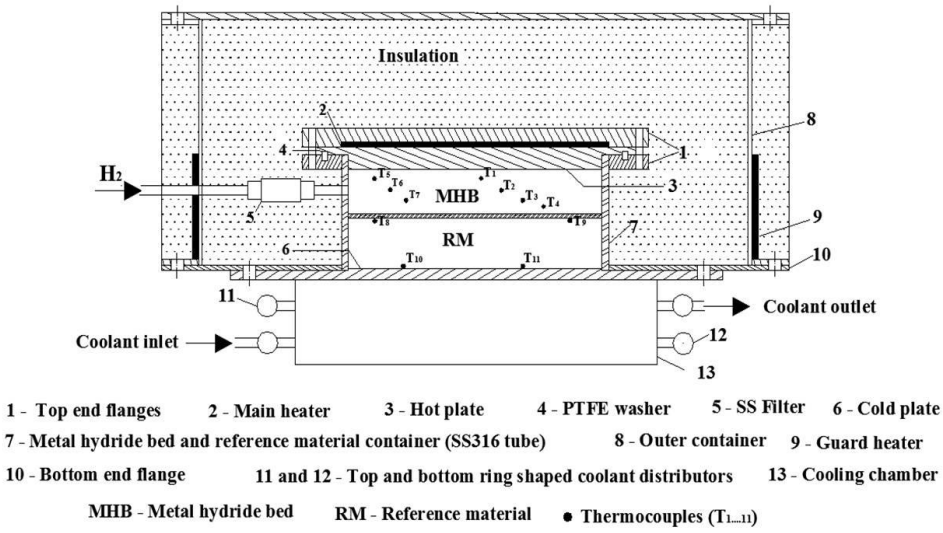

Fig. 1.1 Schematic view of ETC cell used by Anil Kumar et al. [8]

1.3.2 Transient method

Transient temperature profile measurement may be accomplished by one of the following techniques:

Hot wire method: In this method, an infinitely long wire (length/radius ratio ≫200) dissipating constant electrical power with uniform initial temperature is used as heat source. It is encased in the material to be tested and its temperature change with time as a result of step change in voltage applied is measured [27-30]. Kallweit and Hahne [27] measured the ETC of a low temperature hydride HWT 5800

Table 1.1 Experimental details of ETC measurements using steady state method

Author	**Material**	**Reference material/ Absolute**	**Thermal conductivity of reference material ($Wm^{-1} K^{-1}$)**	**Pressure (bar) /Temperature (K)**	**Sample Volume/mass (Bed Void fraction)**	**Initial Packing Density (kgm^{-3})**	**ETC ($Wm^{-1}K^{-1}$)**	**Accuracy**
Kempf and Martin [18]	$TiFe_{0.85}Mn_{0.15}$ hydride	Absolute	----	10^{-8} to 55 /273-423	238.6 g (0.53) and 298.9 g (0.52)	3008 and 3072	0.1-1.5	----
Anil Kumar et al. [8]	$MmNi_{4.5}Al_{0.5}$	PTFE	0.0016T +0.1507	0-50/ 273-373	530 g	4670	0.1-1.2	±5.75%
Suda et al. [20]	$TiMn_{1.5}$ hydride	Combination of ethyl alcohol and lead shots	1.64-0.0019t_s ($0^oC<t_s<60^oC$)	0.1-50/---	3540 cm^3 (0.442 at 20ºC)	3440	0.25-1.2	±3 %

Suissa et al. [23]	Mg_2NiH_4	Stainless Steel	14 to 16	45/ 373	170 g(0.27-0.41)	---	0.83 (at 373 K)	15 %
Suissa et al. [23]	$MmNi_4FeH_{5.2}$	PTFE	0.21	45/ 273	700 g (0.32-0.43)	---	1.05 (at 273 K)	15 %
Sun and Deng [9]	$MlNi_{4.5}Mn_{0.5}$ Hydride	PTFE	---	0 – 30 /300 ---/	267.42	---	0.3-1.3	---
Lloyd et al. [25]	$LaNi_5$ (Compacts)	SS 304	14.9±0.4	<363-423	~386 x 10^{-3} cm^3	----	2.9-6.4	---

($Ti_{0.98}Zr_{0.02}V_{0.43}Fe_{0.09}Cr_{0.05}Mn_{1.5}H_x$) and a medium temperature hydride $LaNi_{4.7}Al_{0.3}H_x$ using a set-up developed on the basis of hot wire technique. Fig. 1.2 shows the ETC cell developed by them. The measuring cell was made up of stainless steel and it had 217 cm^3 inner volume. To serve the requirement of ETC measurement at a very high temperature (up to 370ºC) and a wide range of pressures (from vacuum to 62 bar) this measuring cell was enveloped by a pressure chamber designed to sustain the required temperature and pressure conditions. Porous steel plates were applied at both ends of the measuring cell for hydrogen supply to the packed bed [27].

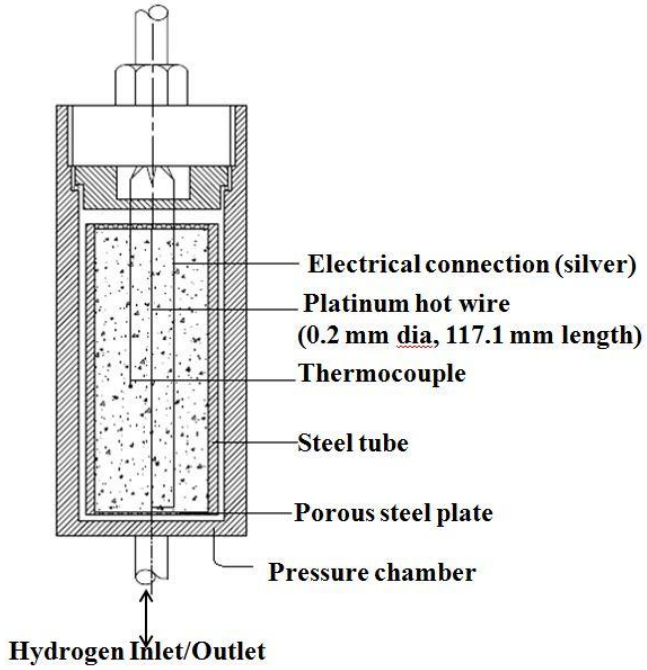

Fig. 1.2 Schematic view of ETC measurement cell used by Kallweit and Hahne [27]

The temperature rise of the hot wire surface can be determined with the approximate solution to the transient heat conduction equation given as:

$$\Delta T = T\left(r_w, t\right) - T_0 = \frac{q_L}{4\pi k_e} \ln \frac{4\alpha_e t}{r_w^2 C} \qquad (1.1)$$

For small temperature range, effective thermal diffusivity (α_e) was considered as constant and ΔT was differentiated with respect to $\ln t$ to obtain ETC, k_e as:

$$k_e = \frac{q_L}{4\pi} \Big/ \frac{d(\Delta T)}{d(\ln t)} \qquad (1.2)$$

The values of $d(\Delta T)/d(\ln t)$ was obtained from the graph plotted between ΔT vs $\ln t$. A brief overview of ETC measurement of MH packed beds using hot wire method is given in Table 1.2.To utilize the benefit of dual purposes (that of heating element as well as of temperature sensor) many authors have used platinum as hot wire material.

Thermal probe method: This method is based on ASTM D5334 standard. This method is very similar to *hot wire method* except that in this case the *hot wire* is replaced by a needle (of diameter around 3 mm) containing a heater element and a thermistor. Fig. 1.3 shows schematic of one such probe. This method was used by Dedrick et al. [31] to measure the ETC of sodium alanate packed bed. They had developed a customized set-up to determine the variation of ETC and the wall heat transfer coefficient with pressure (the pressure range being 1 to 100 atm) and hydrogen concentration of sodium alanate ($NaAlH_4$) system. Fig. 1.4 shows the measuring cell used by Dedrick et al. which was designed to accommodate the complex decomposition and recombination of sodium alanate. The sample space in the apparatus was 219 cm^3. Twelve thermocouples were provided in the measuring cell which were arranged appropriately to record the radial and axial temperature profile of the sample bed. The temperature time data obtained experimentally was compared with the temperature profile obtained by solving one dimensional heat transfer equation [31].

$$T(t) = C_1 \ln(t) + C_2 + C_3 \frac{\ln(t)}{t} + C_4 \frac{1}{t} \qquad (1.3)$$

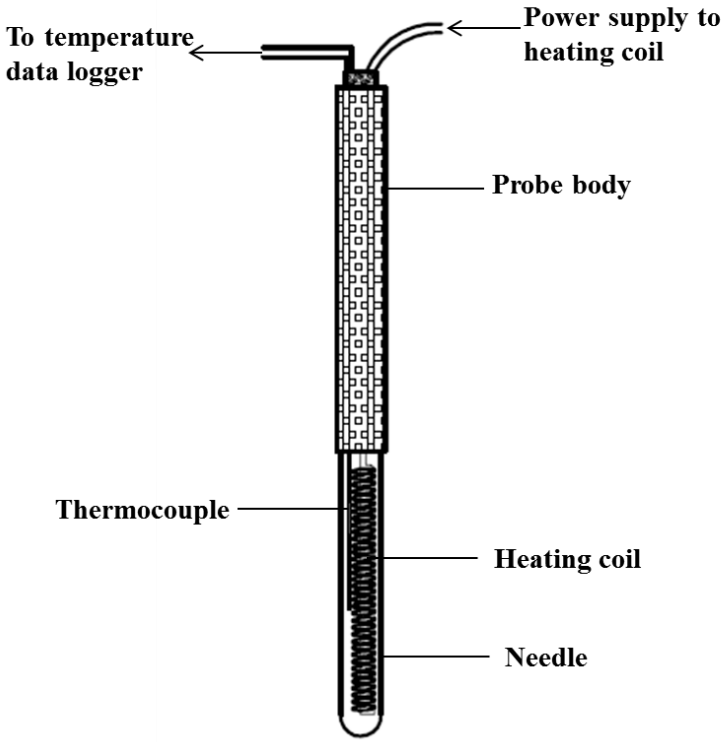

Fig. 1.3 Needle for thermal probe method

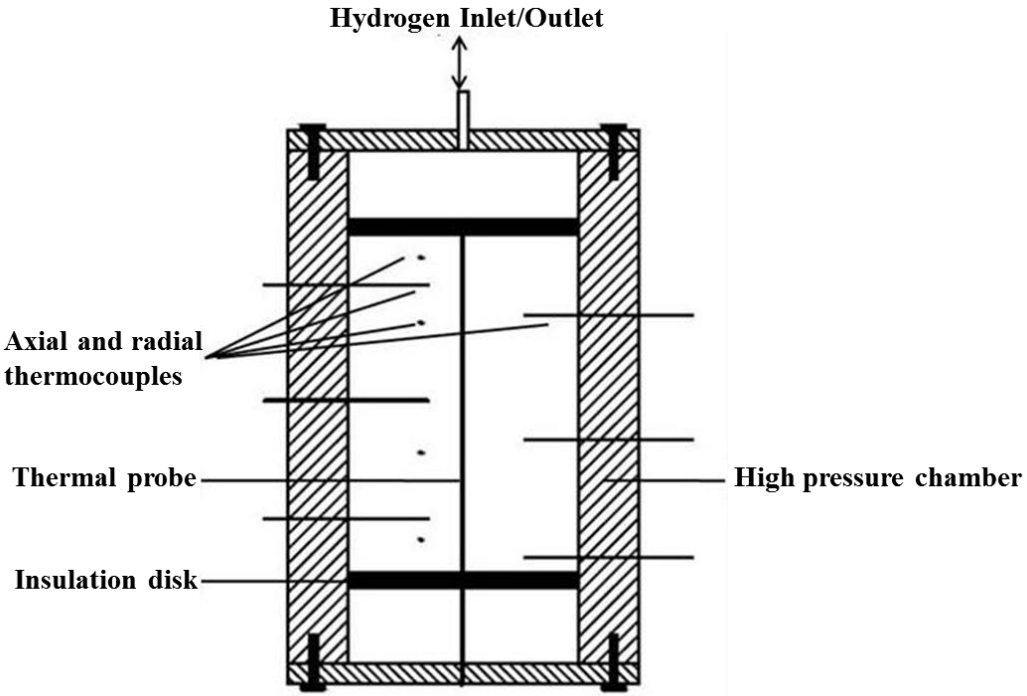

Fig. 1.4 Schematic view of ETC measurement cell used by Dedrick et al. [31]

Table 1.2 Experimental details of ETC measurements using transient hot wire method

Author	**Material**	**Hot wire diameter (Wire material)**	**Temperature Range (˚C)**	**Pressure Range (bar)**	**ETC Range W/m K**
Ishido et al.[26]	Sodium Alanate	0.3 (Nichrome)	30 to 200	1 to 50	0.8 to 1.2
Kallweit and Hahne[27]	HWT 5800	0.2 (Platinum)	- 80 to 20	10^{-5} to 60	0.01 to 1.1
Hahne and Kallweit[28]	$LaNi_{4.7}Al_{0.3}H_x$	0.2 (Platinum)	- 20 to 140	10^{-5} to 60	0.1 to 1.1
Cristopher[29]	Sodium Alanate	0.508 (Platinum)	20 to 240	1 to 100	0.4 to 0.6

Table 1.3 Summary of experimentations for measurement of ETC using different transient methods

Author	Material	Pressure (bar)	Temperature (K)	ETC (W/m K)	Testing method
Kapischke and Hapke [19]	Mg and 2% Ni	0.1 to 50	573 to 673	4 to 9	Transient radial
Kapischke and Hapke [21]	$Mg\text{-}MgH_2$	0.1 to 50	523 to 653	2 to 8	Oscillating heating technique
Flueckiger et al. [33]	$Ti_{1.1}CrMnH_x$	2.9 to 253	283 to 290	0.3 to 0.7	Transient Plane Source
	$TiFeH_x$	---	298	1.49	Transient temperature measurement
	$LaNi_5H_x$	---	298	1.32	
Goodell [35]	$LaNi_5$	---	298	1.32	Non Isothermal KineticsTestMethod
	FeTi	---	298	1.49	
Pons et al. [36]	$LaNi_5H_x$	0.01 to 10	---	0.1 to 1.5	Transient, 2D, Identification technique
Pons and Dantzer [37]	$LaNi_5H_x$	0.03 to 30	---	0.13 to 2.3	Transient Identification Method

The ETC was given as:

$$k_e = \frac{r_p q_L}{2A} \tag{1.4}$$

Where C_1, C_2, C_3 and C_4 are fitting coefficients.

Transient plane source method: The third type of transient method is *transient plane source* (TPS) method. This method is useful in determination of a large number of transport properties of different materials (morphologies and geometries). Similar to hot wire method, resistive element is chosen so that it can be utilized as both heating element and temperature sensor. This element is made in the form of a pattern, which for the sake of experimental and/or theoretical simplification is usually given a regular shape, may be a double spiral disc or a square [33]. Similar to Kallweit and Hahne [27], Flueckiger et al. [33] integrated the thermal plane source apparatus with a pressure vessel to make it suitable for measurement of ETC of metal hydrides at high pressure (up to 275 bar). The thermal conductivity values of non-reactive (oxidized) and activated $Ti_{1.1}CrMn$ under various hydrogen pressures were determined. Figs. 1.5 (a) and 1.5 (b) show the arrangement of apparatus for the measurement of ETC of $Ti_{1.1}CrMn$ hydride sample and the typical element (sensor) for TPS method respectively. For evaluation of the ETC of the sample, the TPS element is slightly heated by an electrical current pulse. Care must be taken to keep the current pulse short enough to verify the consideration of contact between TPS element and sample for the period of transient recording. The ETC evaluation method is exactly similar to hot wire technique [22, 32]. Table 1.3 summarizes transient methods of experimental determination of ETC of hydriding packed beds.

1.3.3 Non-Conventional methods

Other than the conventional methods described above some researchers have proposed innovative methods for the measurement of ETC of reactive packed beds of hydriding materials.

In one such method to determine the ETC and wall heat transfer coefficient of $LaNi_5$ hydride, the packed bed was heated at one of its surfaces while allowing to get cooled naturally (through convection) at the opposite surface i.e. the other surface was not an adiabatic surface thus changing the boundary condition although the lateral surfaces were heavily insulated [36, 37]. Fig. 1.6 shows the schematic arrangement of the apparatus used for ETC measurement. To record the axial and radial temperature profiles thermocouples were staggered in both the directions. The experimental temperature evolutions in two directions were matched with the calculated temperatures obtained from the solution of two dimensional transient heat transfer equation. The comparison of experimental temperature evolution with calculated ones resulted in determination of wall heat transfer coefficient in addition to ETC. The ETC values obtained for $LaNi_5$ hydride bed were in the range of 0.13 to 2.3 $Wm^{-1} K^{-1}$ for the pressure range of 3 kPa to 3 MPa.

Isayev and Schur [38] have developed a method in which solving ill-defined problems have been proposed to determine ETC of metal hydrides. In another method, to obtain ETC, the sinusoidal temperature profile heating of MgH_2 packed bed was done in an oscillating pattern instead of continuous heating [21]. ETC was calculated by tailoring the problem-specific mathematical result to the experimentally recorded temperature time function.

From the above discussion it is clear that the ETC of reactive packed beds of hydriding materials lie in the range of 0.01 to 1.5W $m^{-1} K^{-1}$unless the

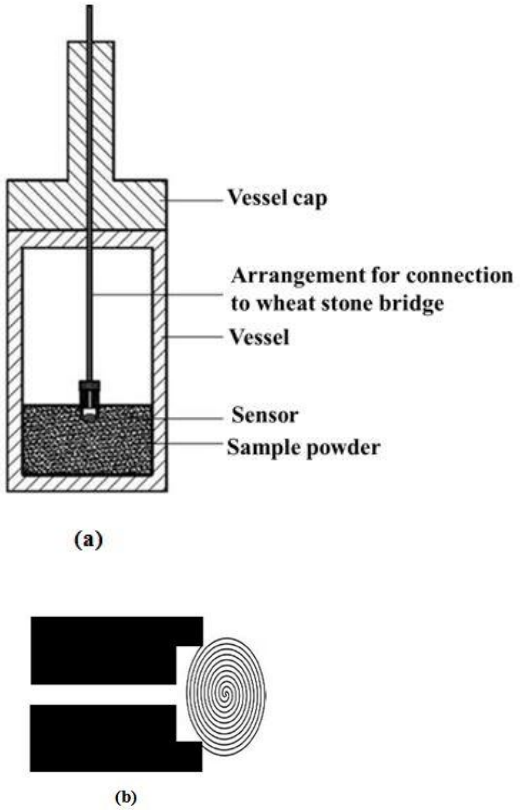

Fig. 1.5 (a) Apparatus used by Flueckiger et al. [33],
(b) Sensor for TPS method [33]

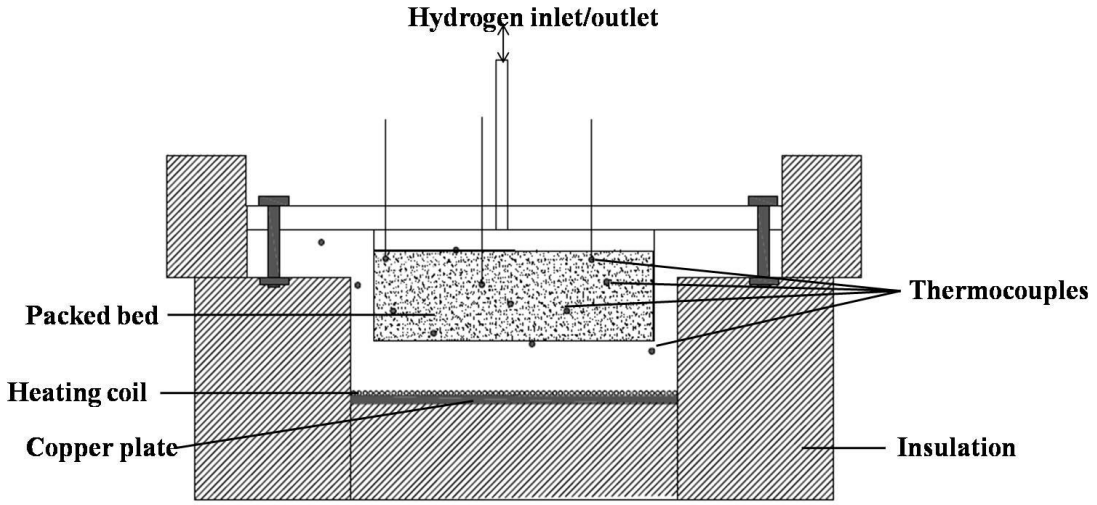

Fig. 1.6 Schematic view of ETC measurement cell used by Pons et al. [36]

metal/alloy in the packed bed is not magnesium or its alloy. Packed beds with magnesium as solid phase possess high ETC values in the range of 1-9 W m^{-1} K^{-1}athigh temperature (250 – 350°C).

1.4 Simulation of MH Packed Beds for Estimation of ETC

The primary parameters influencing ETC (k_e) of MH packed beds are:

- Thermal conductivity of the solid (k_s)
- Thermal conductivity of the gas (k_g) and
- The relative proportion of these phases in the bed [8, 9, 26].

Generally structure of the metal hydride bed is described by the term porosity φ. The porosity is equal to the volume of gas phase per unit volume of the system. Therefore,

$$k_e = f\left(k_s, k_g, \varphi\right) \tag{1.5}$$

The additional factors affecting effective thermal conductivity are solid to solid heat transfer at the contact, gas pressure and heat transfer by radiation. Taking these factors into consideration the ETC of MH packed bed is a function given as:

$$k_e = f\begin{pmatrix} k_s, k_g, \varphi, P, T, d, \text{ Particle Shape and Distribution, Mechanical Properties} \\ \text{of Particles, Thermodynamic Properties of Gas and Particle Flattering} \end{pmatrix} \tag{1.6}$$

Estimation of ETC by mathematical or empirical methods requires the equation (1.6) to be defined in an appropriate form.

Different mathematical models have been developed for estimation of ETC of porous beds providing an insight on the dependencies of ETC on various operating parameters [39, 40]. These models acted as base for the development of models to simulate the ETC of MH beds. The significant differences between non reactive bed and hydriding beds in modeling ETC are; the solid conductivity is constant in non reactive packed beds, whereas due to hydrogen absorption and desorption it varies in metal

hydride beds. Due to the expansion and contraction of particle the contact resistance between the particles varies and also the porosity of the bed varies. Few researchers have extended / modified the models developed for non-reactive packed beds to make them suitable for metal hydride beds. For simulation of ETC of MH beds, usually the MH bed is considered to be made up of an arranged matrix of repetitive elements. This element is termed as unit cell. The set of mathematical expressions formed from the modeling of MH bed can be solved either analytically or by applying suitable approximation technique. One such technique is homogenization method. Alternatively the MH bed can be divided into a huge number of cells by meshing the bed and this structure can then be studied by using FEA software. These techniques of simulation of ETC of MH beds are discussed briefly in following sections.

1.4.1 Analytical method

In this method, the packed bed is considered to be made up of spherical particles of similar geometric features. Utilizing the assumption of symmetrical arrangement, a fraction of a solid particle and the enveloping gas is taken as pivotal element and the packed bed is seen as a systematically arranged matrix of numerous such elements (unit cells). The analysis is made on such an element by taking into consideration, different mechanisms of heat transfer through the unit cell, estimating the heat transfer coefficients for each mechanism of heat transfer by forming an appropriate network of thermal resistances. The expression obtained by this analysis (of the unit cell) is then integrated over the extents of the bed to obtain the value of ETC of the bed. Applying this method, Sun and Deng [41] extended Masamune and Smith model [40] for estimation of effective thermal conductivity of $MlNi_{4.5}Mn_{0.5}$ (Ml: Lanthanum rich misch metal). The heat transfer was considered to be taking place through three mechanisms in parallel to each other as shown in Fig. 1.7. The three heat

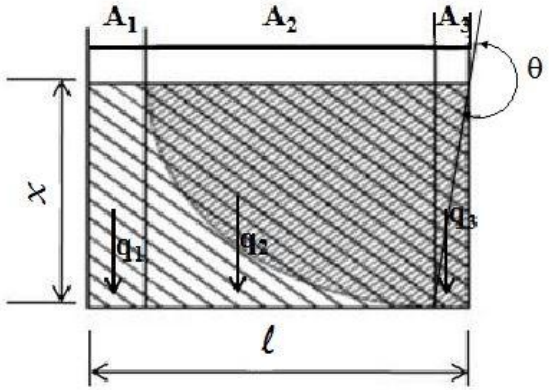

Fig. 1.7 Differential element considered by Sun and Deng [41]

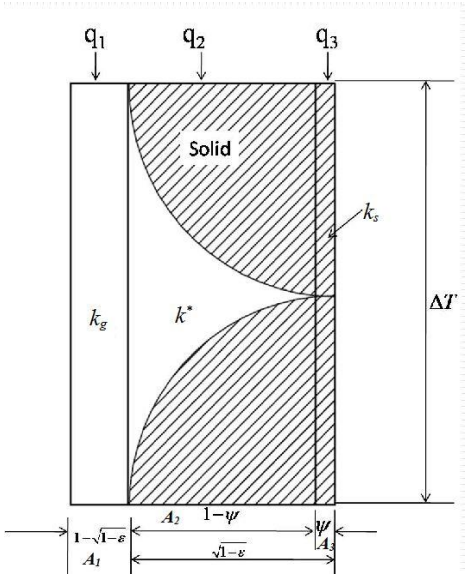

Fig. 1.8 Unit cell considered in Zehner, Bauer and Schlunder model [27]

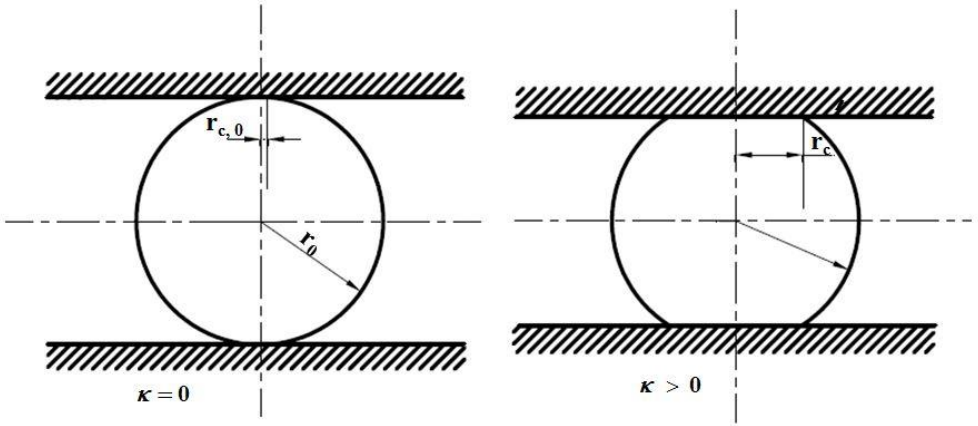

Fig. 1.9 Variable flattened radius considered in Kallweit and Hahne [27]

transfer mechanisms were; (i) conduction and radiation through voids (q_1), (ii) through a series path comprising of effective solid path and effective gas path (q_2), (iii) through diffusion between solid particles (q_3). The summation of the three fractional heat transfers gives total heat transfer which is then used to calculate the ETC of bed. The Masamune-Smith model is given in eq. (1.7)

$$k_e = A_1 k_g + \frac{A_2}{\frac{\varsigma}{k_g^*} + \frac{1-\varsigma}{k_s}} + A_3 k_s \tag{1.7}$$

where,

A_1 = Area fraction for heat transfer through mechanism 1
A_2 = Area fraction for heat transfer through mechanism 2
A_3 = Area fraction for heat transfer through mechanism 3
ς = Gas path length / Total length, for mechanism 2
$k_g^* = f(P, k_g, l_v)$ for the pressure range where, $\lambda \approx l_v$

As an extension to the Masamune-Smith model (eq. (1.7)), Sun and Deng [41] accommodated the effect of volume swell of solid particles due to hydrogenation. This was done by making the thermal conductivity of solid linearly dependent on hydrogen concentration of the MH bed. Also, unlike Masamune-Smith model the radiation heat transfer in mechanisms 1 and 2 were not neglected and heat transfer coefficients were defined accordingly. The model suggested by Sun and Deng is given in eq. (1.8)

$$k_e = A_1\left(k_g^* + x h_{rv}\right) + \left[\frac{A_2}{\frac{1-\varsigma}{k_s^*} + \frac{\varsigma}{k_g^* + 0.215 x h_{rs}}}\right] + A_3 k_s^* \tag{1.8}$$

where, h_{rs} and h_{rv} are radiation heat transfer coefficients for solid path and gas path respectively.

Kallweit and Hahne [27] have developed a similar model based on Zehner, Bauer and Schlunder model, which was devised for non-reactive packed beds. The heat transfer mechanisms suggested in Zehner, Bauer and Schlunder (ZBS) model were very similar to those in Masamune-Smith model with the difference being the radiation effects in ZBS model were modified using Knudsen number and Nusselt number. Another difference was that single effective thermal conductivity for mechanism 2 (q_2) was considered unlike Masamune-Smith model in which separate thermal conductivities were considered for gas and solid parts. Eq. (1.9) gives the ZBS model expression to calculate ETC of non-reactive packed bed.

$$k_e = A_1 k_g + A_2 k^* + A_3 k_s \tag{1.9}$$

where, k^* is the equivalent thermal conductivity for area fraction A_2. Fig. 1.8 shows the unit cell considered in ZBS model.

Kallweit and Hahne suggested the following extensions to ZBS model to make it suitable for MH packed beds and validated the extended model with the experimental values for HWT 5800 and $LaNi_{4.7}Al_{0.3}$ hydride beds.

1. Variable porosity:

$$\varepsilon = \varepsilon_0 - \frac{3.4654\times10^{-9}\kappa_{\max}\rho_s}{M_s}(1-\varepsilon_0) \tag{1.10}$$

2. Variable thermal conductivity of solid:

$$k_s = k_{s,0} + \left(k_{s,0} - k_s^*\right)\frac{\kappa}{\kappa_{\max}} \tag{1.11}$$

3. Variable flattening coefficient:

$$\varphi = f\left(\text{flattened radius, force between two particles, particle radius}\right) \tag{1.12}$$

Variable flattened radius is described in Fig. 1.9. All the above modified parameters are incorporated in the equation 1.9 to calculate the ETC of hydride bed.

Matsushita et al. [10] incorporated the effect of change in contact area and bed porosity caused due to hydrogenation/dehydrogenation by modifying the contact area model and obtained a better conformation with experimental results on ETC of MH bed than shown by other models.

1.4.2 Homogenization method

The behaviour of materials, which are heterogeneous on microscopic level but can be considered homogeneous on macroscopic level, can be modeled using homogenization methods. Homogenization considers the macroscopic domain of the material to be made up of matrix of rather homogeneous periodic unit cells thus replaces a heterogeneous material by an equivalent effectively homogeneous material. For the analysis to be accurate, it is necessary that the unit cell should have minimum possible size and the macroscopic domain can be formed by periodic arrangement of unit cells [42].Unlike analytical method, the assumptions involved in this method are less. Also this method is expected to provide a better insight to the microstructure of MH bed [43].Asakuma et al. [43] applied a homogenization method for calculation of ETC of $LaNi_{4.7}Al_{0.3}H_x$ bed. The change in contact area due to hydrogenation/dehydrogenation was examined and the effect of particle size depreciation on the ETC of MH bed was accommodated. The packed bed of metal hydride was considered as a periodic composite and analysis was done on a unit cell of that composite. The unit cell was assumed to be divided into two domains, solid domain and gas domain. A set of generalized equations for multi-scale steady state periodic heat conduction was devised and homogenization method was applied to the set of equations to finally obtain an expression for ETC of unit cell. The results obtained from this study were validated with the experimental results of Hahne and Kallweit

[27] and was reported to have a good conformity. Due to the underestimation of contact area, some discrepancies between the simulation and experimental results were observed for a certain range of operating parameters [44]. Ueoka et al. [44] considered both point and plane contact areas for better evaluation of contact area.

1.4.3 Numerical methods

Numerical methods have been utilized for simulation of heat transfer characteristics and their improvement but exclusive use of such methods for estimation of ETC of MH bed is not available. Melnichuk et al. [45] optimized the fin design for heat transfer improvement in a MH bed. Effective thermal conductivity of a cell was considered as a function of thermal conductivities of metal hydride and fin material (aluminum). Both these thermal conductivity values were taken as constants. Veerraju and Ram Gopal [46] developed a two-dimensional transient model to study the heat and mass transfer characteristics of plate fin-and-elliptical tube type metal hydride reactors. For this analysis, the thermal conductivities of metal hydride and reactor tube material (copper) were taken as constants. Freni et al. [47] devised a finite element based three-dimensional model to simulate MH based hydrogen storage tank. All thermo-physical properties were considered to be constant for this simulation. On the similar track, P. Muthukumar et al. [48] developed a two-dimensional numerical model using COMSOL Multiphysics software for the performance analysis of an industrial scale MH based hydrogen storage container embedded with cooling tubes. The ETC of hydride bed was assumed to be independent of pressure and temperature for this analysis.

1.4.4 Other methods

Ghafir et al. [49] used Raghavan and Martin [50] model and Hahne and Kallweit's [27] experimental results to estimate the solid thermal conductivity of metal hydrides. Suda et al. [51] proposed an empirical

Table 1.4 Mathematical models for estimation of ETC

Author	Equation	Physical Model	Simulation method	ETC dependency
Pons and Dantzer [36]	$k_e = \left\{ \left(1-\sqrt{(1-\varepsilon)}\right)\varepsilon \left[\frac{k_g}{\varepsilon + \frac{\sigma^*}{D_p}} + k_{ir} \right] + \sqrt{1-\varepsilon}\left[\varphi k_s + (1-\varphi) k_s^* \right] \right.$	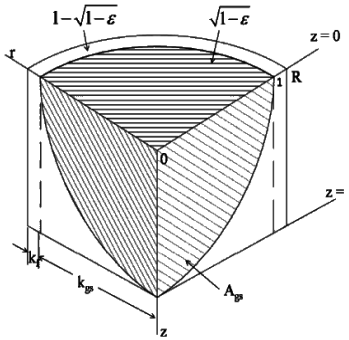	Exact Solution (Modified Zehner Bauer Schlunder Model)	Fractions of heat transfer through solids, through fluid and through a series path of solid and fluid applying Knudsen effect
Suda et al. [38]	$k_e = 0.56 + 0.19(\ln P) + 6\times10^{-3}(\ln P)^2 - 5.2\times10^{-3}(\ln P)^3 + 0.46\overline{H/M}$	----	Empirical	Gas pressure and hydrogen concentration
Asakuma et al. [43]	$k_e = \frac{1}{\Omega}\int_{\Omega} \alpha \left(\delta_{pq} - \frac{\partial \chi_q}{\partial y_p} \right) \mathrm{d}y$	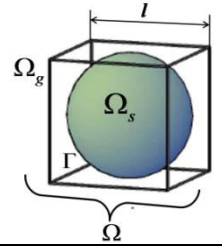	Homogenization method	Mass fraction of solid and gas; Temperature

correlation for estimation of ETC of MH bed based on their experimental results. The empirical correlation may not be considered as generalized expression for calculating ETC of MH beds as dependencies on various parameters vary with changes in operating conditions also and no normalizing factors were given in the said empirical correlation. A brief overview of some of the above discussed simulation works is given in Table 1.4.

1.5 Effect of Operating Parameters on ETC of MH Beds

Effect of gas pressure, temperature, hydrogen concentration, particle size, particle decay and number of absorption–desorption cycles and solid thermal conductivity on ETC of the hydriding beds is reviewed in this section.

1.5.1 Effect of pressure

The variation of ETC of reactive packed beds of hydriding materials with pressure shows a trend of a tilted 'S' shaped curve[7-9, 20, 23, 38].This dependency of ETC on pressure can be explained using Knudsen number (Kn). In the low pressure region ($Kn<<1$) the variation in pressure does not affect ETC. The variation in hydrogen pressure does not influence ETC in this region. The value of hydrogen pressure up to which its effect is not significant on ETC, varies for different metal hydride beds as the characteristic features like particle size, solid thermal conductivity, packing density (or porosity) of metal hydride bed etc. are the deciding factors for the value of ETC in this region. The heat transfer in this region is derived from conduction between solid particles only as the usual range of temperature and very low surface area of particles generally nullify the chances of thermal radiation. Hence depending on these parameters the values of ETC in this region for different metal hydride beds are in the range of 0.2 to 1 W m^{-1} K^{-1} as shown in Fig. 1.10.The sharp increase in ETC in the intermediate pressure range can be attributed to the Knudsen

effect (Kn≃1) and hydrogen-metal hydride interaction. The contribution of Knudsen effect in this increase in ETC can be estimated by exposing metal hydride bed to helium gas at varying pressure. Helium has thermal conductivity close to that of hydrogen but it does not react with metal alloys to form compounds. The difference in the ETC values obtained with helium and those with hydrogen for the same metal hydride bed and same operating parameters can be considered as the contribution of hydrogen-metal hydride interaction in the increase in ETC of metal hydride beds [52]. As the interaction of hydrogen with different metal hydrides will be at different pressure and temperature conditions and will lead to different changes in parameters like bed porosity, contact between solid particles etc., the ETC variation for different metal hydride beds with pressure are different. The ETC increased by 0.95 W m^{-1} K^{-1} for the pressure increase of 3.06 bar for HWT 5800 hydride bed [28] whereas for a $TiMn_{1.5}H_x$ bed [20] an increase of 32 bar resulted in the increase of ETC by 0.88 W m^{-1} K^{-1} . The ETC of MgH_x bed [26] was reported to increase by 0.31 W m^{-1} K^{-1} for the pressure increase of 32 bar while the ETC increase was very less for almost the same pressure increase in case of a $MgNi_2H_x$ (refer to Fig. 1.10).The contribution of Knudsen effect on ETC increase ceases to occur as the hydrogen pressure in the MH bed reaches the *break even pressure*. Therefore beyond break even pressure, where $Kn \gg 1$, the ETC becomes independent of pressure.

1.5.2 Effect of temperature

The thermal conductivity of gas is a stronger function of temperature as compared to thermal conductivity of solid. Moreover the temperature variation has opposite effects on thermal conductivity of gas and solids. While the thermal conductivity of solids decrease with increase in temperature, the thermal conductivity of gases increase due to the increase in molecular kinetic energy. The effect of temperature variation on ETC of MH beds is defined by the relative weightage of variation of thermal

conductivity of gas or that of solid particles. As shown in Fig. 1.11, the ETC of Mg hydride bed [26] and that for $TiFe_{0.85}Mn_{0.15}$ hydride bed [18] increased with temperature while ETC for $MmNi_{4.5}Al_{0.5}$ hydride [8] and that for Mg_2Ni hydride [23] linearly decreased with the increase in temperature. Hence it can be said that the variation of ETC with bed temperature is depended on bed parameters like solid fraction, bed geometry etc. and no fixed trend for this can be suggested.

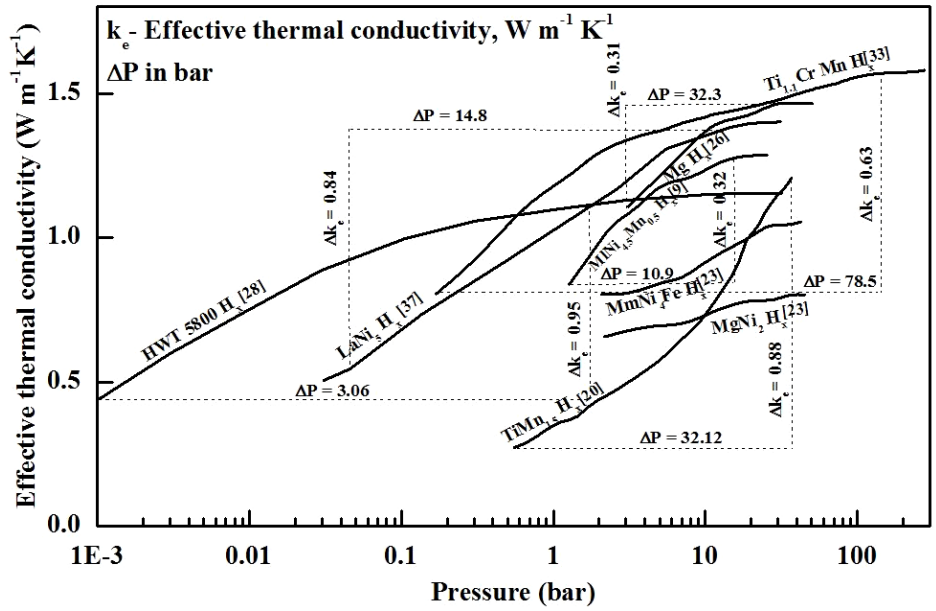

Fig. 1.10 Variation of ETC with pressure

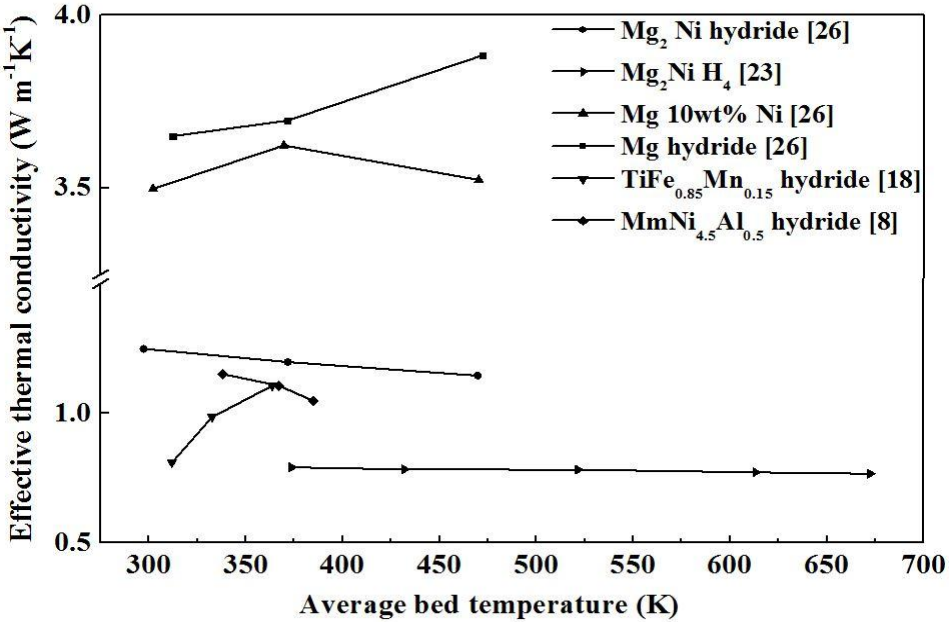

Fig. 1.11 Variation of ETC with temperature

1.5.3 Effect of hydrogen concentration

It is expected that the ETC of reactive packed beds of hydriding materials increases with increase in hydrogen concentration [7-9, 20, 23]. Suda et al. [20] observed a linear variation of ETC with hydrogen concentration with a slope of 0.46(W m^{-1} K^{-1}) / (H-atom/Metal atom). Few authors [28, 49] have observed that the variation of ETC with hydrogen concentration is similar to *pressure concentration isotherm* curve as shown in Fig. 1.12. In contrast, Kapischke and Hapke [19] observed that in case of Mg/ 2 wt% Ni hydride the ETC decreases with hydrogen concentration, whereas in case of magnesium hydride it follows an arch shaped trend [21].Kempf and Martin [18] reported that the hydrogen concentration does not have any effect on ETC.

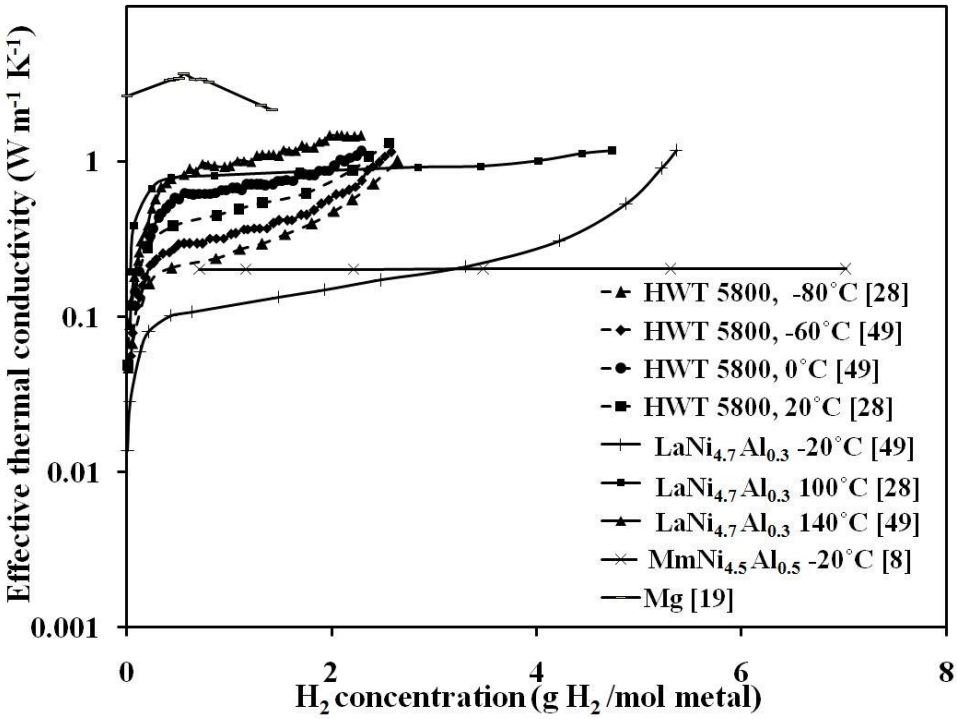

Fig. 1.12 Variation of ETC with Hydrogen concentration

1.5.4 Effects of particle size

Unlike non reactive packed beds, the particle size of MH does not remain constant. With continuous hydrogenation and dehydrogenation cycles, the

particle size decreases significantly due to cyclic expansion and contraction. The particle size ultimately defines the surface area of particle available for heat transfer. With the decrease in particle size the heat transfer through particles (by conduction as well as by radiation) gets reduced significantly. As a consequence the contribution of solid particles towards ETC of MH bed decreases thus decreasing the ETC value. Heat transfer by conduction through the particles may not be affected as much as the radiation component gets affected [9, 26]. The heat transfer through collisions of gas molecules with particle wall is considered in the accommodation coefficient '*a'* used in mathematical modeling of ETC of MH beds [8, 19] thus taking into consideration the effect of variation in particle size on ETC of MH beds. With decrease in particle size, the ETC decreases [9, 18-20, 26]. The particle size also affects the range of pressure dependency of ETC. This is obvious due to the change in void volume and hydrogen-MH interaction caused due to variation in particle size of the MH. The theoretical studies [36] using Bauer and Schlunder model showed that the variation of particle diameter induced a horizontal translation of S shaped curve.

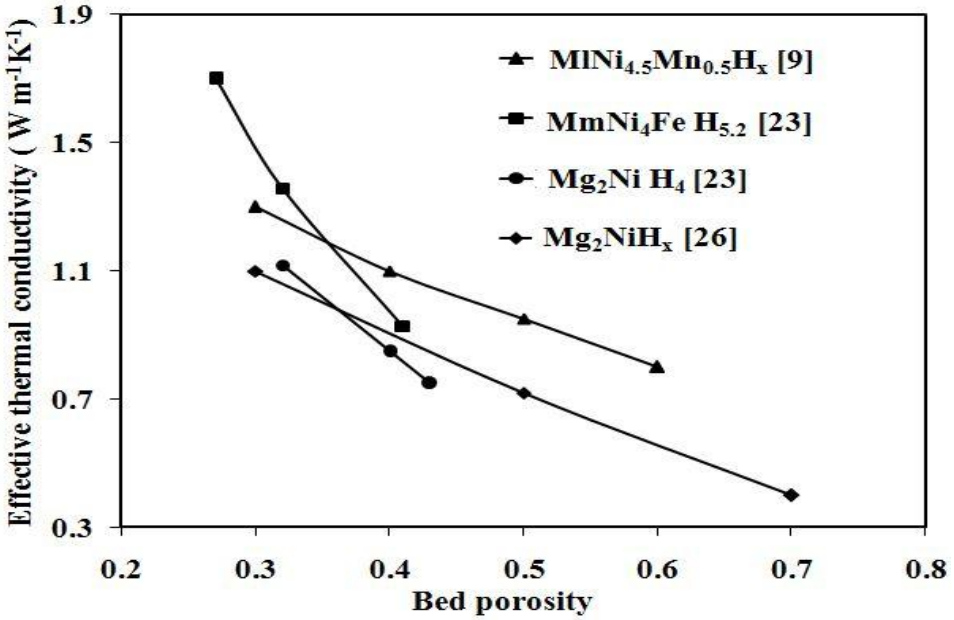

Fig. 1.13 Effect of bed porosity on ETC of MH beds

1.5.5 Effect of number of cycles

With repeated number of hydrogenation-dehydrogenation cycles the parameters like bed porosity, solid thermal conductivity, particle geometry, amount of hydrogen absorbed/desorbed by the MH varies considerably. Also a certain number of cycles are essentially required to convert the metal alloy into metal hydride, this number of cycles is a material dependent parameter [8-9, 20]. The variations of parameters causing decrement of ETC with increasing number of cycles of hydrogenation-dehydrogenation are, decrease in particle size, hydrogen concentration reduction, etc. The MH particle size keeps on decreasing continuously with repeated cycles of hydrogenation and dehydrogenation.ETC of Hydralloy® C5 metal hydride- ENG composite was found to decrease from 40 W m^{-1} K^{-1} for first cycle to 12.7 W m^{-1} K^{-1} after 250 cycles [53]. Hence a general conclusion that can be reached to is that with hydrogenation-dehydrogenation cycles, the ETC of the MH bed decreases up to a certain number of cycles and hence a particular number of cycles are essentially required to obtain ETC value independent of number of cycles in metal-hydrogen systems [23, 28].

1.5.6 Effect of bed porosity

Unlike non-reactive beds, the bed porosity in case of MH beds does not remain constant. With the increase in bed porosity the ETC of MH bed decreases as the contact between solid particles decreases with increase in porosity. As discussed in above sections, the repeated hydrogenation-dehydrogenation of MH bed causes particle size reduction. A consequence of this is increase in packing density or decrease in bed porosity. The decrease in bed porosity results in linear increase in ETC of MH bed as shown in Fig. 1.13. As shown in figure the variations of ETC with bed porosity are steeper for $MmNi_4FeH_{5.2}$ and Mg_2NiH_4 beds [23] as compared to that of $MlNi_{4.5}Mn_{0.5}H_x$ [9] and Mg_2NiH_x [26] beds. This

difference in trend is not only because of difference in metal hydrides rather it is due to differences in packing density, measurement techniques and operating parameters. The porosity of MH bed may vary due to some augmentation techniques also, like compaction and pelletization of MH powder or high thermal conductivity metal structure incorporation etc. The increase in ETC of MH bed due to reduction in bed porosity is at the cost of amount of hydrogen absorbed / desorbed by the MH bed.

1.5.7 Effect of hydrogenation and dehydrogenation of particles

The hydrogen absorption by the MH particles in the bed results in swelling or expansion of the particles thus improving the contact between solid particles and increase in surface area of MH particles. Both of these phenomena have positive effect on ETC of MH bed. These MH particles contract during dehydrogenation of the MH bed. The contraction of particles obviously has the reverse effect of the above, on ETC of MH bed. This frequent hydrogenation and dehydrogenation act as cyclic loading on the solid particles and stresses caused due to such cyclic loading leads to deterioration of solid particles hence bringing about changes in packing density and bed porosity.

1.5.8 Effect of solid thermal conductivity

MH beds are made up of solid particles as discrete phase and hydrogen as continuous phase [8]. As discussed in above sections, the variation of ETC of MH beds has complex dependencies on different parameters. The apparent thermal conductivity of solid particles within the bed also varies continuously with cycles of hydrogenation and dehydrogenation. The effect of variation in solid thermal conductivity on ETC is appreciable only when it is amplified due to the interaction between solid particles and hydrogen. The experimental studies of Suissa et al. [23] and theoretical studies of Pons and Dantzer [54] have shown that solid thermal

conductivity has less effect on ETC except in low pressure region. Solid thermal conductivity has different levels of effects on ETC depending on the bed porosity. With the decrease in bed porosity, the effect of solid thermal conductivity on ETC of MH bed increases [23]. This is obvious, as the solid content of the bed increases with decrease in bed porosity. Even a large variation in k_s caused a small change in ETC.

1.6 Augmentation Techniques

All the experimental and theoretical studies conclude that the micrometric size of the solid particle is the main reason for low value of ETC of hydriding packed beds. For applications of hydriding packed beds like hydrogen storage in metal hydride, chemical heat pump, chemisorption based refrigeration systems, thermal energy storage, etc., lower heat transfer characteristic causes poor performance of the system and hence enhancement of heat transfer is a very important requirement[1-5, 11-13, 55, 56].

Among the parameters effecting heat transfer in hydriding packed beds, ETC finds appreciable importance. Hence augmentation of ETC has been studied by a considerable number of researchers since a long time. For augmentation of ETC (or heat transfer characteristics) in hydriding packed beds, techniques like inclusion of high conductivity material matrix, mixing of fibrous materials, fins, forming compacts, inclusion of metallic structure or high conductivity material foams have been tried and implemented in several cases with varying degree of successes. But increase of parasitic weight and decrease in hydrogen absorption rate or quantity is the hindrance in the implementation of augmentation techniques. An optimal technique is one which takes care of these issues. This section discusses some of the augmentation methods applied to hydriding packed beds.

Table 1.5 Summary of ETC augmentation techniques

Author	**Metal Hydride**	**Augmentation Technique**	**ETC ($Wm^{-1} K^{-1}$)**
Lloyd et al.[25]	$LaNi_5$ Hydride	Cu plating of metal hydride powder and subsequent cold compaction with Sn binder	2.9-6.2
Suda et al. [48]	$MmNi_{4.5}Al_{0.5}$	Porous aluminum packing	4
Nagel et al. [49]	$MmNi_{4.46}Al_{0.54}$	Copper wire net matrix	0.5- 2.75
Suda et al [50]	$MmNi_{4.51}Al_{0.47}$	Multilayer waved sheet of copper	14
Ron et al.[57]	$LaNi_5$ Hydride	Porous metal matrix and MH compacts	8-23
Kim et al.[58]	$LaNi_5$ Hydride	Compacts with recompressed expanded graphite	3-6
Sanchez et al. [62]	$LmNi_{4.85}Sn_{0.15}$	Expanded natural graphite + metal hydride compacts	11.2
Yasuda et al.[63]	$TeFe_{0.9}Ni_{0.1}$; $La_{0.6}Y_{0.4}Ni_{4.9}Al_{0.1}$	Sheet formation with Aramid Pulp and Carbon Fiber	3.20
Shim et al.[61]	MgH_2	Compacts with ENG flakes	9.3

1.6.1 Filling of heat transfer enhancement structures

Filling of structures although augments the ETC but it leads to additional parasitic weight and consecutively decreases the hydrogen rate/quantity with the ultimate effect of decrease in effectiveness/efficiency of the dry sorption systems. Incorporation of copper wire screen in hydriding beds resulted in a marginal improvement in ETC [57, 58]. A complex waved structure made of copper was said to have given a considerable improvement which resulted in a value of ETC as high as 14 W m^{-1} K^{-1} [57]. Aluminum foam is another material generally used for ETC augmentation of packed bed. Suda et al. [57] reported good results, while Wang et al. [58] did not found it justified to increase the aluminum foam content more than 10% in the packed bed, as it results in increase in ETC but at the cost of decrease in the quantity of hydrogen. Helical coil heat exchanger [59] and internal fins [60] have also been tried and reported to show an improvement in heat transfer characteristics of the metal hydride packed beds. To achieve better performance and efficiency of MH based hydrogen compressor, copper structure (with inner fins) was applied resulting in satisfactory augmentation of ETC [60]. Heat transfer or ETC enhancement structures have also been used in sorption cooling/heating systems based on MH packed beds [13].

1.6.2 Augmentation through mixing of high thermal conductivity material

In this method a high thermal conductivity material is mixed with solid particles and compacts (composites) are made to allow heat transfer in a continuous path and thus leading to an increase in ETC of reactor bed. The pressure force applied for making the composites has also been reported to have some effect on the ETC values of compacts as the density of compacts directly depends on this pressure force. The increase in this pressure leads to decrease in permeability of the compacts thus creating a

negative effect on its absorption properties. [61-63]. Making porous metal hydride (PMH) compound by mixing aluminum powder results into good level of improvement in ETC values which reached a range of around 8 to 23 W m^{-1} K^{-1} for a feasible volume fraction of aluminum powder ($0.15 < V_{A1} < 0.5$; V_{Al} being the volume fraction of aluminum powder in PMH compound) [61-63]. In an alternativetechnique the metal hydride particles were plated with thin copper shells and cold plated with low melting point metal binder normally Sn. Variation of mass fraction of the binder and compaction resulted into a range of ETC values from 2.7 ± 0.7 to 6.4 ± 0.5 W m^{-1} K^{-1}. In almost similar experiment, ETC value of around 5 W m^{-1} $K^{-1}$for a fixed proportion of metal alloy (absorbent), binder (Sn) and coating material (Cu) was reported. To decrease the negative effect on permeability of compacts a hole was drilled along the center of each pellet to allow the hydrogen to access entire reactor [64, 65]. For augmentation of ETC and heat transfer characteristics of $LaNi_5$or $LaNi_{4.75}$ $Al_{0.25}$ hydrides, for the application of MH based hydrogen compressor, PMH compacts of copper coated MH particles were utilized and were reported to have the ETC value of more than 6 W m^{-1} K^{-1} [66].

Mixing of carbon and graphite (or expanded graphite) has resulted into augmentation of ETC with comparatively less negative effect on permeability of absorbent/ compacts [65, 67]. It was purported that the ENG-MH compacts gave better kinetics as compared to that in case of Al foam etc. [68]. ETC of 3.2 W m^{-1} K^{-1} was reported in case of a metal hydride sheet comprising of metal hydride powder, aramid pulp and carbon fiber by wet paper method [69].

In a comparatively different technique a Single Walled Carbon Nano Tube (SWCNT) was synthesized directly on $TiMn_2$ and $LaNi_{4.5}Co_{0.5}$ hydrides with the view to reduce boundary thermal resistance. The effect of the SWCNT grown in the intermediate spaces between metal hydride particles was calculated as the function of the particle filling ratio (ε) to the whole volume and the SWCNT filling ratio (X) to the vacuity. The value of ETC

reached 10 W m^{-1} K^{-1}at $X = 0.34$. The maximum achievable value for ETC was suggested as 14 W m^{-1} K^{-1} although no experimental evidence was made available to support this claim [70]. Table 1.5 presents a summary of ETC augmentation techniques applied by different researchers. Fig. 1.14 shows the comparison of ETC values obtained by different augmentation techniques. The ETC value for MH powder bed except for magnesium based hydrides is in the range of 0.5 to 1.2 W m^{-1} K^{-1}. In case of MgH_2 the ETC value is slightly higher because of comparatively higher solid thermal conductivity.

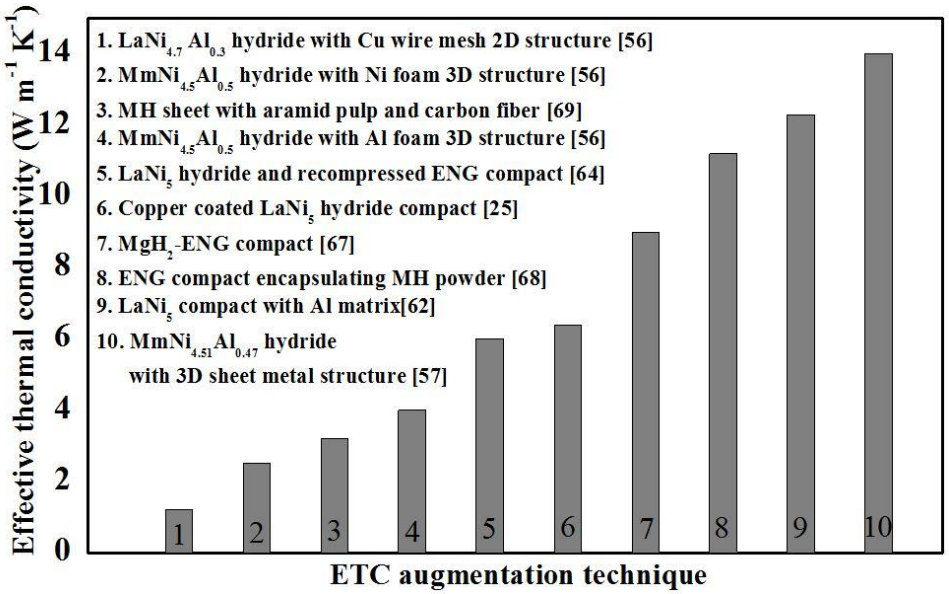

Fig. 1.14 Comparison of different ETC augmentation techniques

As shown in Fig. 1.14, the inclusion of two dimensional structure of copper wire mesh results in only a slight increase in ETC of MH bed. The inclusion of metallic foam offers somewhat better advantage while compaction/pelletization has proven to be the best among the augmentation methods discussed here. Inclusion of expanded natural graphite with compacts has resulted in further improvement in ETC of MH beds.

1.7 Motivation for the Present Work

Poor heat transfer characteristics of metal hydride beds act as hindrance in the applicability of metal hydrides for different applications. Effective thermal conductivity is one of the important parameters defining the heat transfer characteristics of these beds. Mere augmentation of ETC, neglecting its effect on hydrogen absorption/desorption characteristics, may not be fruitful. Several works on augmentation of ETC of MH beds have been reported in literature but the effect of that augmentation on sorption characteristics of MH beds has been rarely studied. Hydrogen sorption characteristics of MH bed comprise of both, the hydrogen absorption/desorption quantity and kinetics and hence the effect of ETC augmentation on these characteristics is needed to be considered to make the ETC augmentation fruitful. Compaction and pelletization along with mixing of graphite/carbon flakes has been considered as relatively better technique for ETC augmentation. The compaction pressure and the mass proportion of graphite flakes are the deciding factors for the effect of ETC augmentation on hydrogen sorption characteristics of MH pellets bed. Inclusion of porous structure made up of material of high thermal conductivity has also been found as a suitable technique for ETC augmentation. A combination of inclusion of three dimensional porous structure and pelletization has never been reported for ETC augmentation of MH beds. Also, the effect of ETC augmentation on sorption characteristics of metal hydride beds is not available in the literature.

An alloy based on $LaNi_5$ with cerium replacing a proportion of lanthanum, $La_{0.8}Ce_{0.2}Ni_5$ was tried for the application of metal hydride based hydrogen compressor (MHHC).

It is revealed from the literature that pure magnesium although has good hydrogen absorption capacity but it has got characteristic limitation of poor kinetics. To improve the sorption kinetics, composites are developed mixing lanthanum based alloy with magnesium in suitable proportion. In

this work such a composite of magnesium and $LaNi_{4.6}Al_{0.4}$, in equal proportion (Mg + 50 wt% $LaNi_{4.6}Al_{0.4}$), has been developed for the application of thermal energy storage system.

A comprehensive literature review on ETC measurement, simulation and augmentation of metal hydride beds resulted in framing the following objectives for the present work.

1. To simulate the effective thermal conductivity of metal hydride packed beds for analyzing the dependencies of different parameters on ETC.

2. To design and fabricate the experimental set ups for measurement of ETC of MH beds along with the quantification of amount of hydrogen absorbed/desorbed and for measurement of performance of MHHC and MHTES.

3. To design and fabricate the copper wire mesh augmentation structure and pellets.

4. To measure the ETC of the three configurations of MH beds, namely lose metal powder bed (LMP), bed of pellets of metal powder and graphite fibers (PMPGF) and bed of pellets of metal powder and graphite fibers embedded with copper wire mesh structure (PMPGFCu) for both the materials, $La_{0.8}Ce_{0.2}Ni_5$ and Mg + 50 wt% $LaNi_{4.6}Al_{0.4}$.

5. To study the level of ETC augmentation achieved using different techniques along with the effect of ETC augmentation on hydrogen absorption/desorption quantity.

5. To study the effect of ETC augmentation on hydrogen sorption kinetics of MHs and hence on the performances of MHHC and MHTES.

1.8 Structure of the Thesis

The overall scope of the thesis is to study the level of ETC augmentation obtained by two different augmentation techniques and the effect of ETC augmentation on hydrogen absorption/desorption quantity and kinetics of metal hydride beds with respect to MHHC and MHTES applications. The

thesis is organized into six chapters. The topic is introduced in this chapter along with the comprehensive review on measurement, simulation and augmentation of effective thermal conductivity of metal hydride beds.

Chapter 2 presents the simulation of effective thermal conductivity of metal hydride packed beds. The mathematical simulation is done by extending four well-known mathematical models developed for non-reactive packed beds. The suitability of the extended models for the simulation of ETC of MH bed ($MmNi_{4.5}Al_{0.5}$) is discussed in this chapter.

Chapter 3 describes the design and fabrication of experimental setup and ETC cell, fabrication of pellets, experimental procedure and data reduction for the measurement of the ETC. The results obtained from the measurement of ETC of three types of beds, LMP, PMPGF and PMPGFCu are discussed.

Chapter 4 details the fabrication of experimental setup and design of reactors for studying the effect of ETC augmentation on the hydrogen sorption kinetics of metal hydrides and consequent effect on the performance of MHHC and MHTES.

Chapter 5 enlists the important conclusions drawn from the present study and the scope of future work.

Chapter 2

Simulation of Effective Thermal Conductivity of Metal Hydride Packed Beds

Several mathematical models are available for estimation of effective thermal conductivity (ETC) of non-reactive packed beds. Keeping in view the salient differences between metal hydride beds in which chemisorption of hydrogen takes place and conventional non-reactive packed beds, modified models are proposed here to predict the ETC. Some well-known models developed by Yagi and Kunii [71], Zehner and Schlunder [72], Dietz [73] and Masamune and Smith [40] have been extended to incorporate the consequences of hydrogen absorption and desorption. The extended models are then used for simulation of ETC of $MmNi_{4.5}Al_{0.5}$ hydride packed bed. The experimental data was taken from Anil kumar et al. [8]. Applicability of the extended models for estimation of the ETC at different operating conditions such as pressure, temperature and hydrogen concentration is discussed.

2.1 Analysis Procedure

In non-reactive packed beds, the ETC depends on a large number of parameters, namely, the thermal conductivities of solid and fluid, porosity of the bed, accommodation coefficient, contact area between solid particles, void dimensions, size and geometry of particles, geometry of bed, pressure and temperature. For a given packed bed, all these parameters, except pressure and temperature, are generally taken to be constant. However, in the case of MH beds, porosity, contact area between solid particles, void dimensions, and geometry of particles change due to the volumetric and structural changes that occur due to the absorption of hydrogen by the metal alloy. Moreover, the thermal conductivity of the solid particles decreases as a consequence of hydrogen absorption. Hence,

modifications to the conventional mathematical models are required to incorporate these effects as discussed in the following sections.

2.2 Variation in Porosity of bed

Due to hydrogen absorption, the porosity continuously decreases due to swelling of the MH bed which is confined within a given volume. Equation (2.1) gives the *maximum expansion factor* due to hydrogen absorption in MH packed beds, while equation (2.2) can be used to obtain the expansion factor as a function of hydrogen concentration

$$f_{VE} = \frac{2\times10^3 \Delta V N_A X_{\max} \rho_s}{M_{H_2}} \tag{2.1}$$

$$\upsilon = \frac{f_{VE} X}{X_{\max}} \tag{2.2}$$

Using equations (2.1) and (2.2), the porosity of the bed can be obtained from equation (2.3) assuming linear variation of porosity with the hydrogen concentration.

$$\varphi = \varphi_0 - (1-\varepsilon_0)\upsilon \tag{2.3}$$

On substitution of values from equation (2.1) and (2.2) in equation (2.3), it yields

$$\varphi = \varphi_0 - 1.7321\times10^{-3}(1-\varepsilon_0)\rho_s X \tag{2.4}$$

2.3 Effect on Heat Conduction through Solid Particles and Gas in Voids

Unlike non-reactive packed beds where the contact area between particles remains unchanged, in case of MH beds, contact area between the particles increases with hydrogen absorption, thus decreasing the contact thermal resistance between solid particles. On the other hand, the thermal conductivity of individual solid particles decreases due to hydrogen

absorption. Hence, in the present work, thermal conductivity of solid particles is taken as a function of hydrogen concentration, and not a constant.

$$k_s^* = k_s + \xi X \tag{2.5}$$

The accommodation coefficient for solid ξ is a parameter dependent on solid-gas combination of the MH bed. In the present case, it is assumed as 0.48. As discussed in section 1.5.7, hydrogenation and dehydrogenation causes variation in geometry of solid particles thus affecting the solid thermal conductivity and the configuration of voids in the MH bed. This variation in voids configuration results in appreciable variation in thermal conductivity of the gas present in the voids. Hence the variation in thermal conductivity of gas in voids needs to be taken into consideration. Apparent thermal conductivity of gas in the voids, k_g^*, can be obtained using the expression suggested by Chapman and Cowling (equation (2.6)).

$$\frac{k_g}{k_g^*} = 1 + \frac{2l_{mf}}{X_e}\left(\frac{2}{\psi} - 1\right) \tag{2.6}$$

The mean size of void (X_e)in the present analysis is assumed to be equivalent to mean diameter of particles (d_s). To obtain the value of d_s, Eq. (2.7) can be used, where breakaway pressure (P_b) is dependent on solid-gas combination of the bed and in the present case it is taken as 15 bar [8]. The accommodation coefficient for gas (ψ) is empirically assumed to be 0.15.

$$P_b = 1770 \times 10^{-24} \frac{\left(T + 491.67\right)}{d_H^2 d_s} \tag{2.7}$$

The mean free path of hydrogen is given by [8]

$$l_{mf} = \frac{3.7206 \times 10^{-15} T}{P} \qquad (2.8)$$

2.4 Extended Mathematical Models

For the sake of accounting the effects of hydrogenation and dehydrogenation on the bed porosity, solid thermal conductivity and thermal conductivity of gas in voids, these parameters (which were taken as constants in the original models) are replaced with the expressions obtained from Eq. (2.4), Eq. (2.5) and Eq. (2.6) respectively. The models obtained after these implementations are presented below which are applicable for MH beds.

2.4.1 Yagi and Kunii Model

Considering a randomly packed bed of spherical particles with seven heat transfer mechanisms broadly classified on the basis of their dependence on fluid flow, Yagi and Kunii [71] found that for small Reynolds number (which generally is the case for MH packed beds), only four heat transfer mechanisms were predominant, viz. thermal conduction through solid particles, thermal conduction through the contact surfaces of two particles, radiation heat transfer between particles and conduction heat transfer through the fluid film in the voids. Their assumptions stipulated that the convection heat transfer in packed beds is not considerable and the conduction heat transfer through the fluid film in the voids is unaffected by the fluid flow. They obtained good agreement of the calculated values of ETC for different types of particles and different fluids with the experimental data reported by several investigators. The expression suggested by Yagi and Kunii was given as eq. (2.9).

$$\frac{k_e^0}{k_g} = \delta\left(\frac{k_s}{k_g}\right) + \frac{(1-\varphi-\delta)\beta}{\psi\left(\frac{k_g}{k_s}\right) + \frac{1}{\frac{1}{\varepsilon} + \frac{D_p h_{rs}}{k_g}}} + \varphi\beta\frac{D_p h_{rv}}{k_g} \qquad (2.9)$$

For bed of fine particles, with motionless gas, the above equation reduces to;

$$\frac{k_e^0}{k_g} = \beta \frac{1-\varphi}{\frac{k_g}{k_s} + \varepsilon} \tag{2.10}$$

The incorporation of proposed extensions (replacement of constant values of bed porosity, solid thermal conductivity and thermal conductivity of gas in voids with variables given by Eqs. (2.4), (2.5) and (2.6) respectively) to Yagi and Kunii model results in the expression given by equation (2.11) for ETC of MH packed beds. The value of ε for the present case is taken as 0.078, and β is taken as unity as discussed by Yagi and Kunii.

$$k_e = \frac{k_g \beta}{1 + \frac{7.4412\times10^{-15} T}{PX_e}\left(\frac{2}{\psi} - 1\right)} \left\{ \frac{1-\varphi_0 + (1-\varphi_0)\times 1.7321\times10^{-3}\rho_s X}{\frac{k_g}{k_s^* \left\{1 + \frac{7.4412\times10^{-15} T}{PX_e}\left(\frac{2}{\psi} - 1\right)\right\}} + \varepsilon} \right\} \tag{2.11}$$

2.4.2 Zehner and Schlunder model

The unit cell considered by Zehner and Schlunder [72] was basically an eighth part of a cylinder. Thus they assumed the bed to be made up of cylindrical cells filled with solid spherical particles. The remaining part of the cylinder was considered to be filled by a low conductivity fluid (hydrogen in present case). As, is clear from eq. (2.12), Zehner and Schlunder model does not consider the effect of contact areas between the particles of the packed bed and thus the model under predicts the values of ETC for packed beds in many cases.

$$\frac{k_e}{k_g} = 1 - \sqrt{1-\varphi} + \sqrt{1-\varphi}\left[\frac{2}{1 - B/\varpi}\left(\frac{\left(1-\frac{1}{\varpi}\right)B}{\left(1 - B/\varpi\right)^2}\ln\frac{\varpi}{B} - \frac{B+1}{2} - \frac{B-1}{1-1/\varpi}\right)\right] \tag{2.12}$$

To determine the shape factor B, following geometric condition is used:

$$\varphi = 1\text{-}\left(\frac{B\left(3-4B+B^2+2\ln B\right)}{\left(B-1\right)^3} \right)^2 \qquad (2.13)$$

This expression is approximated with

$$B = C\left(\frac{1-\varphi}{\varphi} \right)^m \quad \text{with C=1.25 and m=} \frac{10}{9}$$

On substitution of value of B obtained from Eq. (2.13) in Eq. (2.12) the ETC of non-reactive packed beds can be obtained. With the substitutions (as made in case of Yagi-Kunii model) for accounting the effects of hydrogen absorption / desorption by the MH bed, Eq. (2.12) takes the form as given by equation (2.14).

$$k_e = \left(1-\sqrt{1-\varphi_0+\left(1-\varphi_0\right)1.7321\times10^{-3}\rho_s X}\right)k_g + \frac{\sqrt{4-4\varphi_0+\left(1-\varphi_0\right)6.9284\times10^{-3}\rho_s X}}{E}\left\{\frac{\left(1-\varpi\right)B}{E^2}\ln\frac{1}{\varpi B}-\frac{B+1}{2}-\frac{B-1}{E}\right\} \qquad (2.14)$$

where:

$$\varpi = \frac{k_s^*\left(P\times10^5\times X_e+\left(1-\varphi_0\right)1.135\times10^{-8}T\left(\frac{2}{\psi}-1\right)\right)}{k_g P\times10^5\times X_e} \qquad (2.15)$$

$$B = -6.49\varphi + 3.35 \qquad E = \left(1-\varpi B\right)$$

2.4.3 Dietz model

Dietz [73] analysed a particular geometry of packed bed considering a special case of a hexagonal array of touching spheres. Each spherical particle was said to be in contact with neighboring eight similar particles, six in the horizontal plane and two in the vertical plane. Heat flux was assumed to be unidirectional and steady state energy equation was obtained for the said geometry. The analysis was particularly suitable for the cases where k_s^*/k_g^* is much greater than unity. However the calculated results were claimed to be in very good agreement with the experimental

results for the range $1 < k_s^* / k_g^* < 10^4$. The generalized model proposed by Dietz was dependent on the ratio of thermal conductivities of gas and solid, more than other parameters, like bed geometry, particle size, porosity, etc. and is given as equation (2.16).

$$\frac{k_e}{k_g} = \pi \left(\frac{2\theta_0 k_s}{3k_g} \right)^{1/2} \frac{K_0 \left[\left(\frac{8k_g}{\theta_0 k_s} \right)^{1/2} \right]}{K_1 \left[\left(\frac{8k_g}{\theta_0 k_s} \right)^{1/2} \right]} \tag{2.16}$$

Equation (2.17) is the model extended for metal hydride beds $\left(\theta_0 = \pi / 16 \right)$ with the proposed extension.

$$k_e = 1.14 \sqrt{k_s^* k_g^*} \frac{K_0 \left[\left(\frac{40 k_g^*}{k_s^*} \right)^{0.5} \right]}{K_1 \left[\left(\frac{40 k_g^*}{k_s^*} \right)^{0.5} \right]} \tag{2.17}$$

Compared to models of Yagi-Kunii and Masamune-Smith, this model is very simple, where the relation between ETC of bed and ratio of thermal conductivities of solid and gas is given in form of Bessel functions of zeroth and first orders.

2.4.4 Masamune-Smith model

Masamune-Smith [40] assumed the voids between the solid particles to be pendular. Accordingly they suggested the model for ETC considering three mechanisms of heat transfer to be major contributors in overall heat transfer in a packed bed. According to them, these mechanisms were, heat transfer through contact area between solid particles, heat transfer through fluid, heat transfer through the fluid film present in the voids. The expression suggested by Masamune – Smith is given as equation (2.18) The inclusion of suggested extensions in the original Masamune-Smith model results equation (2.19).

$$k_e = \psi\varphi k_g + \frac{(1-\psi\varphi)(1-\delta)}{\frac{\varepsilon}{k_g^*}+\frac{1-\varepsilon}{k_s}} + (1-\psi\varphi)\delta k_s \qquad (2.18)$$

$$k_e = \psi\varphi k_g + \frac{(1-\psi\varphi)(1-\delta)}{\frac{\zeta}{k_g^*}+\frac{1-\zeta}{k_s^*}} + (1-\psi\varphi)\delta k_s^* \qquad (2.19)$$

where:

$$\psi = 1-\frac{3}{2}\left(\frac{1-\varphi}{\varphi}\right)\zeta$$

$$\zeta = n\left\{(\sec\theta_2 - 1)^2\left[1-\left(\frac{\pi}{2}-\theta_2\right)\tan\theta_2\right]\right\}$$

$$\delta = \left(\frac{1}{1-\lambda\varphi}\right)\frac{k_e^0}{k_s^*} \qquad \theta_2 = \cos^{-1}\left(1-\frac{1}{n}\right) \qquad n = 6.93-5.51\frac{\varphi-0.26}{0.216}$$

2.5 Results and Discussion

The results obtained from the extended models were compared with the experimental results [8]. As elaborated in section 1.5.1, experimental data available in literature clearly show that the variation of ETC of MH packed beds with pressure can be divided into three regimes due to Knudsen effect. This division of regimes is done on the basis of the size of voids (X_e) as compared to the mean free path of hydrogen (l_{mf}). In the first regime, where the pressure is low, (mean free path is much greater than average void size). Hence, the change in pressure does not affect the thermal conductivity of gas and thus there is no change in the effective thermal conductivity of the bed. In the second regime, in the intermediate range of pressure, $l_{mf} \leq X_e$, the increase in pressure results in the decrease in mean free path and thus increasing the rate of collisions between the hydrogen molecules, consequently increasing the thermal conductivity of hydrogen as per kinetic theory of gases. This ultimately results in the increase in ETC of the bed. This increase in thermal conductivity with

pressure occurs up to *break away pressure*, given by equation (2.7). After P_b the thermal conductivity of gas is not dependent on pressure (mean free path is much less than average void size) and thus there is no variation in the ETC with the increase in pressure in this regime. Fig. 2.1 (a) shows the comparison of ETC values predicted by original models and Fig. 2.1 (b) shows the comparison of ETC values predicted by extended models. It is clear from these two figures that while the trend of ETC variation with bed pressure predicted by original models is not conforming with the experimental results, the extended models predicted the trend conforming with the experimental results which shows the modification obtained due to extension of models. The extended versions of Yagi-Kunii [71] and Zehner-Schlunder [72] predicted the values of ETC which are closely matching with the experimental results [8]. The maximum deviations from the experimental results were obtained as 7% for extended Yagi-Kunii model, 16% for extended Zehner-Schlunder model, 25% for extended Masamune-Smith model and 39% for extended Dietz model. The parameter 'B' in Zehner-Schlunder model was found to be almost linearly dependent on porosity after incorporating the variation in porosity effect into the model. Extended Masamune-Smith [40] model was also very close in the lower pressure region while some deviations are observed in the higher pressure region. The reason behind this could be the consideration of pendular voids by Masamune-Smith. In case of MH beds, the geometry of voids cannot be assumed to remain same for all ranges of pressure. The swelling of hydride particles results in variation in the void geometry also. Dietz model [73], while predicting the trend similar to that obtained in experimental results [8], under-predicted the ETC values throughout the pressure range. Dietz has suggested contact between particles to be point contact and also has fixed the geometry of bed and arrangement of particles in the bed. Moreover variation in porosity due to hydrogen absorption could not be incorporated into this model as the model did not suggest the ETC to be directly dependent on porosity of

bed. The hydrogen concentration in MH beds plays a critical role on the ETC of the bed. As the hydrogen concentration increases, the size of the particles increases due to swelling, thereby increasing the packing density and decreasing the porosity of bed. Consequently conduction heat transfer through solid particles increases with increase in hydrogen concentration. But hydrogen absorption in the MH molecules causes disturbance in the electronic configuration of particles, thus decreasing the solid thermal conductivity [8].

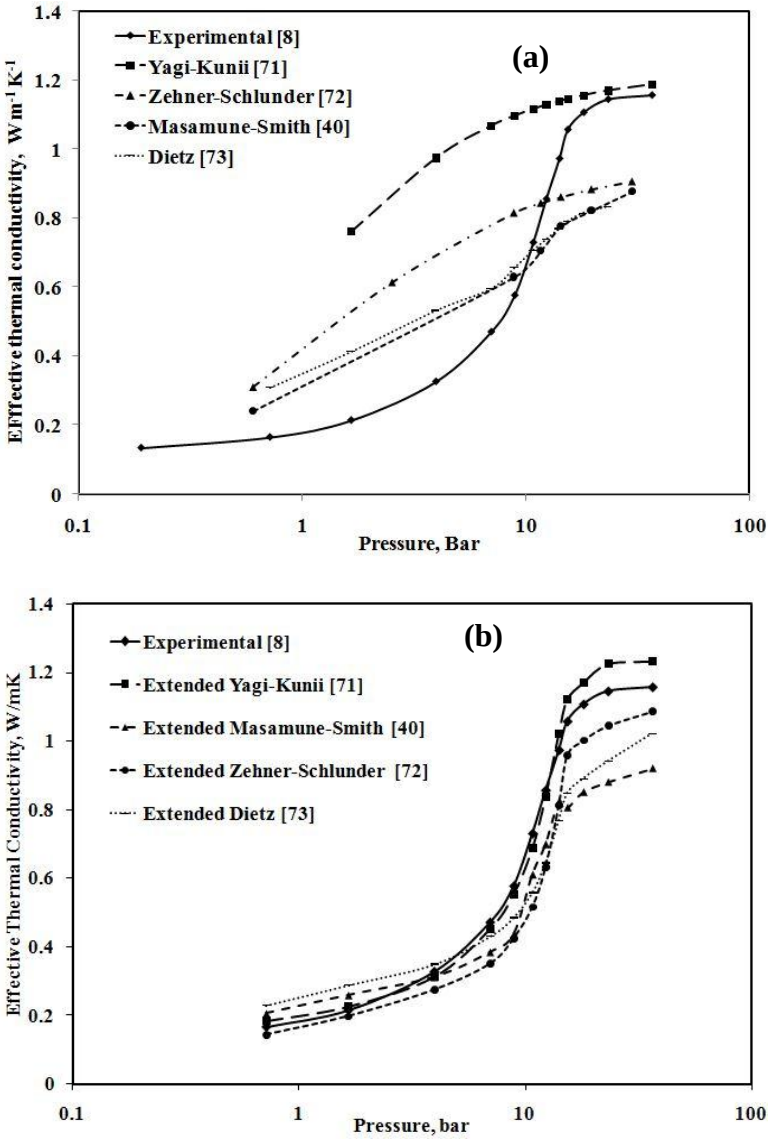

Fig. 2.1 Comparison of models for variation of ETC with pressure at average bed temperature of 60^{O}C
(a) for original models (b) for extended models

The former effect dominates the later, thus the ETC of MH bed increases with hydrogen concentration.

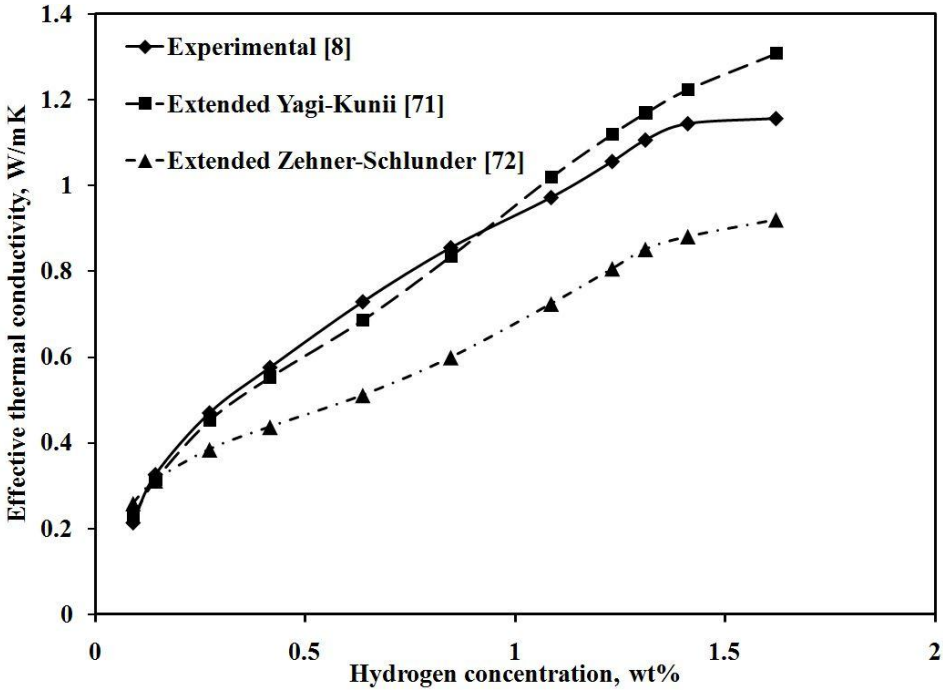

Fig. 2.2 Comparison of models for variation of ETC with hydrogen concentration at average bed temperature of 60^{O}C

The simulation results using Zehner-Schlunder and, Yagi and Kunii models are appropriately conforming the experimental results for the variation of ETC with hydrogen concentration as shown in Fig. 2.2. From literature, the effect of temperature on ETC of MH packed beds is unclear. While some of the researchers have reported increase in ETC with temperature for certain metal hydrides, others have reported the opposite. The probable reason for the decrease in ETC with increase in temperature can be that the decrease in solid thermal conductivity might be dominating over the increase in gas thermal conductivity. Also, at a particular pressure, since the solid thermal conductivity variation with temperature is dependent on the hydrogen concentration, a clear variation of ETC with temperature cannot be concluded.

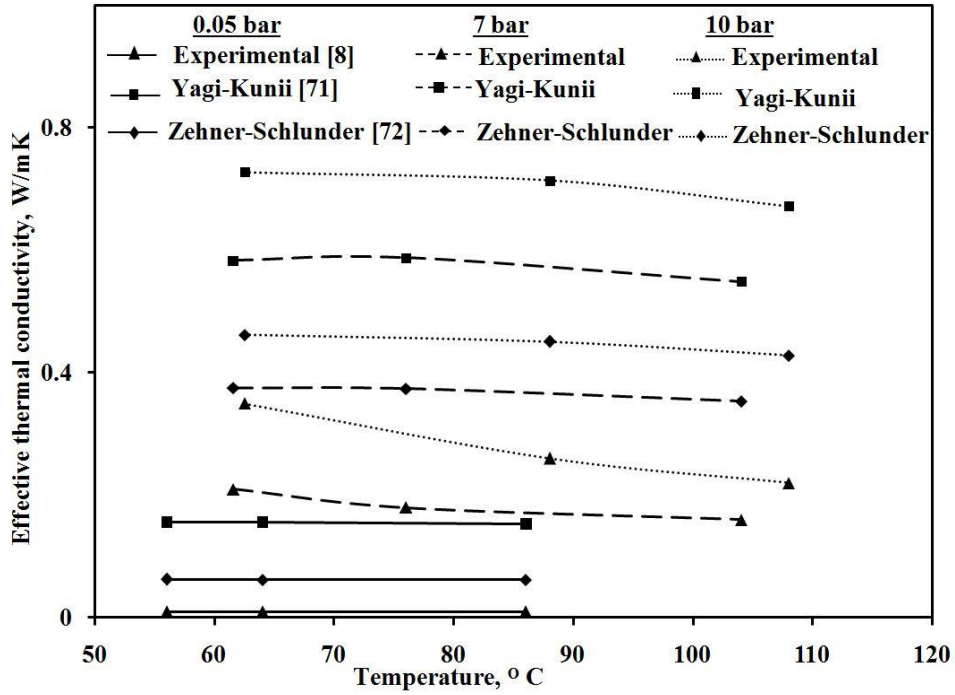

Fig. 2.3 Comparison of models for variation of ETC with temperature

The effect of temperature is also considered in the above models as can be seen in Fig. 2.3, which shows the variation of ETC with temperature for different pressures. The change in temperature is seldom showing any change in ETC at low pressures. But as the pressure is increased, ETC is seen to be decreasing with the increase in temperature. The increase in bed temperature results in increase in thermal conductivity of gas and decrease in the thermal conductivity of solid particles as hydrogen concentration decreases. The decrease in ETC of bed with increase in temperature suggests that later effect is dominating in the high pressure region. In the simulation results, the variation of ETC values with temperature is for average bed temperature. These ETC values are simultaneously dependent on temperature, pressure, hydrogen concentration and bed porosity. It can be seen from PCI diagrams [8] that the values of hydrogen concentration corresponding to a particular pressure are different for different temperatures. The values of hydrogen concentration used in the present simulation are taken from the PCI diagrams. The PCI characterisation was done in a different experiment and with a different reactor. The reactor

used for PCI measurement was smaller in size and hence it was easily maintained at a particular temperature. The hydrogen concentration value corresponding to a particular pressure, when the whole bed is maintained at the same temperature (say 'T'), may be different from the hydrogen concentration value when the bed is large and the temperature gradient exist within the bed (and the *average* bed temperature is 'T'). The significant difference between the variation of ETC values with temperature from various models and experimental results may be because of probability of difference in the hydrogen concentration values in simulation and experimentation. Bed porosity is an important parameter influencing the ETC of MH bed. In case of MH bed since the porosity is assumed to decrease with the increase in hydrogen concentration of the bed (refer to eq. (2.4)), the ETC must show the inverse trend with variation of bed porosity to that with variation of hydrogen concentration. This is verified from Figs. 2.2 and 2.4. Fig. 2.4 shows the variation of ETC with bed porosity as predicted by the four extended mathematical models.

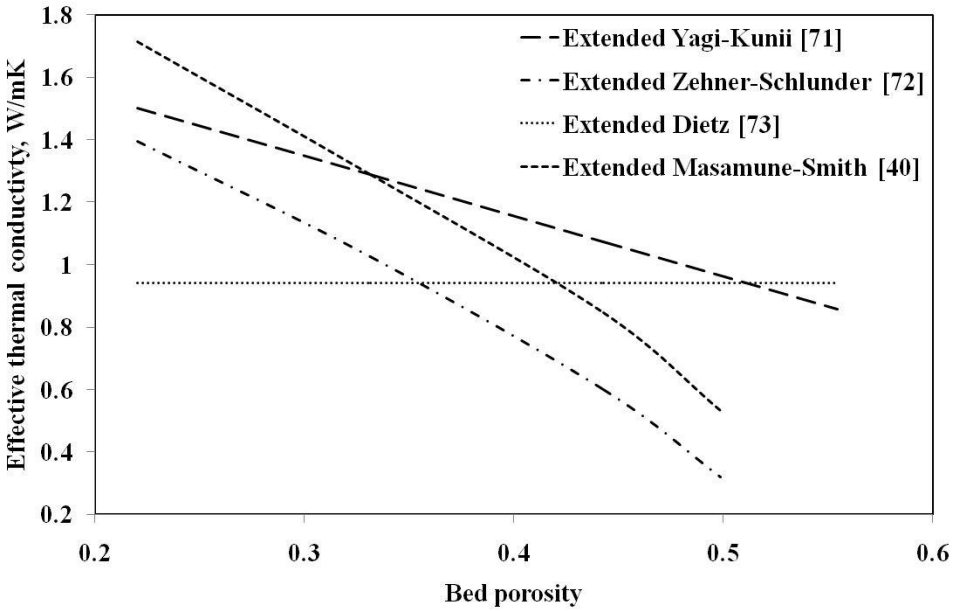

Fig. 2.4 Comparison of models for variation of ETC with bed porosity

As is clear from the figure, among the four models, the extended Dietz model is unable to predict the variation of ETC with bed porosity. This

was very much expected as Dietz [73] had not considered any direct relation between the bed porosity and ETC of packed bed and hence extended Dietz model (eq. (2.12)) also could not show variation of ETC with bed porosity. Other three models are quite satisfactorily verifying the fact that variation of ETC with bed porosity should be opposite to that with hydrogen concentration.

Figs. 2.5 and 2.6 show the variation of ETC with solid conductivity and packing density respectively at moderate pressure (about 22 bar) and temperature (333 K). With the increase in solid conductivity, it is obvious that the ETC will increase as the gas conductivity has dominating effect only in certain pressure ranges by the virtue of Knudsen effect. In the remaining parts of hydrogenation/dehydrogenation curve, the solid conductivity dominates the ETC.

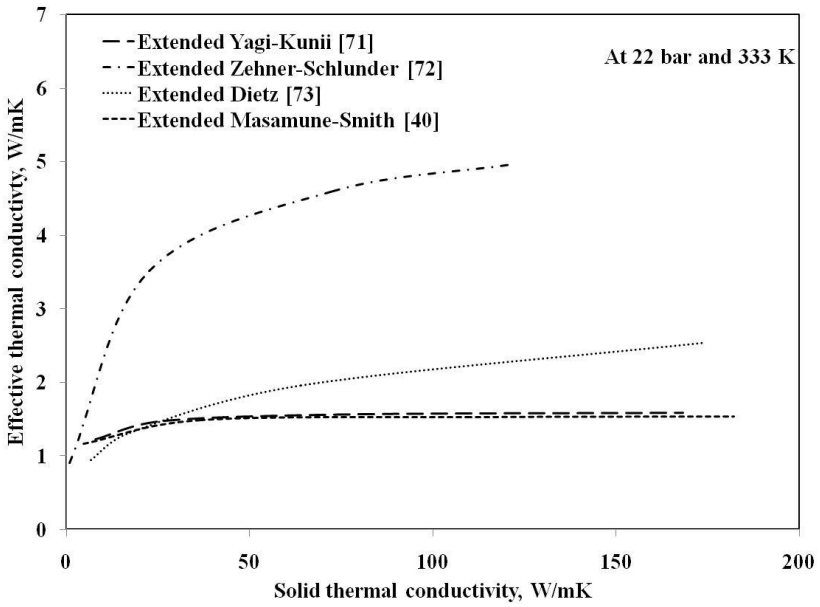

Fig. 2.5 Comparison of models for variation of ETC with solid thermal conductivity

Hence the increase in solid thermal conductivity causes the increase in ETC in most of the regions as shown in Fig. 2.5. Whereas extended Dietz model and extended Zehner Schlunder model are correctly showing the gradually decreasing effect of increase in solid thermal conductivity on the

ETC of the bed, the other two models, viz., extended Yagi-Kunii and extended Masamune-Smith are showing very little effect of increase of solid thermal conductivity on the ETC of the bed and that too up to a very short limit. This is due to the different forms of dependence of ETC on solid thermal conductivity given by different models.

Packing density of the packed bed has significant influence on the rate of heat transfer. As with the increase in packing density, the particle to particle contact and hence the heat conduction through the solid has to increase. This fact is confirmed with the trend obtained in Fig. 2.6 for the variation of ETC with packing density.

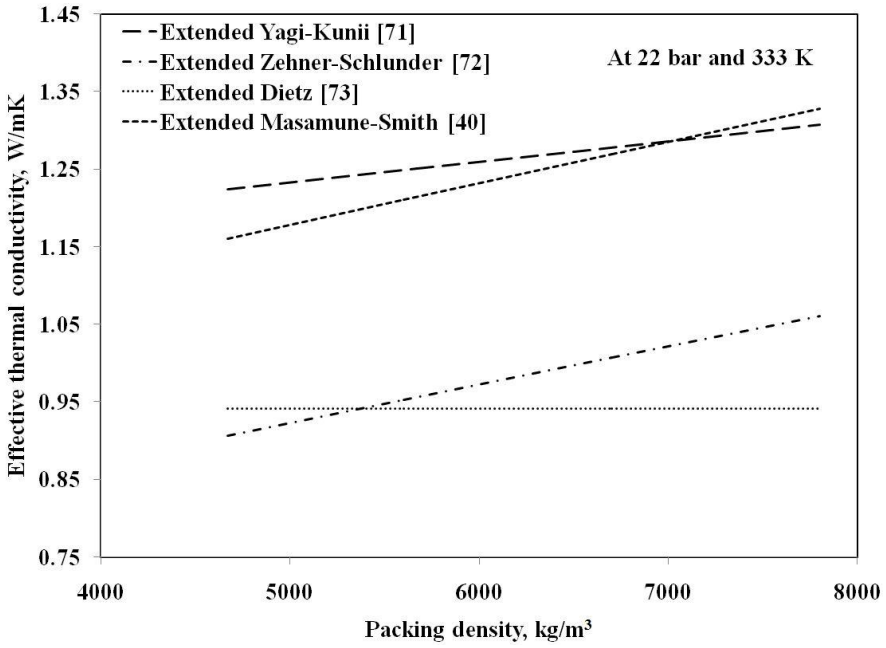

Fig. 2.6 Comparison of models for variation of ETC with bed packing density

Similar to variation of ETC with bed porosity, the extended Dietz model is not predicting the variation of ETC in this case also. All other models are predicting nearly linear variation of ETC of the bed with the initial packing density as shown in Fig. 2.6.

Closure

Four well known mathematical models developed for estimation of ETC of conventional non-reactive packed beds are extended to take into account the effects of hydrogenation on the ETC of MH beds. Hydrogenation results in a number of changes like variation in particle size, packing density, ETC (when compared with beds with non-reactive gases), void fraction etc. These effects were included in the mathematical models to obtain the extended models. The extended models consider effective thermal conductivity of solid to vary linearly with hydrogen concentration, while the variation in thermal conductivity of hydrogen is negligible. The variation in void fraction with hydrogen concentration plays a crucial role in the calculation of ETC of MH beds. The extended models of Yagi-Kunii and Zehner-Schlunder predicted ETC which closely match with experimental results for $MmNi_{4.5}Al_{0.5}$ hydride over a wide range of operating parameters and thus were able to account for the changes resulting due to hydrogenation. The detailed conclusion drawn from this mathematical analysis is given in Chapter-5.

Chapter 3

Measurement and Augmentation of Effective Thermal Conductivity of Metal Hydride Beds

The previous chapter provides an overview of simulation of ETC of metal hydride packed beds using extended mathematical models. The details of ETC measurement and augmentation techniques are discussed in this chapter. Two materials $La_{0.8}Ce_{0.2}Ni_5$ hydride and Mg + 50 wt% $LaNi_{4.6}Al_{0.4}$ hydride, which are suitable for the development of metal hydride based hydrogen compressor and energy storage system are used in the present study. The two materials $La_{0.8}Ce_{0.2}Ni_5$ and $LaNi_{4.6}Al_{0.4}$ were purchased from Lab Tech, Bulgaria in powder form. Mg is procured in powder form (particle size <300 microns) from Sigma Aldrich. An ETC cell was fabricated using one dimensional steady state radial heat transfer absolute method. Two types of pellets, with and without copper wire mesh, were fabricated by mixing metal alloy powder and graphite flakes. ETC of three types of beds, with lose metal alloy powder and two types of pellets, were measured at different operating conditions. The synthesis and characterisation of the composite, construction of ETC cell and experimental set up, fabrication of pellets, experimental procedure and results obtained from ETC measurement are discussed in the following sections.

3.1 Synthesis and Characterization of Mg + 50 wt% $LaNi_{4.6}Al_{0.4}$ Composite

Blended powders of magnesium (purity 99.8%, average particle size of 300 microns) and $LaNi_{4.6}Al_{0.4}$ (average particle size of 80 microns) in equal proportion, were subjected to planetary ball milling under wet milling conditions (toluene) with 6 mm diameter stainless steel balls and

stainless steel vials. The ball to powder ratio was maintained at 15:1. The milling speed was kept at 250 rpm for a period of 15 h. The quantity of powder used for each run was 150 g. The loading and unloading of powder was carried out in a glove box under argon atmosphere. The powders were characterized for identification of phase content by x-ray diffraction in a Rigaku smartlab XRD machine using Cu Kα radiation. The scan rate for XRD was kept as 1 s per step of 0.02º (2θ) and the range of all the measurements were restricted to 20 - 80º (2θ). Fig. 3.1 shows the XRD pattern for Mg, $LaNi_{4.6}Al_{0.4}$ and Mg + 50 wt% $LaNi_{4.6}Al_{0.4}$. The XRD pattern for the composite Mg + 50 wt% $LaNi_{4.6}Al_{0.4}$ showed Mg and $LaNi_5$ peaks. It confirms that in casting, no formation of intermediate phases took place. The XRD pattern indicated induced strain due to milling.

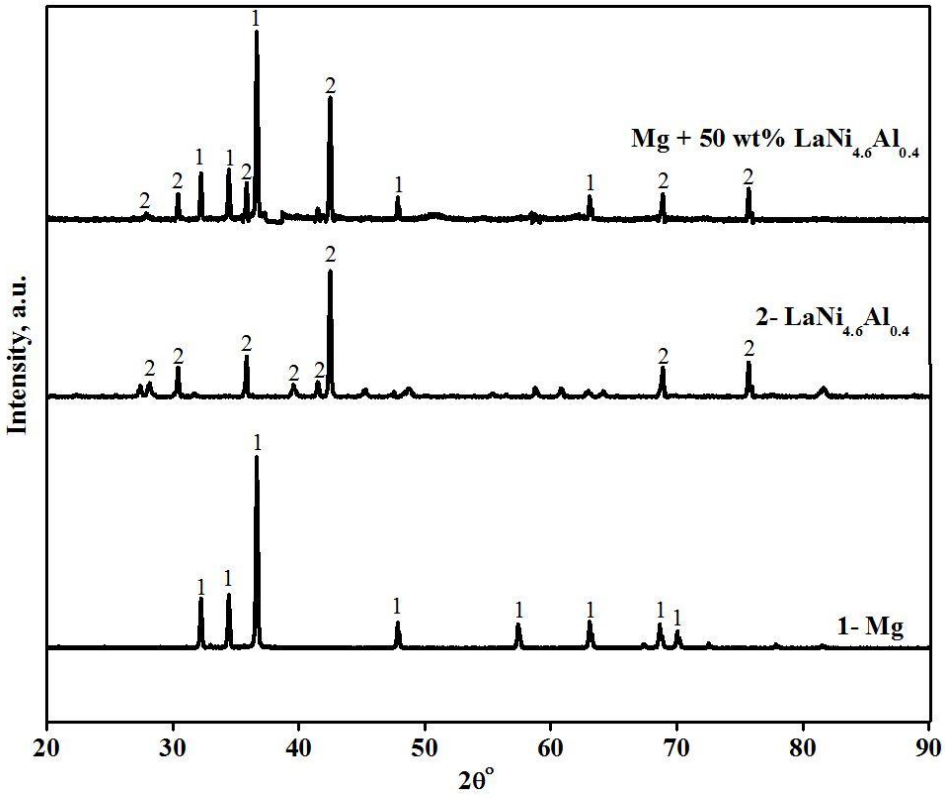

Fig. 3.1 XRD patterns for Mg, $LaNi_{4.6}Al_{0.4}$ and Mg + 50 wt% $LaNi_{4.6}Al_{0.4}$

3.2 Experimental Details

In this work one dimensional, steady state, radial heat transfer, absolute method was used for ETC measurement. Temperature profile prevailing in the MH bed is measured with 'K' type thermocouples with probe of 1 mm diameter. The steady state method is time consuming and some loss in accuracy is seen due to non-fulfillment of assumption of homogeneous beds caused by the presence of thermocouples within the bed [31]. In the present case, the thermocouple probes (each of 1 mm diameter and 2.04 cm^2 surface area) have occupied only 0.2% of bed volume. Therefore the problem of loss in homogeneity was negligible. Taking this into consideration, steady state method becomes more accurate and reliable than transient methods of ETC measurement and hence was chosen for the present study.

3.2.1 ETC cell

Fig. 3.2 shows the schematic diagram of ETC cell. The ETC cell was a cylinder made up of SS 316 and was designed and fabricated to attain the required conditions of one dimensional, steady state, radial heat transfer. For achieving unidirectional radial heat transfer the aspect ratio (L/D) of the reactor was kept as 4.33:1. To ascertain steady-state heat transfer two constant temperatures (at heat source and heat sink) were maintained at the inner and outer radii of the hollow cylindrical MH bed. The MH bed in powder form (1) assumed a hollow cylindrical shape with a capsule heater (2) of 10 mm diameter, 130 mm length and 60 W rated capacity, at the inner radius and enveloped by the inner surface of high pressure cylinder (3) of 30 mm inner diameter, 38 mm outer diameter and 170 mm height, at the outer radius. Coolant jacket (4) has an annular volume between the outer surface of high pressure cylinder and inner wall of another cylinder of 45 mm inner diameter, 49 mm outer diameter and 170 mm length. Suitable fittings were provided to this cylinder for coolant inlet (5) and

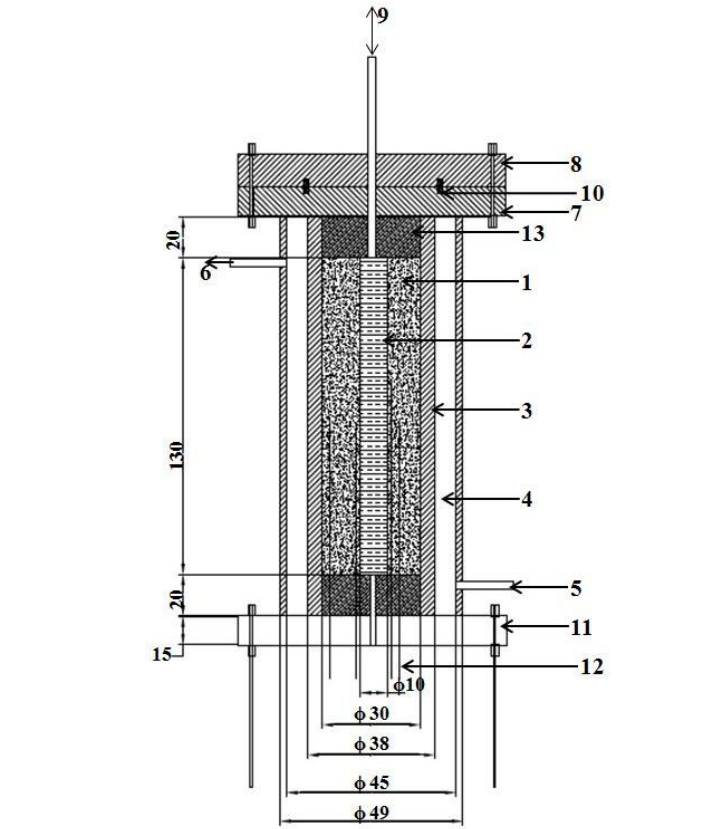

1- MH powder; 2- Capsule heater; 3- High pressure cylinder;
4- Coolant jacket; 5- Coolant inlet; 6- Coolant outlet; 7- Top flange;
8- Lid; 9- Gas inlet/outlet; 10- PTFE gasket; 11- Bottom flange;
12- Thermocouple probes; 13- Syndanio sheets
All dimensions in mm

Fig. 3.2 Schematic diagram of ETC cell

Fig. 3.3 Components of ETC cell

outlet (6). Two flanges, one at each end of the cylinders were welded to make this a single assembly. The top flange (7) was made as a hollow disc of 30 mm inner diameter, 120 mm outer diameter and 15 mm thickness. The 30 mm bore was intended to facilitate the filling of material from this end of the cell. A lid (8) of 120 mm diameter and 7 mm thickness was used as the top cover for the ETC cell. It had a hole of quarter inch at its center with a quarter inch tube, fitted to it for gas passage (9) to / from the MH bed. PTFE gasket (10) was fitted into the grooves made in the top flange and lid to assure leak proof sealing of the ETC cell. Six holes of 10 mm diameter were drilled along an appropriate pitch circle diameter on the lid as well as on top flange to fit the lid to the top flange using threaded joint. The lower flange (11) was equipped with a capsule heater (2) and arrangements for leak proof fitting of four probe type thermocouples (12) and connections for one thermocouple junction each brazed on heater surface and inner surface of high pressure cylinder (3). Thus temperatures at five points at different radii and same axial height and at two points at same radius and different axial heights were monitored for measurement of ETC. The temperatures at same radius and different axial heights were monitored to assure that temperature variation in lateral direction was negligible. Arrangement was also made for electrical connection to the capsule heater using an in-house developed high pressure feed-through. The mass of $La_{0.8}Ce_{0.2}Ni_5$ powder, filled in the ETC cell was 310 g, while that in case of composite powder of Mg + 50 wt% $LaNi_{4.6}Al_{0.4}$ was 340 g. The capsule heater of 60 W rated capacity was used as the source for higher temperature. It was fixed coaxially to the MH bed using a PTFE fixture to minimize the heat transfer from heater to the body of the ETC cell. Also the syndanio sheet (a composite made from treated raw asbestos fibers and special grade of cement) was placed between the bottom surface of heater and the lower flange to assure that there was no metallic contact between heater and ETC body. To maintain a constant lower temperature at the outer radius of MH bed, a thermostatic

fluid (Make: Julabo, Model: Thermal H10) was circulated through the coolant jacket at a flow rate of 10 liters per minute. For the circulation and extraction of heat from the thermostatic fluid a thermostatic bath was utilized. The thermostatic bath had the accuracy of maintaining the temperature of coolant within $\pm 0.1^{\circ}C$ at the set temperature. To prevent the heat loss to surroundings through either top lid or lower flange, syndanio (thermal conductivity 0.06 W m^{-1} K^{-1}) sheets (13) were used above and below the $La_{0.8}Ce_{0.2}Ni_5$ powder bed. Fig. 3.3 shows the photograph of components of ETC cell.

3.2.2 Pellets details

Two different types of pellets were developed. First type contained the $La_{0.8}Ce_{0.2}Ni_5$ powder, graphite flakes (Sigma-Aldrich) and tin powder (Source: Sigma Aldrich; Purity: 99.5%). Graphite flakes were used for enhancement of ETC and tin powder was used as binder. Average flake size of the graphite flakes used in this work was 150 μm. For making pellets, the ingots were initially crushed in the mortar and then ground using a cup mill in dry atmosphere. The graphite flakes (6 wt%) and tin powder (1.5 wt%) were then mixed with the alloy/composite powder. The components were mixed thoroughly by dry milling using a *cup mill*. The rings were not used during milling to avoid deterioration of metal alloy powder and graphite flakes. The mixture of alloy/composite, graphite flakes and tin powder was then taken to a pellet die in measured amount and was pressed on a hydraulic press with a pressure of 200 MPa to obtain the pellets. This pressure for compaction was decided on the basis of similar work reported in literature [61, 64, 68]. The die was designed to provide an axial hole of 10.1 mm in the compacts to accommodate the capsule heater. Fig. 3.4 depicts the steps involved in the making of pellets. While the compaction of metal alloy powder considerably decreases the permeability, the addition of ENG flakes results in overcoming this effect along with significant increase in ETC of the bed. The radial dimensions

of the pellets were designed to fit the ETC cell described in the previous section. Hence the pellets were of 29.8 mm outer diameter and 10.1 mm inner diameter. Holes were drilled in the pellets for accommodating the thermocouple probes. Thermal paste having a composition of aluminium oxide suspended in silicon compound, was applied on the thermocouple probes to fill the micro gaps between pellets and different components of ETC cell. In case of second type of pellets copper wire mesh structure was embedded in the graphite flakes and metal powder mixture. The intentions behind including copper wire mesh structure were; to exploit the benefit of high thermal conductivity of copper while keeping the volume fraction occupied by augmentation source to suitably lower values and to provide a set of fins for radial heat transfer enhancement. Table 3.1 provides detailed information about the copper wire mesh used in this work. Dimension wise, both types of pellets were similar. Fig. 3.5 shows both the types of pellets. For measurement of ETC, the pellets were piled one over the other in the ETC cell, with the capsule heater passing through the axial hole of the pellets.

Table 3.2 depicts the packing densities and bed porosities for the three types of beds. To measure the bed porosity following steps were performed: (i) measuring the volume of the empty reactor (in the present case it was 9.18×10^{-5} m^3) (ii) filling the reactor with the metal alloy (either in powder or compact form) (iii) supply of known mass of argon gas to the filled reactor and recording its pressure and temperature (iv) calculation of void volume in the reactor using the mass of argon, pressure and temperature in the reactor. This void volume and the reactor volume is then used for calculation of bed porosity. The bed porosity decreases from 58 % to 34% due to compaction. The packing density increases from 3.79 to 5.47 $g.cm^{-3}$.

Table 3.1 Physical properties of copper wire mesh used for making pellets

Parameter	**Value**
Surface area per unit volume	8333 m^2 m^{-3}
Density	5.6 g cm^{-3}
Thermal conductivity	392 W m^{-1} K^{-1}
Wire diameter	0.12 mm
Purity	99.9%

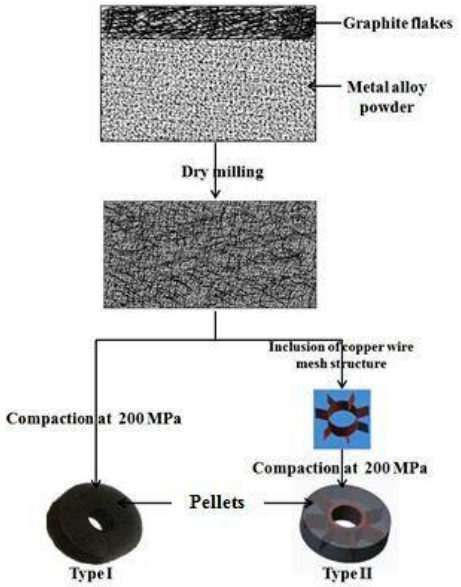

Fig. 3.4 Steps in pellet making

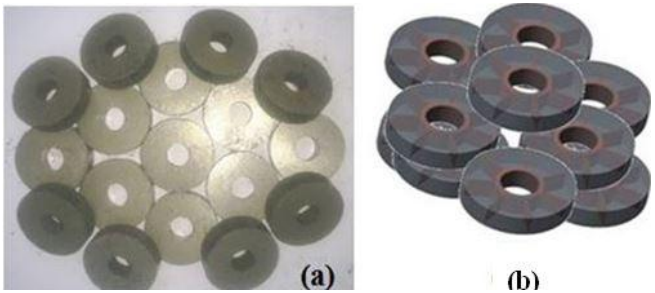

Fig. 3.5 Types of pellets (a) Pellets of metal alloy powder and graphite flakes (b) Pellets with CWM structure

Table 3.2 Packing density and bed porosity of different types of beds

	Packing density ($g.cm^{-3}$)	**Bed porosity (%)**
LMP	3.79	58
CMPGF	4.94	38
CMPGFCu	5.47	34

3.2.3 Experimental set up

In the present work as the intention was not only to evaluate the ETC augmentation achieved through different augmentation techniques but also to evaluate the relative effect of the augmentation technique on the amount of hydrogen absorbed by the metal hydride. To fulfill these intentions, the experimental set-up was designed for activation of metal hydride, quantification of hydrogen absorption / desorption and ETC measurement. Fig. 3.6 shows the schematic diagram of experimental set up used in the present work. Quarter inch seamless SS 316 tubes were used for building the gas flow circuit. These tubes could sustain pressure up to 500 bar. The gas flow in this circuit was controlled through high pressure bellow sealed valves (working pressure up to 172 bar, in the temperature range of -28˚C to 343˚C). Calibrated SS 316 cylinders (2250 ml-1No., 1000 ml-2 No.s) were utilized for supply of hydrogen gas to the ETC cell in metered quantities. One of the two 1000 ml cylinders was used as reference volume while the other two cylinders formed the major part of supply volume. For monitoring hydrogen pressure, piezoresistive type pressure transducers were installed at different locations in the set up. P_1 and P_2 were installed for monitoring the supply pressure and transducer P_3 was used for monitoring the pressure in the ETC cell. The working pressure range for all these pressure transducers was 0 to 100 bar with 0.1% accuracy on full scale. With the aim to minimize the error in the measurement of absorption quantity of hydrogen, a differential pressure transducer DP was used between the reference volume and selected volumes. The operating pressure range of the DP was 0 to 5 bar. 'K' type thermocouples with an accuracy of ± 0.5˚C and time constant of 0.2 s were used at different locations in the hydrogen supply circuit and in the ETC cell to monitor the hydrogen gas temperature as shown in Fig. 3.6. A rotary type vacuum pump was used for evacuating the system as per the requirement. Pirani gauge attached to the vacuum line was utilized for

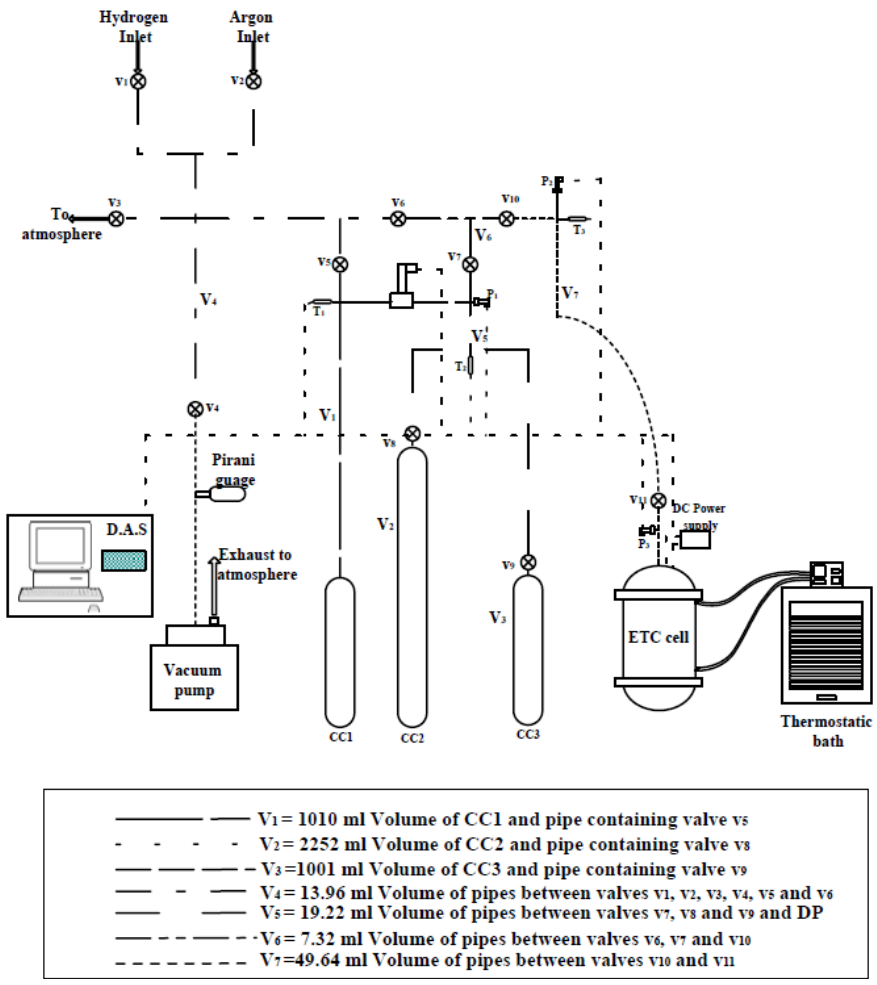

Fig. 3.6 Schematic arrangement for experimental measurement of ETC

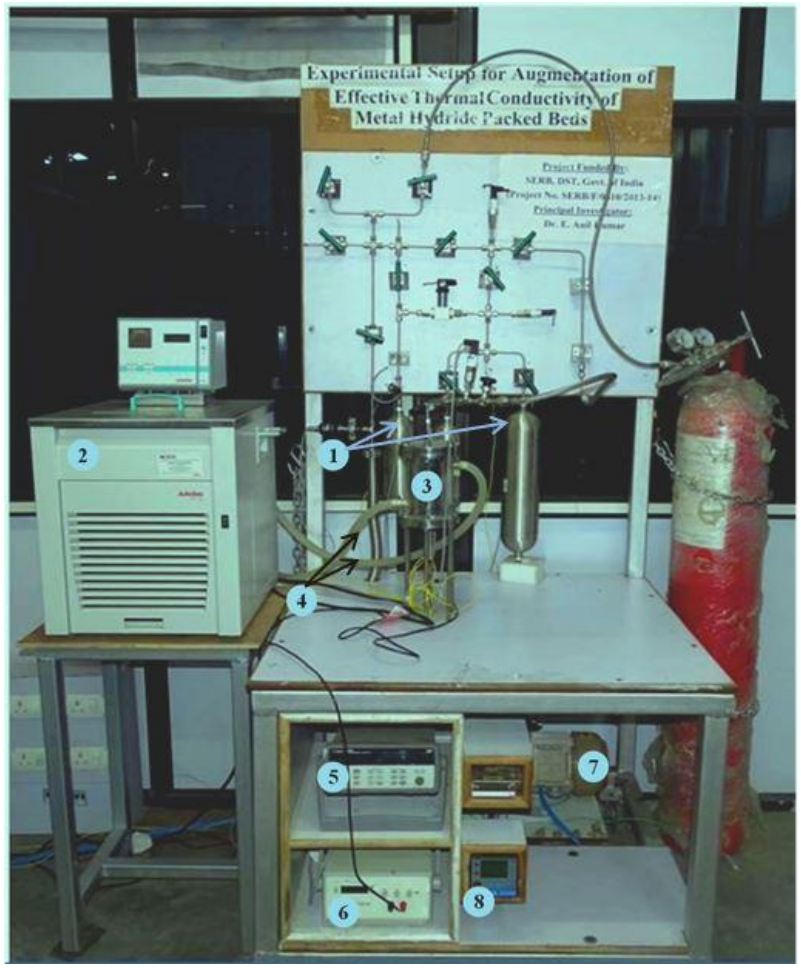

1- Calibrated sample cylinder; 2- Cold/Hot Fluid Circulator; 3- ETC measurement cell; 4- Fluid circulation tubes; 5- Data logger; 6- DC power supply unit; 7- Vacuum pump; 8- Pirani gauge; 9- Vacuum sensor

Fig. 3.7 Experimental set up for ETC measurement

monitoring the vacuum level in the circuit. Computerized data logger system was used for monitoring and recording all the temperatures and pressure data during the experiments. High purity argon (99.999% purity) was used for volume measurement of different parts of the circuit and for leakage tests. The photographic view of experimental set up is shown in Fig. 3.7.

Heat transfer rate **(*Q*)** was calculated from the electrical power supplied to the heater. However to estimate the heat losses along the axial direction, pilot tests were performed using the ETC cell with different test specimens of known thermal conductivity (stainless steel, brass and PTFE) with dimensions, 30 mm outer diameter, 10 mm inner diameter and 130 mm height to resemble the MH bed. Using Fourier's law of heat conduction (Eq. (3.1)), the heat transfer rate was evaluated for the known temperature profile and thermal conductivity data. Tests were performed for different source and sink temperature ranges and different pressures of argon and hydrogen.

3.2.4 ETC measurement of non-activated metal alloy beds

After filling the ETC cell with material, the cell was heated to a temperature of 200ºC and then evacuated for few hours while maintaining the temperature. This was done to remove moisture and foreign gases present in the cell. The ETC was then measured under vacuum and different argon pressures for this configuration of bed when the metal alloy / composite was not converted to hydride.

3.2.5 Volume measurements

The experimental setup was divided into eight volumes as shown in Fig. 3.6. All the volumes were determined using a cylinder of known volume. Volumes are determined based on isothermal expansion of an ideal gas from known volume at room temperature and low pressure. Volumes V_1 to V_7 are fixed and were measured during the fabrication of experimental

setup. Volume of the free space in the ETC cell up to v_{11} (V_8) was determined each and every time the ETC cell was connected, as the volume may change due to change in quantity of material filled and length of connecting pipe. The calculated volumes are given in Fig. 3.6.

3.2.6 Activation of alloy samples

Despite the efforts made to keep the metal alloy/composite powder unaffected from moisture and other gases in the environment, it could not be assured that at the time of filling the metal alloy/composite powder into the reactor the powder sample was free of moisture and other gaseous substances. To remove these infiltrations from the metal alloy/composite powder sample, activation of samples was must.

The process of activation for $La_{0.8}Ce_{0.2}Ni_5$ comprises of four steps; 1. Degassing of the sample at 10^{-3} mbar and activation temperature (80˚C, in the present case) for several hours, 2. Exposure of sample to hydrogen at activation temperature and pressure (60 bar, in this case) for one hour, 3. Sample allowed to cool to 20˚C and held in that state for 5 hours, 4. Bringing the sample to activation temperature to desorb the hydrogen. Steps 1 to 4 are repeated in sequence till the sample reaches its maximum hydrogen absorption capacity. Fifteen such cycles were performed for the complete activation of the $La_{0.8}Ce_{0.2}Ni_5$ in the present case.

To activate Mg + 50 wt% $LaNi_{4.6}Al_{0.4}$ the bed was evacuated for around 2 h, then was exposed to hydrogen at 10 bar at 400ºC for another 10 h. Then bed was again evacuated for 2 h at the same temperature. At this temperature, the bed was exposed to hydrogen at 10 bar for 10 h. Five such cycles of hydrogenation and evacuation were followed to make the composite activated.

3.2.7 ETC measurement of metal hydride beds

The ETC estimation experiment comprised following steps (Refer Fig. 3.6):

1. Evacuation of entire setup to 10^{-3} mbar pressure by opening all valves except v_1, v_2 and v_3.

2. The temperature of coolant was set to a fixed value and coolant circulation is started.

3. Power was supplied to the capsule heater through a DC power supply unit.

4. All the thermocouples readings were monitored in the ETC cell in intervals of 15 minutes till the steady state is reached.

5. Temperatures T_4 to T_{11} were recorded after attaining steady state.

6. The ETC value for the MH bed at vacuum was estimated using equation (3.1) as:

$$ETC = \frac{Q}{2\pi L\left(dT/d\ln r\right)} \qquad (3.1)$$

7. Valves v_4 and v_{11} were closed and hydrogen was supplied to volumes V_2, V_3, V_4, V_5, V_6 and V_7 to a predetermined incremental pressure by opening valve v_1. After reaching steady state, valve v_1 was closed and initial pressures in the volumes V_2, V_3, V_4, V_5, V_6 and V_7 were recorded.

8. Valve v_{11} was opened to allow hydrogen to the ETC cell. The final pressure values after attaining steady state were recorded. The amount of hydrogen absorbed by the $La_{0.8}Ce_{0.2}Ni_5$ hydride powder

was calculated by mass balance on the basis of drop in hydrogen pressure in the supply volumes.

9. Steps 2 to 8 are repeated to estimate the value of ETC corresponding to different hydrogen concentration, pressure and average bed temperatures. The same procedure was adopted for measurement of ETC in case of pellets also.

Effective thermal conductivity of metal hydride beds is generally in the range of 0.1-1.2 W m^{-1} K^{-1}. This leads to poor heat transmission characteristics of hydride beds. For better hydrogen sorption characteristics and more importantly for efficient working of metal hydride based heat exchanging systems the value of ETC must be improved. Several augmentation techniques have been tried with different levels of successes as discussed in chapter 1. Based on the literature, compaction and pelletization technique was adopted for ETC augmentation of metal hydride beds. Two types of pellets were fabricated with $La_{0.8}Ce_{0.2}Ni_5$ and Mg + 50 wt% $LaNi_{4.6}Al_{0.4}$. First type was made by mixing 6 wt% graphite flakes with metal alloy / composite powder while the second type had a three dimensional structure made with copper wire mesh embedded to it in addition to the constituents of first type. The effective thermal conductivity of the three types of beds namely, loose metal powder bed (LMP), bed of pellets of metal alloy / composite powder mixed with graphite flakes (PMPGF) and bed of pellets of metal alloy / composite powder mixed with graphite flakes and embedded with copper wire mesh structure (PMPGFCu) were measured and compared at different hydrogen pressures and concentrations and average bed temperatures. The level of ETC augmentation achieved by different types of pellets for both the materials are studied and compared.

3.3 Results and Discussion

Effective thermal conductivities of three configurations of beds of $La_{0.8}Ce_{0.2}Ni_5$ and Mg + 50 wt% $LaNi_{4.6}Al_{0.4}$ hydrides were measured at various pressures, temperatures, and hydrogen concentrations in the range of 0 – 70 bar, 0 – 100ºC and 0 – 1.45 wt% for $La_{0.8}Ce_{0.2}Ni_5$ and 0 – 70 bar, 120 – 190ºC and 0 – 3.7 wt% for Mg + 50 wt% $LaNi_{4.6}Al_{0.4}$ respectively. As discussed in section 1.5, these operating parameters are known to significantly influence the effective thermal conductivity of metal hydride beds. In the present study, the influence of each parameter on the effective thermal conductivity, the level of augmentation achieved by the two augmentation techniques and the effect of ETC augmentation on hydrogen absorption quantity have been analyzed in detail and the outcomes are discussed in the following sections.

A common phenomenon that can be observed in the graphs from Fig. 3.8 to Fig. 3.14 is that, for the same set of operating parameters, the ETC values obtained with PMPGFCu is around 1.5 times of PMPGF and 6 times of LMP bed for both the materials, thus clearly showing the level of augmentation of ETC achieved by different types of pellets.

3.3.1 Effect of pressure

In case of metal hydride beds hydrogen concentration varies with the hydrogen pressure (at a particular temperature) and to determine the effect of gas pressure (separately), experiments were conducted for non-activated metal alloy/composite bed. Argon, being an inert gas, was used as filling gas. Figs. 3.8 (a) and 3.8 (b) show the effect of variation of gas pressure on effective thermal conductivity of packed bed of $La_{0.8}Ce_{0.2}Ni_5$ and Mg + 50 wt% $LaNi_{4.6}Al_{0.4}$ respectively. To evaluate the effect of gas thermal conductivity on the ETC of the bed, initially the ETC was measured for the non- hydrogenated bed of metal alloy / composite. As shown in Figs. 3.8 (a) and 3.8 (b), the variation of ETC with pressure

forms a tilted ‘S’ shaped curve. The curve can be divided into three regimes depending on the range of pressure. For low pressure region (from 0.001 to 1.5 bar), the gas pressure does not show any effect on the thermal conductivity of gas and consequently the ETC of bed remains almost constant in this region. In this region the density of the gas is low in the voids of the bed. Therefore the mean free path of the gas molecule is large compared to the void size, which is assumed to be equivalent to the average particle size of the bed. However, with the increase in gas pressure (from 1.5 bar to around 40 bar), the density of the gas in the pores increases due to which the mean free path decreases. When it approaches the size of the voids, collision of gas molecules is high resulting in higher gas conductivity, consequently resulting in a drastic increase in ETC. This trend continues till the pressure value reaches break away pressure [8]. When the pressure reaches break away pressure of corresponding gas, the mean free path of the gas molecules becomes much lower than the effective size of the voids. In this region, the process of heat transfer by the gas is similar to that in an infinite space and does not influence the conductivity of the gas. Thus for gas pressures beyond break away pressure, ETC remains nearly constant. Similar to the powder beds, the pellets beds also shown the variation in ETC with respect to gas pressure in the form of a tilted ‘S’ shaped curve. The effect of augmentation techniques is clearly visible in the relative increment in the value of ETC in this regime. The increase in ETC in this region for LMP/PMPGF/PMPGFCu was recorded to be 102% / 120% / 140% respectively for $La_{0.8}Ce_{0.2}Ni_5$ while it was 70% / 112% / 116% respectively for Mg + 50 wt% $LaNi_{4.6}Al_{0.4}$. The huge difference in increase in ETC in case of pellets beds and that in case of powder bed suggests that the effect of gas pressure is further amplified due to implementation of augmentation techniques. There is a considerable difference in the increase in ETC values in the cases of PMHGF and PMHGFCu which demonstrates the effect of inclusion of copper wire

mesh structure. The effect of variation in pressure is supplemented with other effects when the gas in the bed is hydrogen instead of non-reactive gas, because with exposure to hydrogen, the metal alloy/composite particles react with it to form metal hydride. There is a swelling effect due to hydrogenation of particles changes causing decrease in contact resistance. Thus although the change in pressure has no direct effect on thermal conductivity of solid but due to metal alloy/composite – hydrogen interaction, the ETC amplifies for the same pressure as compared to that with argon (an inert gas).

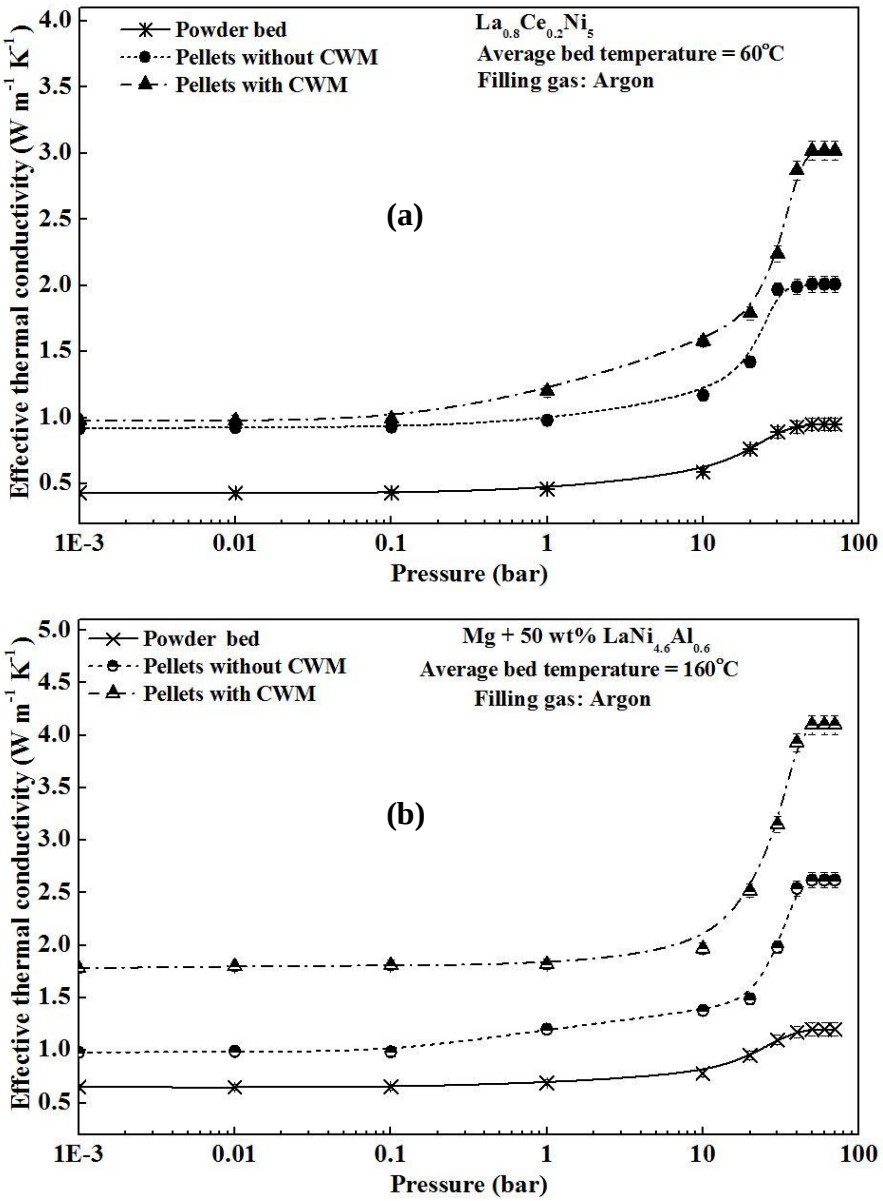

Fig. 3.8 Variation of ETC with pressure with argon as filling gas (a) for $La_{0.8}Ce_{0.2}Ni_5$ (b) for Mg + 50 wt% $LaNi_{4.6}Al_{0.4}$

Figs. 3.9 (a) and 3.9 (b) show the variation of ETC with pressure when the filling gas is hydrogen for $La_{0.8}Ce_{0.2}Ni_5$ and Mg + 50 wt% $LaNi_{4.6}Al_{0.4}$ respectively.

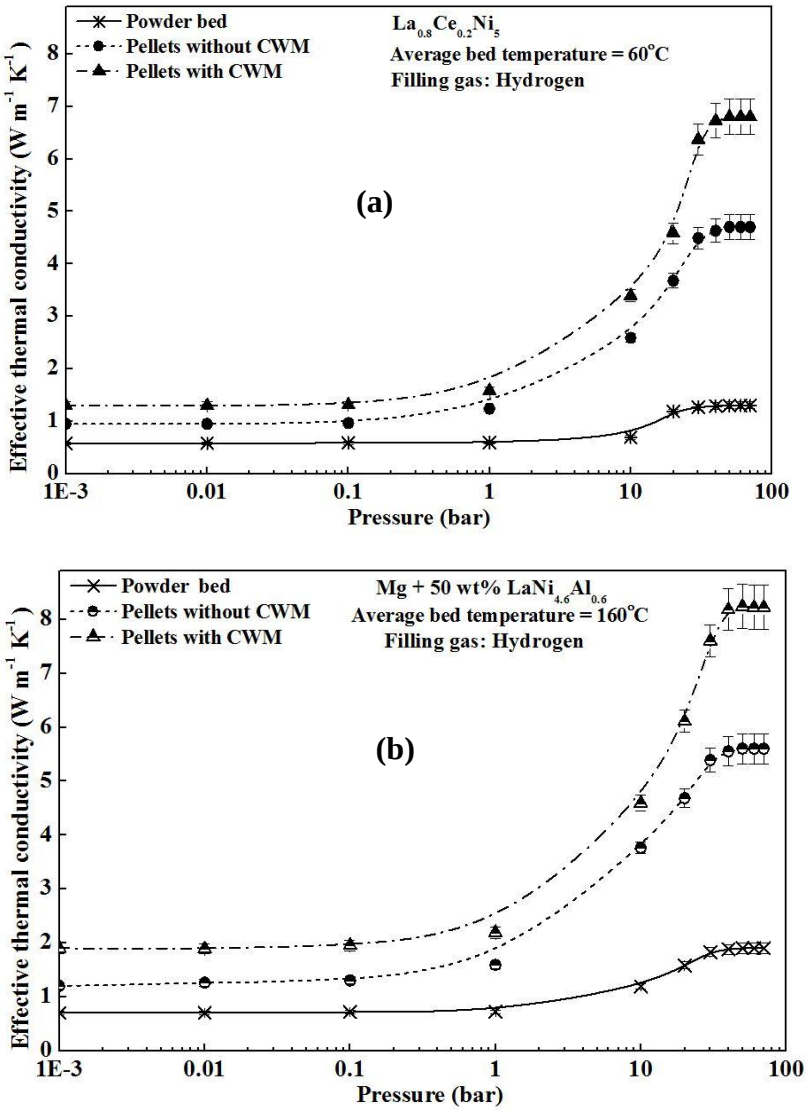

Fig. 3.9 Variation of ETC with pressure with hydrogen as filling gas (a) for $La_{0.8}Ce_{0.2}Ni_5$ (b) for Mg + 50 wt% $LaNi_{4.6}Al_{0.4}$

The trends of ETC variation in the intermediate regime were similar (but larger) to that of argon as filling gas verifying the explanation given for the case of argon. The trend of variation of ETC with pressure was same for all the types of beds as the betterment in heat transfer characteristics will not have any effect on gas characteristics. The increase in ETC value

for LMP/PMPGF/PMPGFCu in this case was 120% / 273% / 326% for $La_{0.8}Ce_{0.2}Ni_5$ hydride while this was 160% / 250% / 275% for Mg + 50 wt% $LaNi_{4.6}Al_{0.4}$ hydride.

3.3.2 Effect of hydrogen concentration

The effect of hydrogen concentration on ETC can be seen as the net effect of the following four phenomena: 1.The reaction between metal alloy / composite particles and hydrogen causes swelling of solid particles and thus increasing contact area between particles which ultimately results in increase in ETC of bed. 2. The increase in hydrogen concentration involves increase in hydrogen pressure thus the effect of increase in pressure gets involved in the effect of hydrogen concentration on ETC. 3. The swelling of solid particles causes increase in contact area between the particles, thereby decreasing the contact resistance between the particles. 4. As the hydrogen atoms get embedded to solid particles, the electronic configurations of solid particles changes.

The comparative consequences of hydrogen concentration variation on ETC of metal hydride beds of different types are shown in Figs 3.10 (a) and 3.10 (b) respectively for $La_{0.8}Ce_{0.2}Ni_5$ and Mg + 50 wt% $LaNi_{4.6}Al_{0.4}$ hydrides. Again the enhancement in heat transfer characteristics resulting from augmentation techniques can be seen from the significant difference between the ETC values of powder bed and those of pellet beds for almost the same hydrogen concentrations. For the same temperature and pressure conditions, hydrogen concentration (in wt%) : ETC (in W m^{-1} K^{-1}) for LMP/PMPGF/PMPGFCu were observed to be 0.8 : 1.22 / 0.76 : 4.39 / 0.78 : 5.67 for $La_{0.8}Ce_{0.2}Ni_5$. and 3.25 : 1.83 / 3.12 : 5.26 / 3 : 7.62 for Mg + 50 wt% $LaNi_{4.6}Al_{0.4}$. The values of hydrogen concentration clearly suggest that although there were significant enhancements in the ETC values with augmentation techniques, the decreases in quantities of hydrogen absorption were nominal. Figs. 3.11 (a) and 3.11 (b) show the variation of ETC with pressure during hydrogen absorption and desorption

processes for powder beds of $La_{0.8}Ce_{0.2}Ni_5$ and Mg + 50 wt% $LaNi_{4.6}Al_{0.4}$ hydrides respectively.

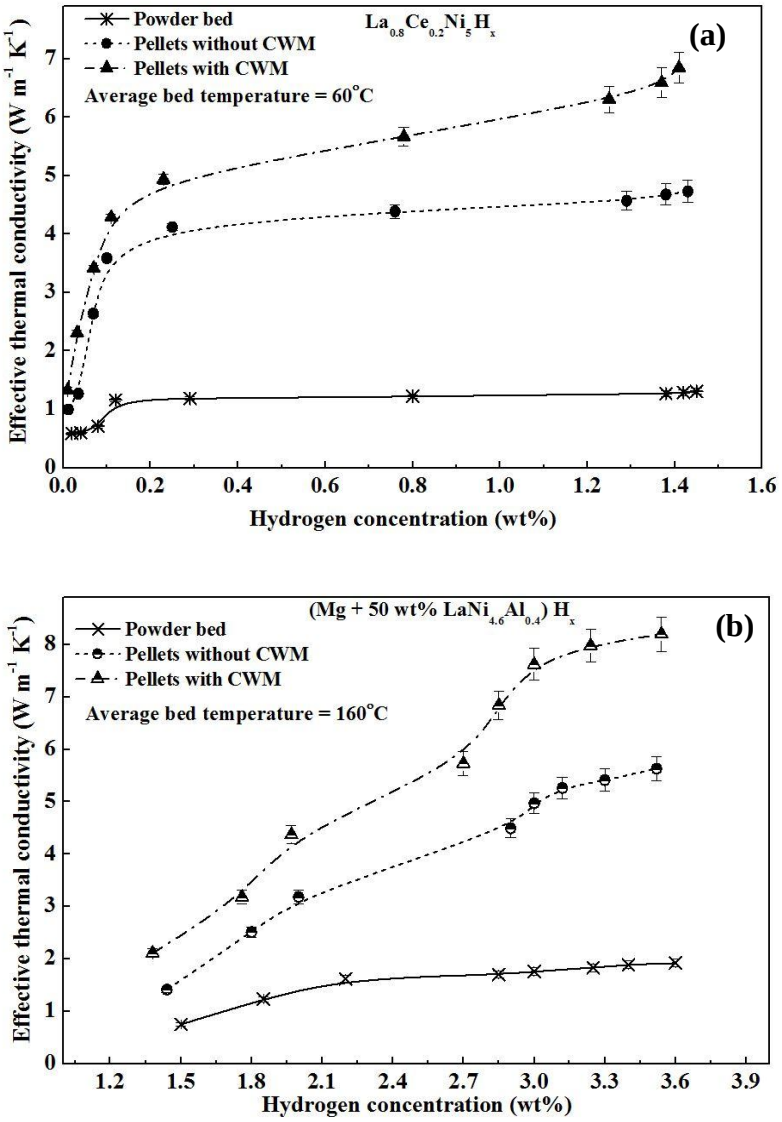

Fig. 3.10 Variation of ETC with hydrogen concentration
(a) for $La_{0.8}Ce_{0.2}Ni_5H_x$ (b) for (Mg + 50 wt% $LaNi_{4.6}Al_{0.4}$)H_x

As shown in figures, the ETC during desorption is marginally more than that during absorption at a particular pressure. This can be explained with the help of PCI characteristics. At a given pressure the concentration of hydrogen in metal hydride is slightly higher in case of desorption curve compared to absorption curve due to hysteresis. Due to the higher

concentration ETC value during desorption is slightly higher than that for absorption.

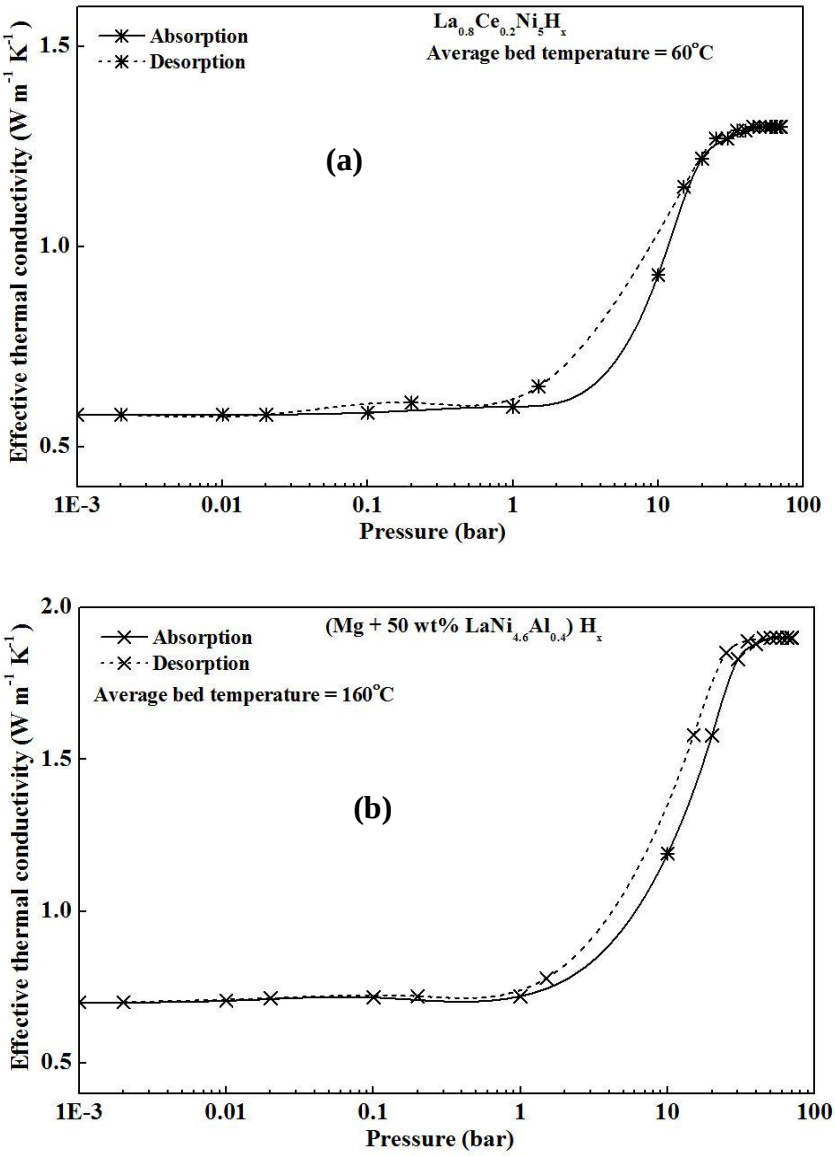

Fig. 3.11 Variation of ETC with pressure during hydrogen absorption and desorption; (a) for $La_{0.8}Ce_{0.2}Ni_5H_x$ (b) for (Mg + 50 wt% $LaNi_{4.6}Al_{0.4}$) H_x

3.3.3 Effect of temperature

Temperature variation is reported to have different types of effects on ETC in different studies [8, 18, 23, 26]. With an increase in temperature, radiation heat transfer comes into play. In addition, the thermal conductivities of gas and solid also change. The total effect of temperature

is the combination of these effects. In the present work, the average temperature variation seemed ineffective in bringing about any change in the ETC of MH beds although the effect of augmentation technique was clearly visible. For an average bed temperature of 30ºC and 50 bar pressure, ETC value was 1.37 for $La_{0.8}Ce_{0.2}Ni_5$ hydride. Whereas for an average bed temperature of 170ºC and 50 bar pressure, for Mg + 50 wt% $LaNi_{4.6}Al_{0.4}$ hydride, ETC value was 1.76.

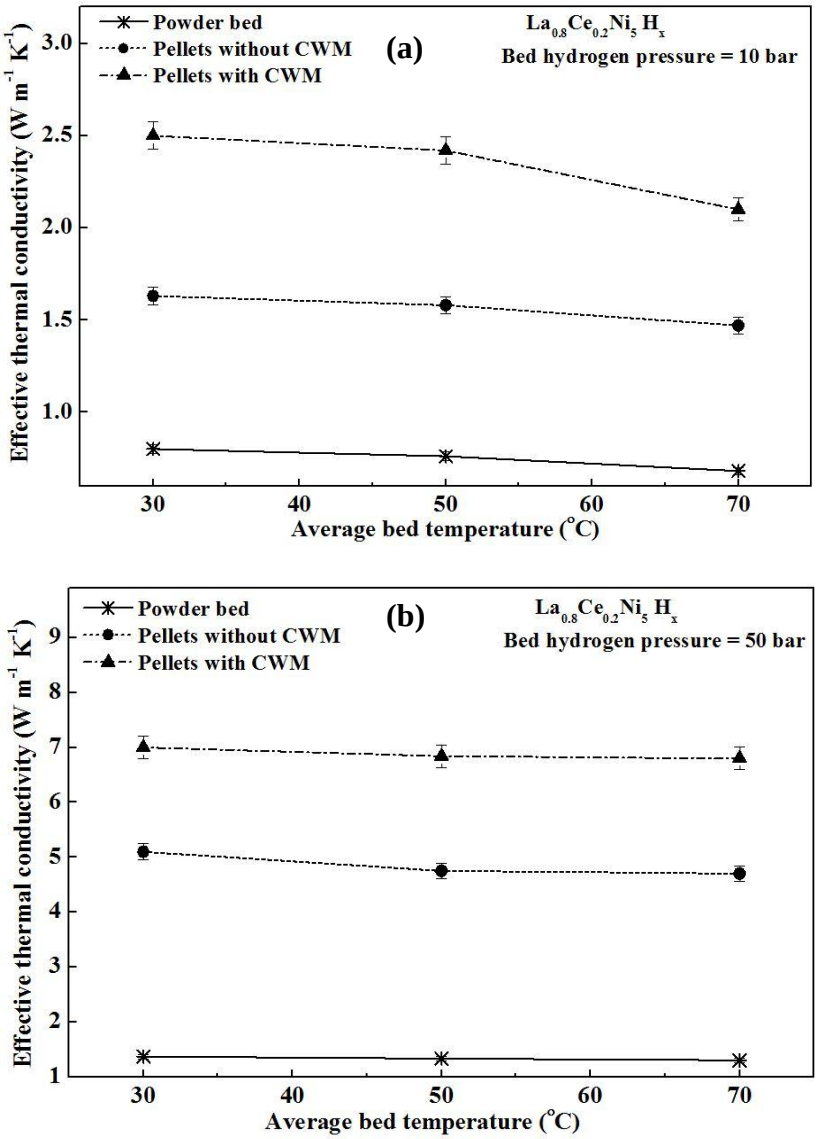

Fig. 3.12 Variation of ETC with average bed temperature for $La_{0.8}Ce_{0.2}Ni_5H_x$ (a) Hydrogen pressure = 10 bar (b) Hydrogen pressure = 50 bar

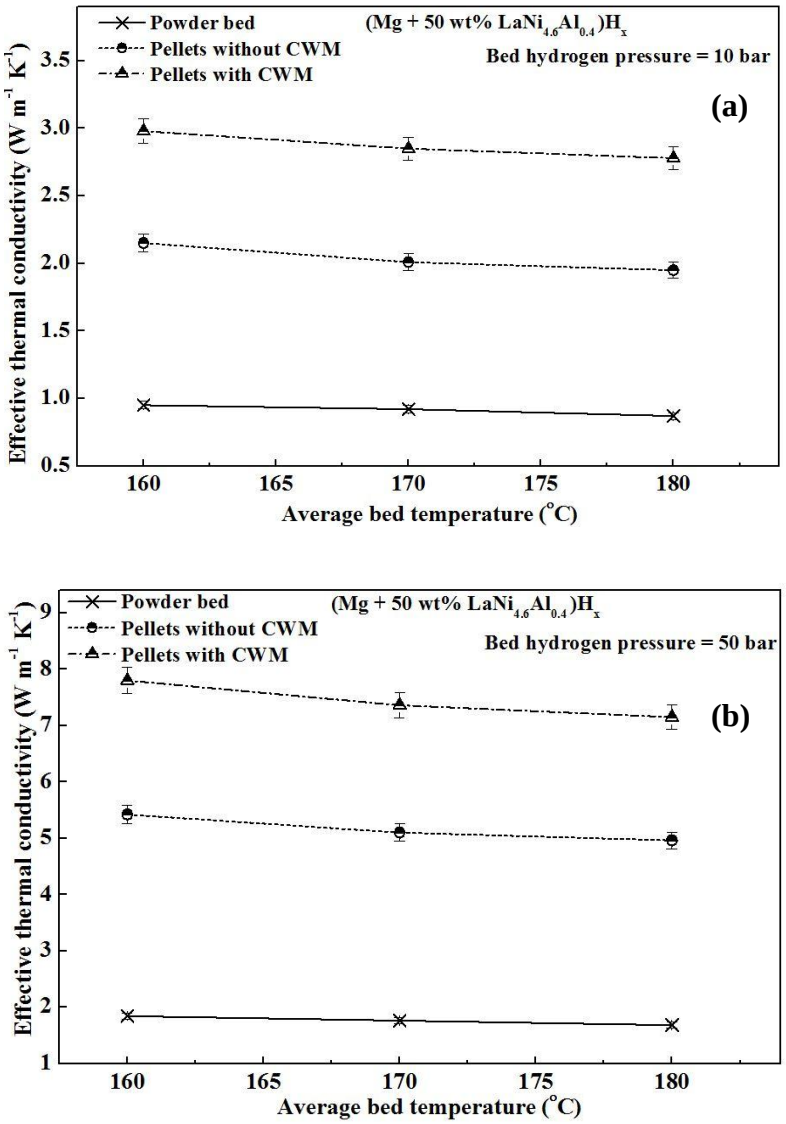

Fig. 3.13 Variation of ETC with average bed temperature for $(Mg + 50\ wt\%\ LaNi_{4.6}Al_{0.4})\ H_x$
(a) Hydrogen pressure = 10 bar (b) Hydrogen pressure = 50 bar

As shown in Figs. 3.12 and 3.13, although the ETC is changing with pressure but the graph between ETC and average temperature remained almost a horizontal line in all the cases. ETC of MH bed is the resultant of thermal conductivity of solid particles (which form the discrete phase) and that of hydrogen (which form the continuous phase). Factors which affect the ETC do so indirectly by affecting either one or both of these factors. The thermal conductivity of solid is a major function of movement of free electrons and it also depends on lattice vibrations. At higher temperatures,

the movement of free electrons decreases and lattice vibrations increases consequently leading to decrease in thermal conductivity (more prominently in case of alloys than in case of pure metals). On the other hand, the thermal conductivity of gases is a function of mean velocity and mean free path of molecules, and specific heat. The increase in temperature results in increase in mean velocity of molecules and specific heat. Hence the thermal conductivity of gases increases with increase in temperature.

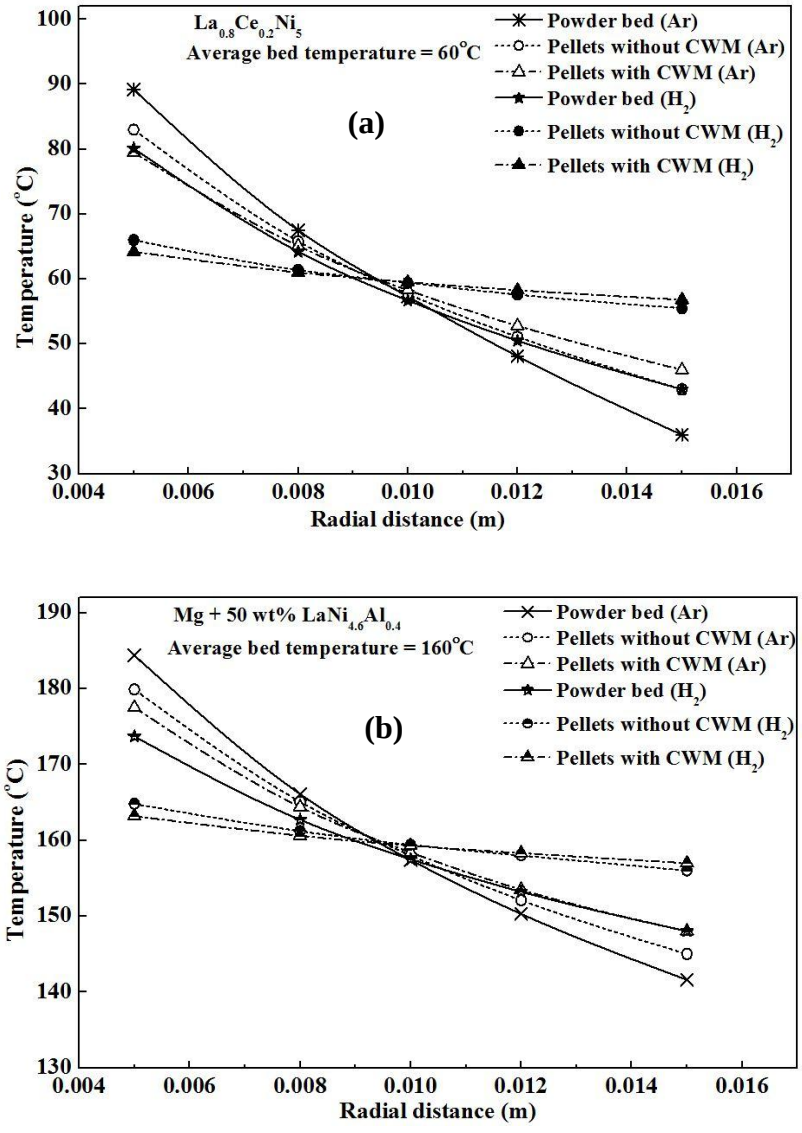

Fig. 3.14 Radial bed temperature profile; (a) for $La_{0.8}Ce_{0.2}Ni_5$ (b) for Mg + 50 wt% $LaNi_{4.6}Al_{0.4}$

The variation of ETC of MH bed with temperature is based on the result of variation of the two competing effects, namely thermal conductivity of solid particles and that of hydrogen. In the present case, probably the increasing effect on ETC, caused due to the increasing thermal conductivity of hydrogen with temperature, might be balanced by the decreasing effect, caused due to decrease in thermal conductivity of the solid particles.

The effect of ETC augmentation is clear from Figs. 3.14 (a) and 3.14 (b), which show the radial temperature profile for the MH beds of different configurations. As can be seen that the slope of the radial temperature profile reduces for PMPGF and it further reduces for PMPGFCu beds for both the MH's when compared to that in case of LMP beds. For $La_{0.8}Ce_{0.2}Ni_5$ the slopes of radial temperature profiles for LMP/PMPGF/PMPGFCu with argon as filling gas were -5255.17 / -3955.17 / -3312.07 K/m whereas with hydrogen these were -3670.69 / -1036.21 / -731.03 K/m respectively. For Mg + 50 wt% $LaNi_{4.6}Al_{0.4}$ the respective values with argon as filling gas were -4234.48 / -3456.9 / -2918.97 K/m and with hydrogen as filling gas the slopes were -2543.1 / -868.97 / -613.79 K/m. This clearly shows the improvement in heat transfer characteristics with the augmentation of ETC. Since the filling of argon gas will result into comparatively lower values of ETC for these beds as compared to those with hydrogen as filling gas, the slopes for the cases of hydrogen are lower than those for argon for the respective beds.

The uncertainties of different measuring instruments used for this work are given in Table C.1. Detailed uncertainty analysis for the experiments of ETC measurement is provided in section C.2.1 (Appendix C). Using these values the maximum uncertainty in the estimation of ETC values was found to be ± 5.1%.

Closure

The effective thermal conductivity of three configurations of beds of two materials, $La_{0.8}Ce_{0.2}Ni_5$ and Mg + 50 wt% $LaNi_{4.6}Al_{0.4}$, were measured for different sets of operating parameters. The effects of gas pressure, average bed temperature and hydrogen concentration on ETC were studied. Additionally, the ETC variation during hydrogenation and dehydrogenation was also analysed. In addition to ETC augmentation levels achieved, the effect of augmentation on hydrogen absorption by the bed is also analysed. The detailed conclusions are reported in Chapter 5.

Chapter 4

Effect of Pelletization on Absorption-Desorption Kinetics

As discussed in the previous chapter, the ETC augmentation by pelletization with appropriate mass fractions of graphite flakes, copper wire mesh and adequate compaction force results in significant increase in ETC and nominal decrease in the quantity of hydrogen absorbed. This chapter introspect the effect of ETC augmentation on hydrogen absorption-desorption kinetics of $La_{0.8}Ce_{0.2}Ni_5$ hydride for metal hydride based hydrogen compressor (MHHC) application and Mg + 50 wt% $LaNi_{4.6}Al_{0.4}$ hydride for metal hydride based thermal energy storage system (MHTES).

4.1 Metal Hydride based Hydrogen Compressor

Metal hydride based hydrogen compressor is one of the several applications of metal hydrides by virtue of exothermic/endothermic reversible reactions of hydrogen absorption / desorption respectively. The MHHC is a proven alternative to mechanical compressors owing to the disadvantages/limitations of the latter namely frictional losses, noise due to moving parts and requirement of high grade energy. The compression of hydrogen using MHHC has added advantage of safety and purity of hydrogen [74-75]. MHHC comprises of a metal hydride container (reactor), with a filter (to allow uniform distribution of hydrogen and to avoid the contamination of gas pipes with fine particles of MH), heat exchanging source and sink for maintaining two different temperatures and low pressure hydrogen supply source. The heat energy required for maintaining the higher temperature in the cycle can be obtained from renewable energy source or industrial waste heat. The compressor operates in a cycle consisting of following four processes [76].

Process 1-2: Hydrogen supplied at low temperature and low pressure is absorbed by the metal hydride

Process 2-3: Sensible heating of MH bed from low temperature T_a to high temperature T_d and consequent compression of hydrogen from P_s to P_d

Process 3-4: High pressure hydrogen is desorbed at high temperature T_d

Process 4-1: Sensible cooling of MH bed from T_d to T_a

Parameters governing the performance of MHHC can be classified as either material related parameters or operation/design related parameters. Reversible hydrogen sorption capacity, heat of absorption/desorption (ΔH), specific heat (c), thermal conductivity and sorption hysteresis are some of the material related parameters. Heat transfer rate from/to MH container, void space of MH bed, bed thickness, hydrogen absorption/desorption temperatures, supply pressure of hydrogen, pressure ratio and hydrogen throughput are operation/design related parameters [74-76].

4.1.1 Parameters affecting performance of MHHC

Important parameters governing the performance of MHHC are hot fluid temperature, cold fluid temperature, supply pressure of hydrogen, pressure ratio and hydrogen throughput. These parameters are interdependent and thus the performance of MHHC ultimately depends on combination of these properties. For a fixed cold fluid temperature, hydrogen throughput initially increases with hot fluid temperature, reaches a maximum and then remains constant. Thus a higher value of hot fluid temperature will not be beneficial after the hydrogen throughput achieves its maximum. If hot fluid temperature is fixed, the hydrogen throughput amount increases with decrease in cold fluid temperature as with the decrease in cold fluid temperature the bed pressure decreases thus raising the pressure gradient and enhancing the mass transfer to the bed. Again after a certain value of cold fluid temperature (of about 285 K), further decrease in cold fluid

temperature results in only marginal increase in hydrogen throughput. Hence, an optimized combination of hot fluid temperature and cold fluid temperature is required to get an optimum value of hydrogen throughput for MHHC.

From literature, it can be depicted that the hydrogen absorption-desorption rates have a great influence on the performance of MHHC. Although the diffusion of hydrogen through the formed hydride phase is one of the rate limiting steps, but the absorption and desorption rate of metal hydride beds also depends on the average temperature of the bed and pressure gradient available for absorption/desorption to occur. All the absorption and desorption kinetics equations proposed in the literature [77-81] consists of these parameters (temperature and pressure differential). Also many experimental and theoretical studies on heat and mass transfer aspects of metal hydride available in the literature [75-76, 82-85] showed that the absorption and desorption rates are heat transfer dependent. The low value of effective thermal conductivity of metal hydride beds leads to poor heat transfer characteristics of the beds thereby causing slower absorption/desorption kinetics. Compaction and inclusion of CWM structure increases the effective thermal conductivity of metal hydride bed as discussed in the previous chapter. Hence in this work, the rates of absorption and desorption with two different techniques of ETC augmentation and without ETC augmentation have been qualitatively studied.

4.1.2 Thermodynamic analysis

$LaNi_5$ alloy and its derivatives based on substitutions for either La or Ni or both have been widely tested and studied for MHHC [83, 86-89]. Partial replacement of La with Ce has been reported to improve reaction rate [89-90]. Also, sorption kinetics of $LaNi_5$ alloy and intermetallics derived from it are heat transfer limited and hence the effect of heat transfer augmentation on the performance of MHHC is studied.PCI and Van't

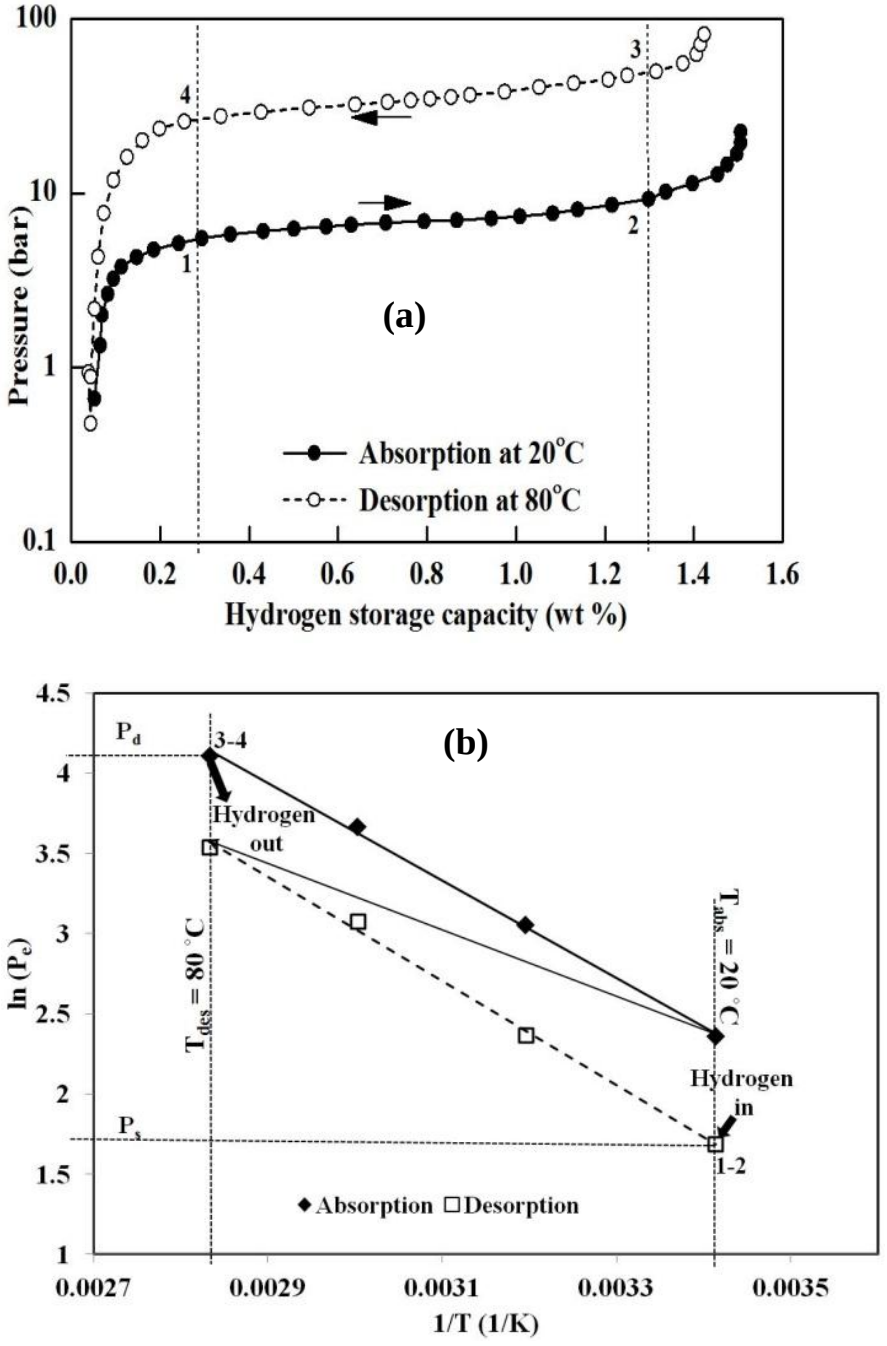

Fig. 4.1 MHHC cycle (a) on PCI curve (b) on Van't Hoff plot [90]

Hoff plots were plotted from the results obtained from the experiments done earlier in our laboratory [90]. Figs. 4.1 (a) and 4.1 (b) show the cycle of operation of MHHC on measured PCI and Van't Hoff plots. Fig. 4.1 (a) shows the compression cycle with absorption temperature of 20˚C and desorption temperature of 80˚C. The plateau pressures corresponding to

20˚C and 80˚C are 6.76 bar and 34.4 bar respectively. The maximum amount of hydrogen for cyclic operation of MHHC for this set of absorption and desorption parameters is 1 wt%. From the representation of compression cycle on PCI diagram it can be inferred that at 20˚C $La_{0.8}Ce_{0.2}Ni_5$ reaches the maximum theoretical hydrogen absorption capacity with the supply pressure of 10 bar. The desorption enthalpy of formation is calculated from the Van't Hoff plot. 13.23 kJ of heat energy is required for desorbing one gram of hydrogen gas. The properties of $La_{0.8}Ce_{0.2}Ni_5$ relevant to the present analysis are given in Table 4.1[91]. The effect of various operating parameters, absorption temperatures (20, 25 and 30˚C), supply pressures (10, 15 and 20 bar) and desorption temperatures (70, 80 and 90˚C), on absorption and desorption kinetics of hydrogen are measured. The details of experimental set up, reactor design and results obtained from the measurement are discussed in the following sections.

Table 4.1 Properties of $La_{0.8}Ce_{0.2}Ni_5$ hydride, reactor material and hydrogen

Parameters	**Values**
$La_{0.8}Ce_{0.2}Ni_5$ hydride	
1. Molecular Weight	432.61 g/mol
2. Enthalpy of Desorption	26.73 kJ/mol H_2 =13.23kJ/g of H_2
3. Specific Heat	0.36 kJ/kg.K
Reactor (Stainless Steel ANSI 316)	
1. Specific Heat	0.51 kJ/kg.K
Hydrogen	
1. Molecular weight	2.016 g/mol

4.1.3 Experimental set up details

The absorption and desorption kinetics were measured using Sievert's type experimental set up based on the mass balance of hydrogen. The

schematic arrangement of experimental setup used in the present work is shown in Fig. 4.2 (a).The gas flow lines were fabricated with ¼ inch seamless SS 316 tubes and PTFE flexible hoses with SS-316 strand and fittings capable to sustain pressure up to 500 bar. Medium pressure bellow sealed valves (working pressure up to 68.9 bar) and high pressure needle valves (maximum pressure rating 236 bar) were used to control the gas flow in the circuit.SS 316 cylinders of calibrated volumes (2250 ml-4No.s) were used as major part of supply volume and a calibrated cylinder of 300 ml was used as storage cylinder for compressed hydrogen.A compact regulator (with rated maximum inlet pressure of 248 bar and outlet pressure in the range of 0 to 103 bar) was utilized to supply hydrogen at a constant pressure from calibrated sample cylinders. For monitoring hydrogen pressure along the flow line as well as in the reactor, piezoresistive type pressure transducers were installed. Two transducers P_1 (pressure range 0 to 50 bar) and P_2 (pressure range 0 to 25 bar) were installed on the inlet and outlet sides of compact regulator respectively for monitoring the supply pressure and transducer P_3 (pressure range 0 to 100 bar) was used to monitor the pressure in the reactor. All these pressure transducers were of 0.1% accuracy on full scale. 'K' type thermocouples with an accuracy of ±0.5˚C and time constant of 0.2 s were used atdifferent locations in the hydrogen supply circuit and in the reactor to monitor the hydrogen gas temperature as shown in Fig. 4.2 (a). For leak test of the gas supply circuit and the reactor and for volume measurement, high purity (99.99%) argon gas was used. Hydrogen gas used in the experimentations was 99.999% pure. Evacuation of system, as and when required, was done using a rotary vacuum pump and a digital Pirani gauge was installed for monitoring the vacuum level. All the temperature and pressure sensors data were recorded using a data acquisition system. Fig. 4.2 (b) shows the photographic view of the experimental set up.

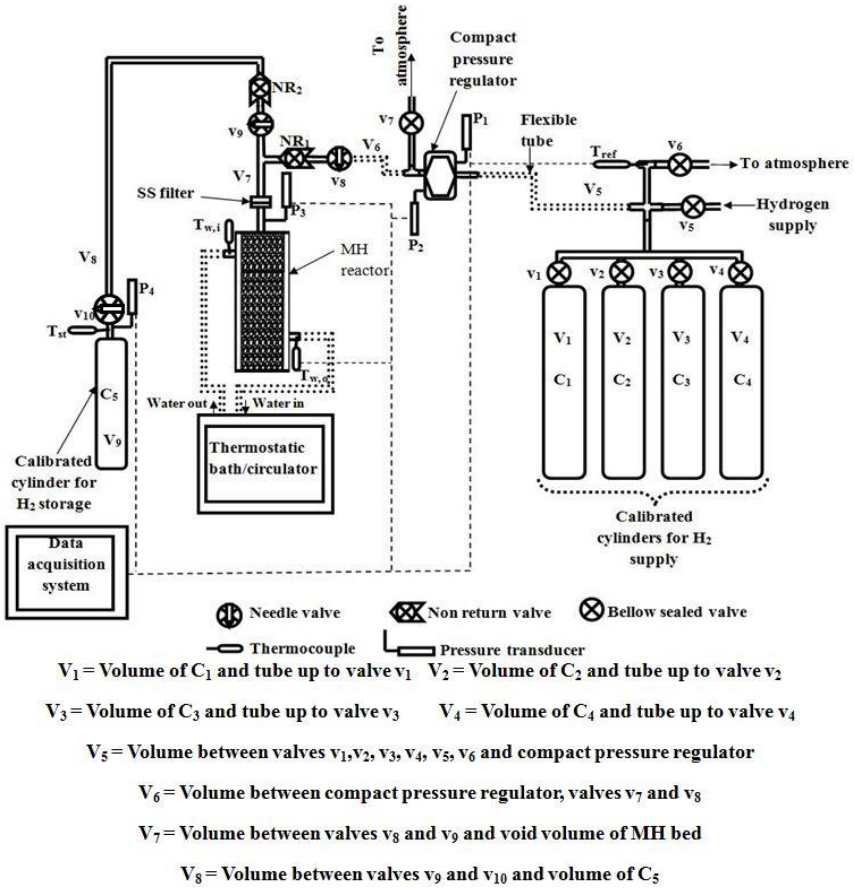

Fig. 4.2 (a) Schematic arrangement for $La_{0.8}Ce_{0.2}Ni_5$ hydride MHHC

Fig. 4.2 (b) Experimental set up for performance measurement of MHHC

4.1.4 Reactor Details

A cylindrical reactor made up of SS 316 was used in the present study. The $La_{0.8}Ce_{0.2}Ni_5$ powder was filled in the annulus formed between the copper tube (1) enveloping the axial filter (2) of 14 mm outer diameter and 130 mm length and the inner wall of the high pressure cylinder (3) with 30 mm inner diameter, 36 mm outer diameter and 130 mm height. The axial filter was SS sintered type with pore size of 2 microns. For the powder bed configuration 250 g of $La_{0.8}Ce_{0.2}Ni_5$ powder was filled in the reactor.A finned structure made up of copper tube and copper plate of 1 mm wall thickness (as shown in Fig. 4.3(a)) was used for two purposes; (i) to accommodate the axial filter attached to the top lid and (ii) to act as a heat transfer augmentation technique. Another annulus between the outer wall of high pressure cylinder and inner wall of a concentric thin cylinder was utilized as the water jacket (4) having the inner diameter of 36 mm and outer diameter of 45 mm. The coolant inlet (5) and outlet (6) tubes were welded to the thin cylinder. To supply/extract heat to/from the MH bed coolant was circulated through the water jacket.For the circulation and heating/cooling of water a thermostatic bath was utilized. The thermostatic bath had the accuracy of maintaining the temperature of water within $\pm$ 1˚Cof the set temperature. Two flanges, one on each end were TIG welded to both the cylinders to make a single assembly. On the top flange (7) six holes were drilled along a PCD for fitting of lid (8) through threaded joints. Provision for filling the reactor was given in the top flange. The lid had an arrangement for gas inlet and outlet (9). To ascertain the leak proof high pressure assembly between top flange and lid, a PTFE gasket (10)was used. The bottom flange (11) was designed with the arrangements for fitting thermocouple probes (12).

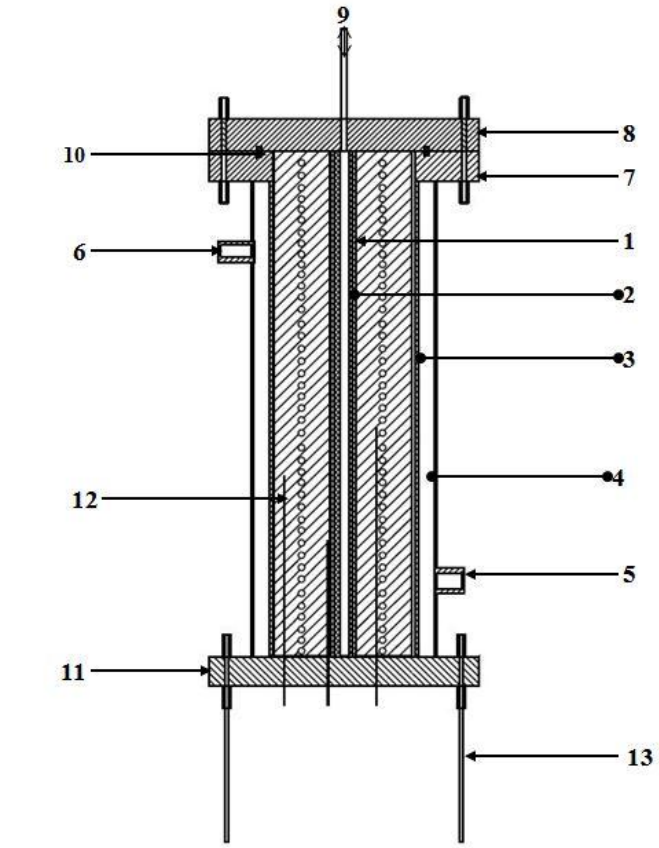

1- Copper tube; 2- Axial filter; 3- High pressure cylinder; 4- Water jacket;
5- Water inlet; 6- Water outlet; 7- Top flange; 8- Lid; 9- H_2 inlet/outlet;
10- PTFE gasket; 11- Bottom flange; 12-Thermocouple probe; 13-Stand

Fig. 4.3 (a) Schematic diagram of metal hydride bed for MHHC; (b) Components of metal hydride bed for MHHC

Three “K” type thermocouples (mineral insulated inconel sheathed with 1 mm diameter) were inserted into the MH bed (at different radii and heights so as to obtain the average bed temperature) through the holes drilledin the lower flange with aremovable arrangement. Figs. 4.3 (a) and (b) show the schematic diagram and photograph of components of the reactor.

4.1.5 Heat Transfer Augmentation Techniques

For heat transfer augmentation to/from $La_{0.8}Ce_{0.2}Ni_5$ hydride bed, three different techniques were implemented in the present work. In the first method, copper finned structure made with 1 mm thick copper plate and 1 mm wall thickness copper tube, perforated all along the extent as shown in Fig. 4.4 (a), was used. The perforation was intended to allow proper exposure of MH particles with hydrogen. Two different types of pellets, as shown in Figs. 4.4 (b) and (c), were used as the other two methods. These pellets were similar to the ones discussed in section 3.2.2in their ingredients, composition and method of formation but to accommodate the axial filter, the geometry of the pellets was appropriately changed. The inner diameter of both the types of pellets in this case was kept 14.2 mm. 1.2 mm diameter holes were drilled at appropriate positions on those pellets which lie towards the bottom of the bed to accommodate thethermocouple probes. Thermal paste was applied between the thermocouple probe andthe holes on the pellets to assure continuous contact and avoid chances of contact resistance. Mass of $La_{0.8}Ce_{0.2}Ni_5$ alloy was kept same in all the three configurations to avoidthe chances of relative effect of mass of metal hydride on the heat transfer characteristics of MH bed.

4.1.6 Experimental Procedure

Despite the efforts made to keep the $La_{0.8}Ce_{0.2}Ni_5$ powder unaffected from moisture and other gases in the environment, it could not be assured that at

the time of filling the metal alloy powder into the reactor the $La_{0.8}Ce_{0.2}Ni_5$ powder sample was free of moisture and other gaseous substances.

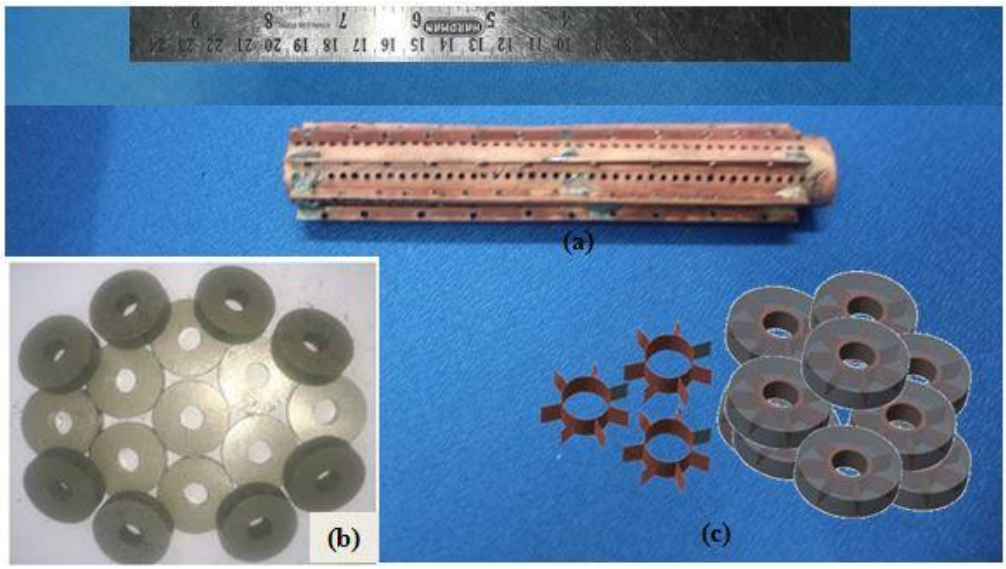

Fig. 4.4 Heat transfer augmentation techniques implemented

To remove these infiltrations from the $La_{0.8}Ce_{0.2}Ni_5$ powder sample, activation of sample was must. The activation was carried out as discussed in Section 3.2.6. After activation of MH bed valves v_1 to v_4 are opened to fill the supply line upstream of compact pressure regulator with hydrogen at high pressure. The hydrogen compression using MHHC is a cyclic process with four processes as discussed in previous section. The experimental procedure for obtaining this cyclic process of MHHC is explained as follows.

1. To start with the cyclic process of MHHC, water is circulated at absorption temperature to bring the MH bed to absorption temperature.
2. Compact pressure regulator is opened appropriately to get the tubes downstream of regulator filled with hydrogen at the desired supply pressure. Valve v_8 is opened to expose the MH bed with hydrogen at supply pressure till the equilibrium pressure of MH

bed becomes equal to supply pressure. The heat of absorption is carried away by the water flowing at constant absorption temperature. Referring to Fig. 4.2 (a), the amount of hydrogen absorbed with time is calculated by hydrogen gas mass balance in the supply volume (consisting of volume V_1=2252 ml, volume V_2= 2253 ml, volume V_3= 2252 ml, volume V_4= 2252 ml and volume V_5=20 ml) and void volume downstream of compact pressure regulator (including V_6=25 ml and V_7 =45 ml). The mass balance was done as follows:

Initial mass of hydrogen in supply volume was calculated as;

$$m_{s,i} = \sum_{j=1}^{5} \frac{P_{1,i} V_j}{Z\left(P_{1,i}, T_{ref,i}\right) R_{H_2} T_{ref,i}} \tag{4.1}$$

where, Z is the compressibility factor for hydrogen which is a function of pressure and temperature and is given as [79]:

$$Z = 1 + (B_0 + B_1 T + B_2 T^2) P + A(C_0 + C_1 T + C_2 T^2) P^2 \tag{4.2}$$

The coefficients are defined as:

$A = 1$ for 280 K $\le T \le$ 428 K and T=0 for 428 K $\le T \le$ 800 K;

$B_0 = 0.00962$ MPa^{-1}, $B_1 = -15.446 \times 10^{-9}$ MPa^{-1}K^{-1}, $B_2 = 82.314 \times 10^{-13}$ MPa^{-1}K^{-2}

$C_0 = 18.167 \times 10^{-8}$ MPa^{-2}, $C_1 = -83.222 \times 10^{-11}$ MPa^{-2}K^{-1},

$C_2 = 9.327 \times 10^{-13}$ MPa^{-2}K^{-2}, P-Pressure, in MPa

Final mass of hydrogen in supply volume was obtained as;

$$m_{s,f} = \sum_{j=1}^{5} \frac{P_{1,f} V_j}{Z\left(P_{1,f}, T_{ref,f}\right) R_{H_2} T_{ref,f}} \tag{4.3}$$

Total mass of hydrogen supplied,

$$m_s = m_{s,i} - m_{s,f} \tag{4.4}$$

The mass of hydrogen present in gaseous form in void volume,

$$m_{v,f} = \sum_{j=6}^{7} \frac{P_{2,f} V_j}{Z\left(P_{2,f}, T_{r,f}\right) R_{H_2} T_{r,f}} \tag{4.5}$$

The mass of hydrogen absorbed by the metal alloy is given as:

$$m_{a,f} = m_s - m_{v,f} \tag{4.6}$$

3. Valve v_8 is closed and set temperature of thermostatic bath is increased to desired desorption temperature.
4. As the MH bed achieves the desorption temperature, valves v_9 and v_{10} are opened. Hydrogen is desorbed by the MH bed till the pressure in storage cylinder becomes equal to the bed pressure. The amount of hydrogen desorbed is calculated by mass balance of hydrogen gas in the storage volume comprising of volumes V_7 and V_8 (= 348 ml) in Fig. 4.2 (a). The mass balance is done as follows:
   Initial mass of hydrogen (after reaching desorption temperature) in the MH bed was determined from Eq. (4.8):

$$m_{d,i} = \frac{P_{r,i} V_7}{Z(P_{r,i}, T_{r,i}) R_{H_2} T_{r,i}} \tag{4.7}$$

   Final mass of hydrogen (after achieving saturation state) in the storage volume was obtained as:

$$m_{d,f} = \frac{P_{r,f} (V_7 + V_8)}{Z(P_{r,f}, T_{r,f}) R_{H_2} T_{r,f}} \tag{4.8}$$

   Mass of hydrogen desorbed was thus given as:

$$m_d = m_{d,i} - m_{d,f} \tag{4.9}$$

5. Valves v_9 and v_{10} are closed and thermostatic bath is set to desired absorption temperature again.

Steps 1 to 5 are repeated for different sets of parameters such as absorption temperature, desorption temperature and supply pressure. Pressures and temperatures data are recorded periodically during the experimentations.

4.1.7 Results and discussion

Two different ETC augmentation techniques, discussed in the previous chapter were tested for hydrogen absorption/desorption kinetics of $La_{0.8}Ce_{0.2}Ni_5$ hydride for the MHHC. The three configurations of MH beds, namely, lose metal hydride powder bed (LMHP), bed of pellets of metal hydride mixed with graphite flakes (PMHGF) and bed of pellets of

metal hydride mixed with graphite flakes and embedded with copper wire mesh structure (PMHGFCu) were tested for wide range of operating parameters. The results obtained are compared thoroughly to study the effect of ETC augmentation on absorption and desorption kinetics in following sections.

4.1.7.1 Hydrogen absorption kinetics: The parameters affecting rate and quantity of hydrogen absorption are: hydrogen supply pressure and average bed temperature. For a fixed hydrogen supply pressure, the variation in average bed temperature with time is defined by the heat transfer characteristics of the bed. The sorption kinetics of MH beds is mass and heat transfer limited. Figs. 4.5 (a) – (c) show the variations of average bed temperature and amount of hydrogen absorbed with time for all the three configurations of MH beds (LMHP, PMHGF and PMHGFCu). Figs. 4.5 (a), 4.5 (b) and 4.5 (c) show these variations for different supply pressures of 10 bar, 15 bar and 20 bar respectively. For a fixed supply pressure, the variation in amount of hydrogen absorbed suggests that in the beginning (initial 60 to 100 seconds, depending on the supply pressure) the diffusion of hydrogen to metal hydride is faster in case of powder bed. The compaction of metal hydrides reduced the surface area and thereby initial diffusion of hydrogen is delayed. Therefore it can be observed that for all the supply pressures, at the beginning of absorption process, the rate of absorption is higher in case of powder beds. Due to this, rate of heat release and rise in average bed temperature is also higher for powder beds in this regime. In addition to diffusion through the formed hydride phase, average bed temperature and available pressure gradient also influence the sorption kinetics of MH [77-81]. The low value of effective thermal conductivity of metal hydride beds leads to poor heat transfer characteristics of the beds there by causing slower absorption/desorption kinetics [76, 82, 84-85, 92]. Initially the LMHP bed shows faster increase in temperature verifying faster kinetics in the initial phase of absorption process. But with time, as the hydrogen absorption

phase progresses, poor heat transfer characteristics of LMHP bed causes decrement in the hydrogen absorption rate. On the other hand, the heat transfer augmentation in case of pellets beds show better absorption rate inthis phase hence the time taken by the bed to reach its initial temperature is less in these beds. This effect can be seen in Figs. 4.5 (a) – (c).

For supply pressure of 10 bar and coolant inlet temperature of 30˚C, in the first 20 seconds the LMHP bed had absorbed 70% (of maximum absorption capacity for this pressure, temperature condition) of hydrogen, while for PMHGF bed, it was 52.4% and for PMHGFCu bed, it was 52.9%. As the average bed temperature increases the driving pressure difference (supply pressure and plateau pressure of the bed) decreases. This leads to a decrease in absorption rate. Due to poor heat transfer characteristics of the powder bed the average bed temperature decreases slowly and therefore the bed takes longer time to reach saturation stage. Better heat transfer characteristics of PMHGF and PMHGFCu beds allow these beds to reach the initial average temperature and saturation stage faster. To achieve a stage of 90% of maximum hydrogen storage (at the above stated supply pressure and temperature) the time taken by LMHP bed was 165 s while those by pellets beds were 130 s and 125 s respectively for the case of PMHGF and PMHGFCu. However, there is little difference between the PMHGF and PMHGFCu beds in reaching saturation stage. The reason behind this may be that the negative effect caused due to additional parasitic dead weight of copper wire mesh would have suppressed the effect of betterment in heat transfer characteristicscaused due to presence of copper wire mesh structure. The maximum difference in time taken by powder bed and that by pellets bed for reaching the saturation stage is around 150 seconds at a supply pressure of 20 bar while this difference is lower for lower supply pressure. With the increase in hydrogen supply pressure, the initial hydrogen diffusion increases as the driving gradient for mass transfer (pressure

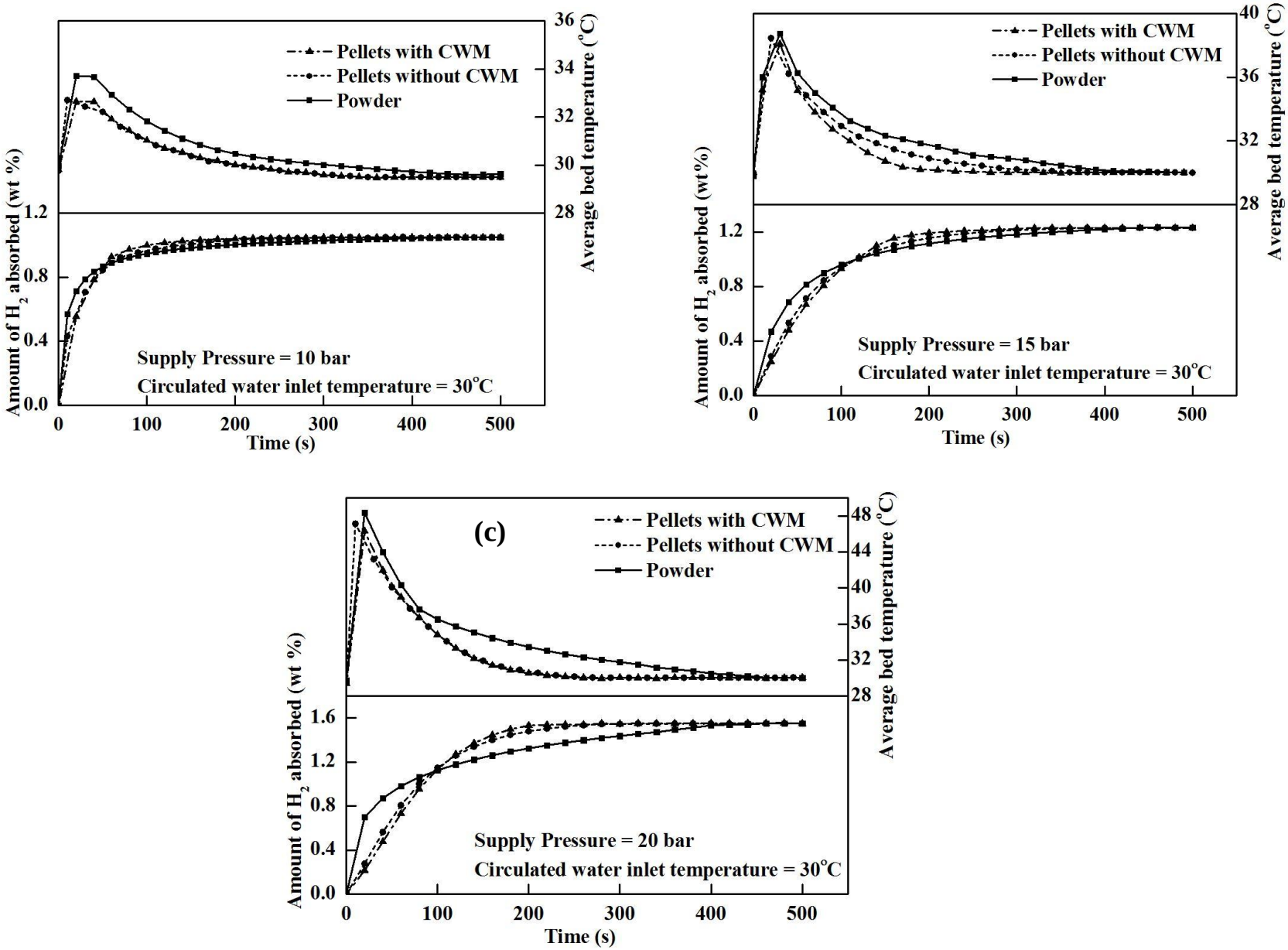

Fig. 4.5 Variation of amount of hydrogen absorbed and average bed temperature during absorption with circulating water inlet temperature of 30˚C (a) Supply pressure = 10 bar (b) Supply pressure = 15 bar (c) Supply pressure = 20 bar

difference) increases. Hence the difference between the amount of hydrogen absorbed in case of powder bed and that in case of pellets is more in the mass transfer limited regime.As the hydrogen absorption quantity increases with increase in supply pressure, the increase in rate of exothermic reaction results in an increase in the average bed temperature rise and it takes longer time for LMHP bed to reach saturation stage. Thus the timedifference for reaching saturation stage between powder and pellets beds increases with increase in supply pressure.

4.1.7.2 Hydrogen compression rate/desorption kinetics: Figs. 4.6 (a) – 4.6 (c)show the variation of average bed temperature and amount of hydrogen desorbed with hot fluid temperature. As shown in the figures the increase in desorption temperature results in increase in amount of hydrogen desorbed, if supply pressure and absorption temperature are same.For the supply pressure of 20 bar and absorption temperature of 30˚C, the maximum amounts of hydrogen desorbed were 1.9 g, 2.2 g and 2.5 g respectively for desorption temperature of 70˚C, 80˚C and 90˚C. Similar to absorption, most of the hydrogen gets desorbed in first few seconds; this is due to the large pressure gradient between the reactor and storage cylinder. With time, this pressure gradient gets decreased and thus the hydrogen desorption rate falls. Time taken to desorb 90 % of total amount of hydrogen desorbed for 20 bar supply pressure and 90˚C desorption temperature were 152 s, 83 s and 57 s respectively for LMHP bed, PMHGF bed and PMHGFCu bed respectively. The differences in rates of hydrogen desorbed in case of powder bed and pellets can be justified with the same reason as for the case of absorption discussedabove. The sudden drop in average bed temperature soon after starting of desorption process is due to the poor thermal conductivity of hydride bed [82]. The thermalenergy required for desorption (Enthalpy of desorption = 13.23 kJ of heat energy per g of hydrogen desorbed) is supplied to the hydride bed through the circulating hot fluid but this heat

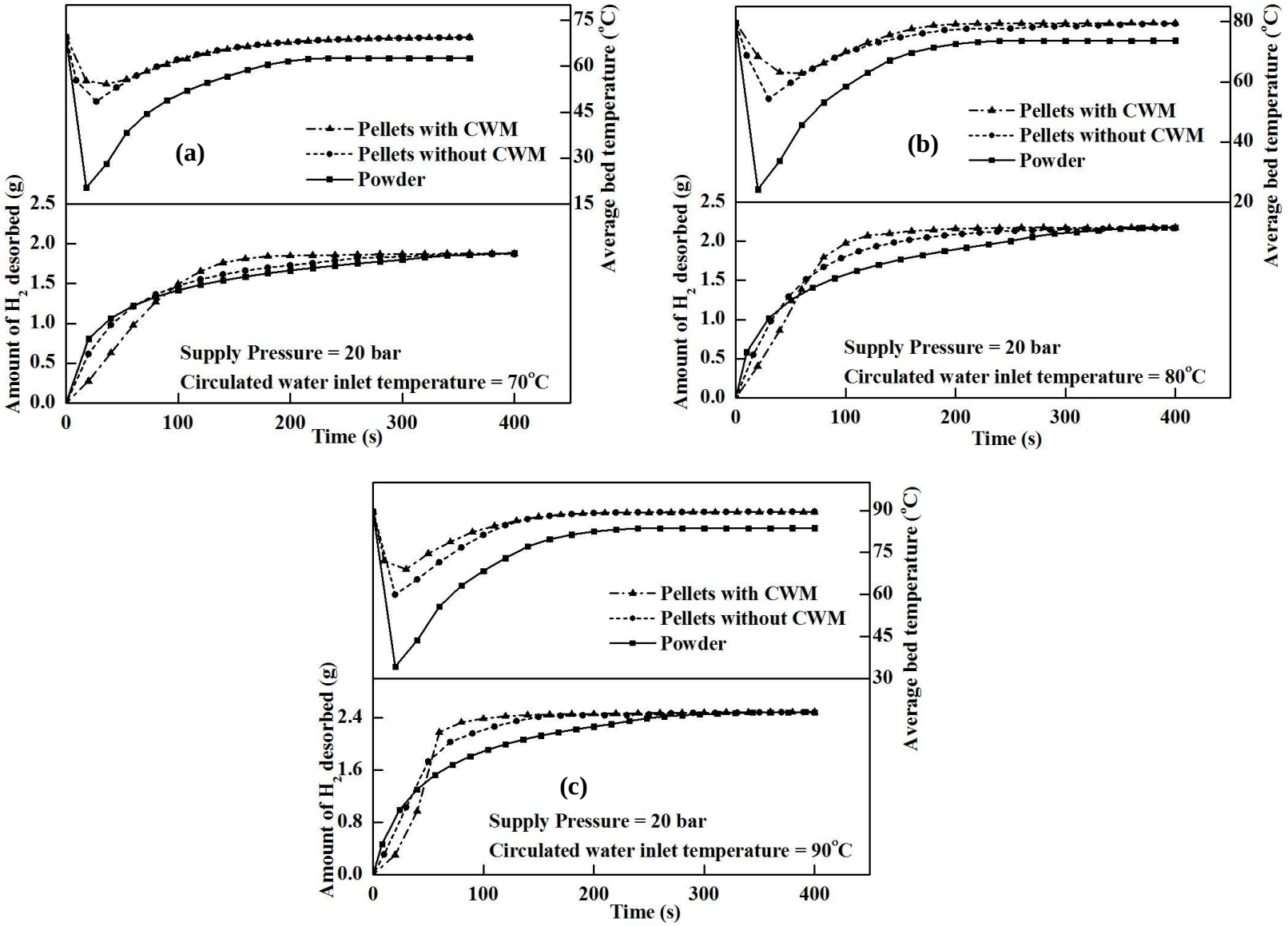

Fig. 4.6 Variation of amount of hydrogen desorbed and average bed temperature during desorption

(a) Water inlet temperature =70˚C (b) Water inlet temperature =80˚C (c) Water inlet temperature =90˚C

could not reach towards the core of hydride bed instantly due to poor thermal conduction. Hence, the portions of hydride bed, not in proximity of heat source take the required heat from itself consequently the average bed temperature drops.The drop in average bed temperature is very high in case of loose powder bed whereas it is less due to better heat transfer from the hot fluid in case of pellets. For the absorption pressure of 20 bar, absorption temperature of 20˚C and coolant inlet temperature of 90˚C, the maximum drop in temperature for LMHP bed / PMHGF bed / PMHGFCu bed were obtained as 54.7˚C / 30˚C / 21˚C respectively. The difference in temperature profile between loose powder bed and beds with pellets were much higher for desorption than that for absorption. Also the difference intemperature profiles and hydrogen desorption rates is more between PMHGF bed and PMHGFCu bed suggesting better heat transfer characteristics in the case of later.

4.2 Metal Hydride based Thermal Energy Storage System

Another important non – hydrogen storage application of metal hydrides exploiting the heat transfer in exothermic / endothermic hydrogen absorption / desorption reactions is Thermal Energy Storage (TES). TES is applied in the places where thermal energy is available for a particular period and for continuous operation of the system the thermal energy needs to be stored so that this stored thermal energy can be utilized when it is not available from the main source. Units based on renewable energy like solar or wind energy are among the main consumers of TES. TES are of three types, namely sensible heat storage, latent heat storage and thermochemical heat storage. Due to higher energy densities in case of thermochemical heat storage, this type is preferred among the three types. With the salient features like high energy densities, good cyclic stability, self regulating and low corrosiveness, metal hydride based TES has been successful in being a leading contender among all types of thermochemical thermal energy storage systems available [93]. A metal

hydride based TES system requires following important components; a MH reactor, a circuit to connect reactor to the hydrogen storage tank, a hydrogen storage tank, a hydrogen supply cylinder at comparatively higher pressure.

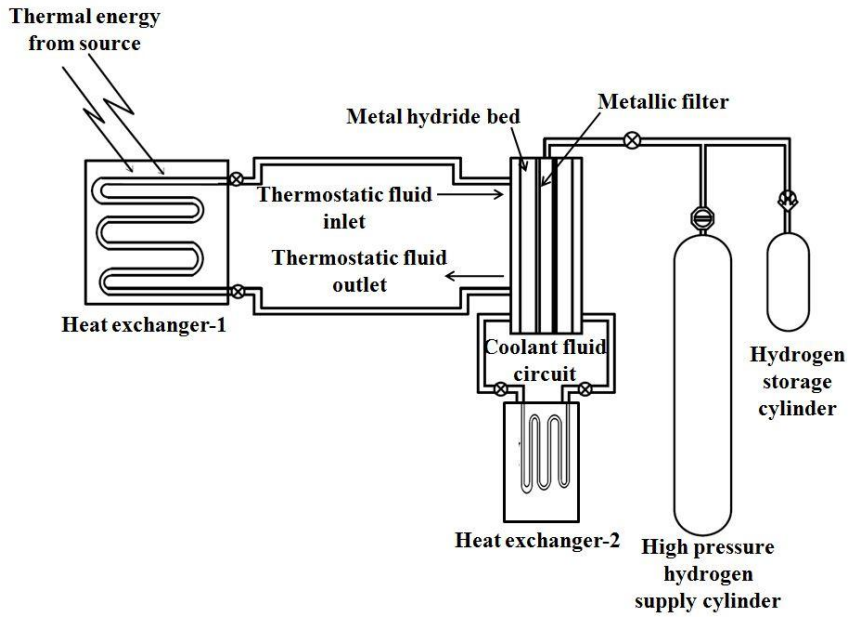

Fig. 4.7 Schematic diagram of MHTES system

Heat transfer between metal hydride, thermal energy source, and the thermal energy utilizing unit is facilitated through a thermostatic fluid. Fig. 4.7 shows a general schematic of a MH based TES system. The operating cycle consists of two processes, charging process and discharging process. The heat energy from the heat source is transferred to the MH reactor through the thermostatic fluid. This heat energy causes the rise in temperature and consequently hydrogen pressure in the MH reactor thus resulting in development of pressure gradient between MH reactor and hydrogen storage tank. This leads to dehydrogenation from the metal hydride bed. The dehydrogenation reaction being endothermic acts as the heat energy storage reaction as the heat energy from the heat source has now got stored in the form of desorbed hydrogen. The end of dehydrogenation due to end of pressure gradient between MH reactor and hydrogen storage tank signifies the end of charging process of MHTES

system. As per the requirement of thermal energy utilizing unit, relatively at low temperature compared to absorption, the hydrogen is supplied to MH reactor (from hydrogen storage tank) and hydrogenation reaction (an exothermic reaction) starts thus resulting into supply of heat energy from MH reactor to the thermal energy utilizing unit through the thermostatic fluid. The end of hydrogenation signifies the end of discharging process of the MHTES system [93-96].

As the complete operation of MHTES is heat transfer dependent, the heat transfer characteristics of MH bed plays a vital role in the functioning of MHTES system. MH powder beds are known for their poor heat transfer characteristics. Hence, measures to improve the heat transfer characteristics are must to make the MH bed appropriate for the application of MHTES [94]. Other than measures to improve the heat transfer characteristics of MH bed, some appropriate changes in design and material of MH holding container have been reported to result in improvement in absorption kinetics of MH bed [97]. In the present work, two different types of pellet beds with improved ETC are tested for determining their suitability for the application of MHTES.

The experimental set up and reactor details and the heat transfer augmentation techniques are same as in case of MHHC. The thermostatic fluid used for the experiments of MHTES system is different from the coolant used in MHHC experiments and the present thermostatic fluid is capable of sustaining 220ºC.

4.2.1 Material selection

Literature on MHTES systems suggests that Mg based metal alloy/composite is best suited for this application due to low material density and high energy density of Mg. The study of characteristics of Mg based hydrides reveals that they exhibit slow kinetics and it requires high temperatures (in the range of 400ºC) for appropriate level of hydrogen absorption/desorption [93, 98-99]. To modify these characteristic

properties, a composite of Mg and $LaNi_{4.6}Al_{0.4}$ was prepared using rigorous ball milling. The composite of Mg + 50 wt% $LaNi_{4.6}Al_{0.4}$was used for this experimentation. This composite starts hydrogen absorption at a much lower temperature of around 110ºC and provides better hydrogen absorption/desorption kinetics as compared to pure Mg.

The activation of Mg + 50 wt% $LaNi_{4.6}Al_{0.4}$composite was done as discussed in section 3.2.6.

4.2.2 Experimental procedure

After activation of Mg + 50 wt% $LaNi_{4.6}Al_{0.4}$composite, hydrogenation and dehydrogenation with appropriate thermostatic fluid temperatures and hydrogen supply and discharge pressures were performed. The temperatures for hydrogenation were taken as 125ºC, 150ºC and 175ºC while temperatures for dehydrogenation were taken as 180ºC and 215ºC. The hydrogen supply pressure during hydrogenation was fixed at 20 bar. The following sections describe the hydrogenation and dehydrogenation processes in detail.

4.2.2.1 Hydrogenation procedure: To start the process of hydrogenation, heat transfer fluid is circulated at desired temperature to bring the MH bed to absorption temperature. Referring to Fig. 4.3 (a), hydrogen pressure is ensured by appropriate opening of compact pressure regulator and the tubes downstream of regulator are filled with hydrogen at the desired supply pressure. Valve v_8 is opened to expose the MH bed with hydrogen at supply pressure till the equilibrium pressure of MH bed becomes equal to supply pressure. The heat of absorption is carried away by the heat transfer fluid flowing at constant temperature. The temperatures at three different locations in MH bed, as well as the temperatures of heat transfer fluid at inlet and outlet and pressures at different locations are recorded in time intervals of 2 seconds using a data acquisition system. The amount of hydrogen absorbed by the MH bed is calculated as explained for MHHC experiment. At the end of hydrogenation process, valve v_8 is closed.

4.2.2.2 Dehydrogenation procedure: During the dehydrogenation or charging process the temperature of thermostatic fluid is increased to the desired desorption temperature and this fluid is then circulated through the thermostatic fluid jacket, enveloping the MH reactor. When the average bed temperature reaches equilibrium with the thermostatic fluid, valves v_9 and v_{10} are opened and hydrogen released from the MH bed is stored in the hydrogen storage cylinder till the pressure in MH reactor equals the pressure in the storage cylinder. The mass of hydrogen desorbed is calculated as discussed in case of MHHC.

4.2.3 Results and discussion

As discussed in section 4.2.1, the Mg + 50 wt% $LaNi_{4.6}Al_{0.4}$compositewas selected for the application of MHTES due to its favourable thermodynamic properties and better absorption/desorption kinetics as compared to pure magnesium based hydride. Encouraged with the improvement in sorption kinetics obtained by applying the ETC augmentation techniques in case of $La_{0.8}Ce_{0.2}Ni_5$ hydride (for MHHC application), the same augmentation techniques were also applied in case of Mg + 50 wt% $LaNi_{4.6}Al_{0.4}$ hydride for the application of MHTES. Following sections discuss the effect of ETC augmentation on the sorption kinetics of Mg + 50 wt% $LaNi_{4.6}Al_{0.4}$ hydride.

4.2.3.1 Effect of ETC augmentation on hydrogen absorption kinetics: The hydrogen absorption kinetics of three configurations of MH beds, namely, LMHP, PMHGF and PMHGFCu were measured at three different absorption temperatures (125ºC, 150ºC and 175ºC). The results are depicted in Figs. 4.8 (a) – (c). As shown in the figures, the amount of hydrogen absorbed was highest for LMHP. This is due to the intrinsic nature of Mg. In case of Mg based materials, the absorption capacity increases with increase in temperature up to 250ºC. As rate and amount of hydrogen absorbed is higher,the average bed temperature rise in case of LMHP is high as compared to those in cases of PMHGF and PMHGFCu.

The average bed temperature profiles suggest the ease of heat transfer within the bed. The maximum temperature rise in case of LMHP were 75.6ºC, 76ºC and 79ºC for absorption temperatures of 125ºC, 150ºC and 175ºC respectively, the respective temperature rises for PMHGF bed were 63ºC, 67.6ºC and 50ºC and those for PMHGFCu bed were 58ºC, 60ºC and 45ºC respectively. This clearly shows the improvement in heat transfer characteristics achieved by the ETC augmentation techniques. As the rise in temperature of thermostatic fluid will be similar to the rise in average bed temperature, in case of LMHP, thermal energy is recovered at a higher temperature compared to metal hydride beds with augmentation. For a particular absorption temperature, the rate of absorption is also high in case of powder bed. However, due to poor heat transfer characteristics, the time taken for the bed to reach initial temperature is higher. Due to this, the overall absorption process takes more or less same time in all the three cases (LMHP, PMHGF and PMHGFCu). Thus ETC augmentation does not seem to show any significant effect on the absorption kinetics of Mg + 50 wt% $LaNi_{4.6}Al_{0.4}$hydride. Consequently the discharging process of MHTES system would not be influenced by ETC augmentation. It is worth to be mentioned here that the insignificant effect of ETC augmentation on absorption kinetics was true for Mg based composite. With other metal hydride (which shows better absorption characteristics at lower temperatures), the effect of ETC augmentation can be expected to be considerable. The amount and rate of hydrogen absorption increases with temperature up to a certain value in case of Mg based materials. The mixing of $LaNi_{4.6}Al_{0.4}$although causes better hydrogen absorption at lower temperatures but studies suggest that with increase in absorption temperature, the hydrogen absorption characteristics (both, rate as well as quantity of absorption) show improvement [93, 98, 100]. As can be seen from Figs. 4.8 (a) – 4.8 (c), as the absorption temperature (thermostatic fluid inlet temperature) increases, the rate of hydrogen absorption increases and this leads to reduction in time required for the metal hydride

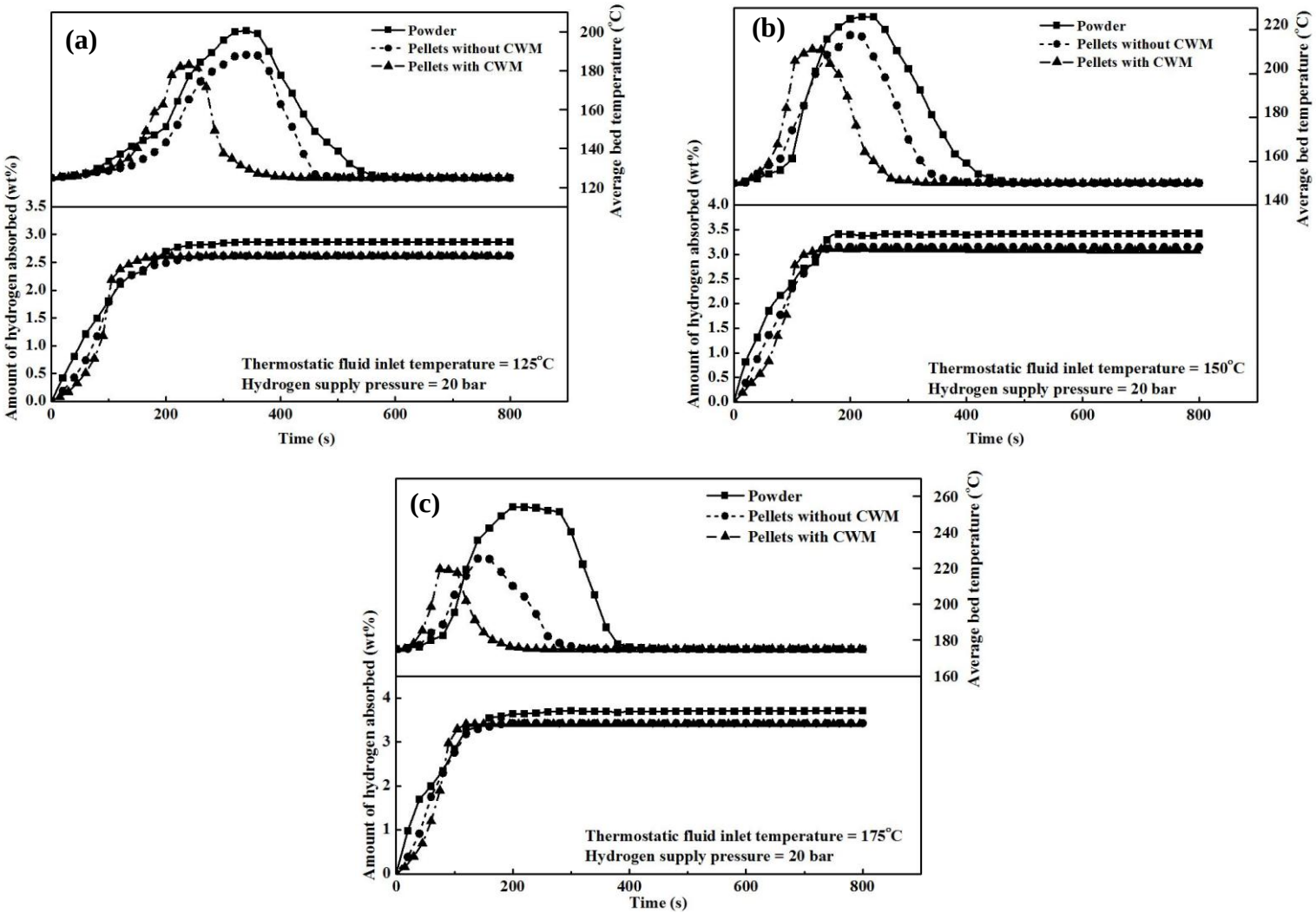

Fig. 4.8 Variation of amount of hydrogen absorbed and average bed temperature during absorption at 20 bar supply pressure: (a) Thermostatic fluid inlet temp =125˚C (b) Thermostatic fluid inlet temp =150˚C (c) Thermostatic fluid inlet temp =175˚C

bed to achieve the saturation stage. This is true for all the three configurations of beds. The time required for the LMHP bed to reach the saturation stage were 400 s, 360 s and 330 s respectively for 125ºC, 150ºC and 175ºC absorption temperatures, while the time recorded for the PMHGF bed were 280 s, 180 s and 160 s and those for PMHGFCu were 195 s, 150 s and 120 s. As the increase in hydrogen absorption rate, the rate of heat release increases, the rise in temperature is greater for higher temperatures.

4.2.3.2 Effect of ETC augmentation on hydrogen desorption kinetics: The hydrogen desorption kinetics experiments were conducted at two temperatures, 180ºC and 215ºC. From Figs. 4.9 (a) – (b), it is clear that the increase in desorption temperature resulted in better desorption kinetics. Similar to absorption kinetics, in case of desorption, the time required for maximum hydrogen desorption decreased with increase in desorption temperature. For LMHP bed, the time required for achieving maximum hydrogen desorption was 200 s for 180ºC desorption temperature, it was 150 s for the desorption temperature of 215ºC. This suggests that the desorption kinetics gets faster with increase in desorption temperature. Following the same trend, the time required for desorbing maximum amount of hydrogen, decreased from 100 s / 75 s to 75 s / 50 s for PMHGF / PMHGFCu beds respectively for 180ºC and 215ºC desorption temperatures. While the maximum amount of hydrogen desorbed by the LMHP bed was 88% (of total absorbed hydrogen), when the desorption temperature was 180ºC, this quantity increased to 90% for 215ºC desorption temperature. Similarly for PMHGF and PMHGFCubeds the quantity of hydrogen desorbed increased from 90 to 92%, when the desorption temperature was increased from 180 to 215ºC. The effect of ETC augmentation can be clearly observed for both the desorption temperatures. Compared to absorption process, the effect of augmentation is better for desorption process as far as average bed temperature variation is concerned. Verifying the reasoning given in section 4.1.7.2, the

implementation of ETC augmentation techniques have resulted in more uniform bed temperature during desorption process. The minimum temperatures in case of LMHP bed for desorption temperatures of 180ºC and 215ºC were 117.6ºC and 158.9ºC respectively while these temperatures for PMHGF/PMHGFCu were recorded as 151.6 and 191.2ºC / 156.8ºC and 193.5ºC.

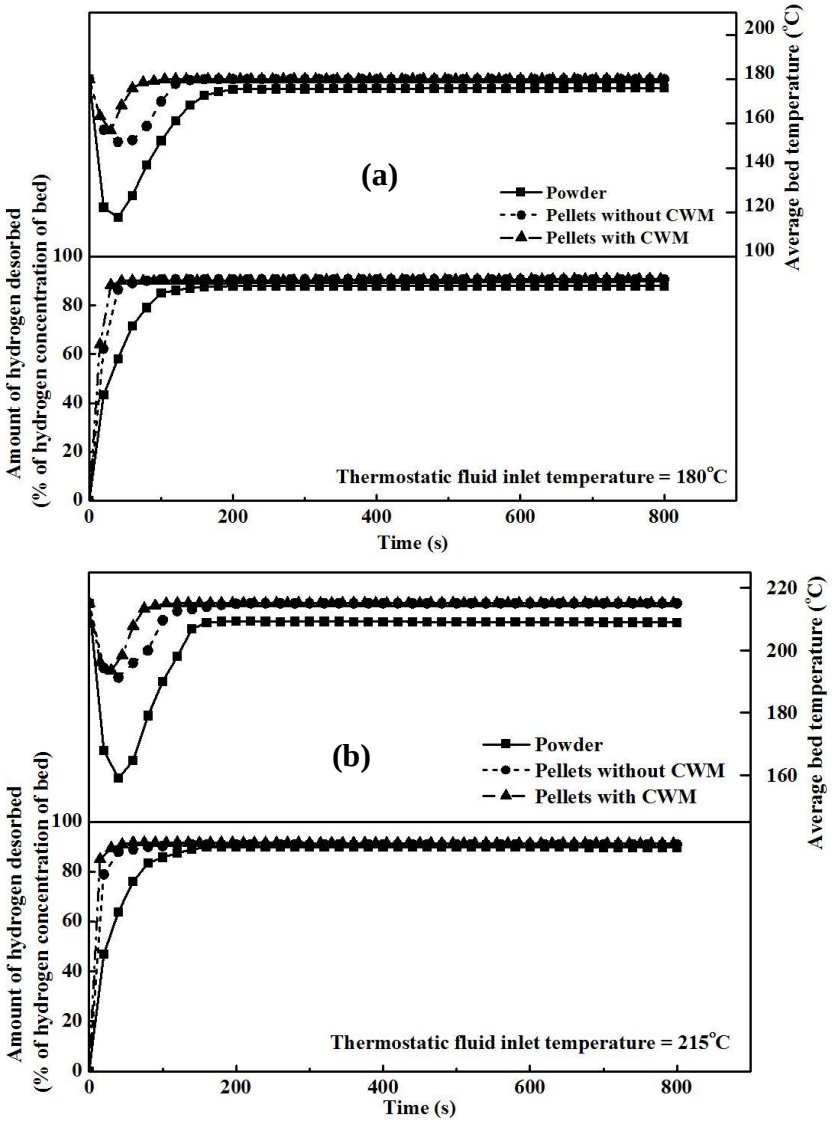

Fig. 4.9 Variation of amount of hydrogen desorbed and average bed temperature during desorption: (a) Thermostatic fluid inlet temp =180˚C (b) Thermostatic fluid inlet temp =215˚C

The higher the minimum temperature the better the heat transfer through the bed.Better heat transfer through the bed will lead to better heat energy utilization from the thermal energy source i.e. better functioning of MHTES system.Hydrogen desorption characteristics also got improved with the implementation of ETC augmentation techniques as ETC augmentation resulted in improvement in both the quantity and the rate of hydrogen desorption.While the LMHP desorbed around 88% of hydrogen, PMHGF and PMHGFCu recorded desorption of around 91% for the same desorption and absorption temperatures. Also the time taken for powder bed to reach saturation stage was 220 s whereas this was around 100 s for pellet beds.Similar to absorption kinetics, better rate of hydrogen desorption will result in decrease in the process time for MHTES system.Maximum errors in the estimation of amount of hydrogen absorbed and amount of hydrogen desorbed were found to be ±3.95% and ±4.6% respectively.

Closure

A single stage MHHC using $La_{0.8}Ce_{0.2}Ni_5$ hydride and a MHTES system using Mg + 50 wt% $LaNi_{4.6}Al_{0.4}$ hydride, both, in three different bed configurations (LMPH, PMHGF and PMHGFCu) were tested for various sets of operating parameters. ETC augmentation resulted in better kinetics and more uniform temperature distribution along the MH bed. The conclusions drawn from the present study are summarized in Chapter 5.

Chapter 5

Conclusions

In this thesis, simulation, experimental measurement and augmentation of ETC of MH beds of $La_{0.8}Ce_{0.2}Ni_5$ and Mg + 50 wt% $LaNi_{4.6}Al_{0.4}$ have been attempted. These metal hydrides were selected on the basis of their suitability for the applications of MHHC and MHTES. The effect of ETC augmentation on the sorption characteristics of these MH beds and consequently on the performance of MHHC and MHTES was studied.

5.1 Conclusions

For simulation of ETC of MH beds, four mathematical models, originally developed for simulation of ETC of non – reactive packed beds were modified to take into account the effects of hydrogenation on the ETC of MH beds. One dimensional-steady state – radial heat transfer – absolute method was used for measurement of ETC of MH beds. To serve the purpose of studying the effect of ETC augmentation on sorption characteristics of MH beds, two experimental set ups were fabricated. For augmentation of ETC, two techniques were implemented and thus two types of pellets were developed. First, by mixing graphite flakes with the metal alloy/composite powder and compaction and the second, by using the same ingredients but embedded with a three dimensional structure made of copper wire mesh. The levels of ETC augmentation achieved by different augmentation techniques and their effect on hydrogen sorption characteristics of MH beds were compared.

These studies lead to the following conclusions.

5.1.1 General

- To design a packed bed of hydriding material for any application, the heat transfer characteristics must be known beforehand. Thus knowledge of ETC is very essential.
- ETC of MH bed is a complex function of several parameters like pressure, temperature, particle morphology, number of hydrogenation / dehydrogenation cycles, hydrogen concentration, etc.
- For measurement of ETC steady state methods claim better accuracy, but homogeneity should be maintained across the bed.
- For simulation of ETC, the analytical method has gained considerable attention over other methods such as homogenization method and numerical method.
- Among the innovative augmentation techniques, inclusion of carbon fibers and expanded natural graphite to MH compacts has led to favourable augmentation of ETC without unduly increasing the 'dead' weight.

5.1.2 Simulation of ETC of MH beds

- The inclusion of variation of bed porosity, solid thermal conductivity and gas thermal conductivity in the mathematical modelsof non – reactive packed bedsresulted in close prediction of ETC of metal hydride beds.
- The variation in void fraction with hydrogen concentration plays a crucial role in the calculation of ETC of MH beds.
- The absence of bed porosity term in Dietz model resulted in under prediction of ETC values throughout the pressure range of simulation, as the variation in bed porosity caused by the metal – hydrogen reaction could not be accommodated to this model.

- The extended models of Yagi-Kunii and Zehner-Schlunder predicted ETC which closely match with experimental results for $MmNi_{4.5}Al_{0.5}$hydride over a wide range of operating parameters and thus were able to account for the changes resulting due to hydrogenation.

5.1.3 Measurement and augmentation of ETC of MH beds

- The space occupied by the thermocouples in the MH bed was kept negligible in the present work, thus assuring no loss in homogeneity the bed.
- Both the types of pellets resulted in significant augmentation of ETC with negligible effect (around 6 %) on amount of hydrogen absorbed for both the materials$La_{0.8}Ce_{0.2}Ni_5$ and Mg + 50 wt% $LaNi_{4.6}Al_{0.4}$.
- While the ETC of bed of pellets of metal alloy/composite powder mixed with graphite flakes (PMPGF) was around 4 times that of the lose metal alloy/composite powder (LMP) bed, the ETC recorded for the bed of pellets of metal alloy/composite powder mixed with graphite flakes and embedded with copper wire mesh structure (PMPGFCu) was about 6 times that of LMP bed for same values of operating parameters. Thus suggesting that the inclusion of copper wire mesh structure has resulted in further augmentation of ETC without any loss in hydrogen sorption characteristics of MH beds.

5.1.5 Effect of ETC augmentation on hydrogen sorption characteristics of MH beds with respect to the performance of MHHC and MHTES

- Theoretically the metal hydride based hydrogen compressor developed using $La_{0.8}Ce_{0.2}Ni_5$ hydride can compress hydrogen

from 10 to 35 bar when operated at absorption and desorption temperatures of 20 and 80˚C respectively.

- Hydrogen absorption rate is higher in case of powder beds compared to pellet beds at the beginning of absorption process due to better mass transfer in loose powder beds. However, time to reach saturation stage and initial bed temperature during hydrogen absorption is less in case of MH pellets beds due to better heat transfer.
- During hydrogen desorption, the temperature drop in case of pellets was far less as compared to that for loose powder bed confirming the improvement in heat transfer characteristics of the bed.
- The minimum temperatures in case of Mg + 50 wt% $LaNi_{4.6}Al_{0.4}$powder bed for desorption temperatures of 180ºC and 215ºC were 117.6ºC and 158.9ºC respectively while these temperatures for PMPGF / PMPGFCu were recorded as 151.6ºC and 191.2ºC / 156.8ºC and 193.5ºC respectively.
- While the Mg + 50 wt% $LaNi_{4.6}Al_{0.4}$powder bed desorbed around 88% of hydrogen, the beds of pellets desorbed around 91% at the same desorption and absorption temperatures.
- The pelletization and inclusion of three dimensional copper mesh structure improved the heat transfer characteristics of the metal hydride beds thereby leading to better sorption characteristics for both the applications.

5.2 Scope for Future Work

- Working models for MHHC and MHTES can be developed with PMPGFCu configuration of appropriate quantities of metal hydrides.
- ETC studies on complex metal hydrides can be performed with the aim to improve sorption characteristics of these hydrides.

Appendix A

List of Instruments

The details of the various instruments used in the present work are given below:

A.1 Weighing Balance

Make	:	Essae
Model	:	DS 852G
Range	:	0 to 1 kg
Accuracy	:	±0.1 g

A.2 Data Logger

Make	:	Agilent technologies
Model	:	34972A
Reading rate	:	600 readings/s
Scanning rate	:	60 channels/s
Scan intervals	:	0 to 99 h; 1 ms step size

A.3 DC Power Supply

Make	:	Scientech
Model	:	Scientech 4181
Output range	:	0-30 VDC, 0.1-10A
Input supply	:	230 V, ±10 %, 50 / 60 Hz

A.4 Thermostatic Bath

Make	:	Julabo
Model	:	FP 50
Temperature range	:	-50 to 200°C
Stability	:	±0.01°C
Flow range	:	11 to 16 1/min
Heating Capacity	:	2000 W

A.5 Heating Circulator

Make	:	Julabo
Model	:	HE-4
Temperature range	:	20 to 250°C
Stability	:	±0.01°C
Flow range	:	22 to 26 1/min

Heating Capacity	:	2000 W

A.6 Capsule Heater

Make	:	Marathon Heaters
Rated Power	:	60 W

A.7 PID Controller

Make	:	Yudian
Model	:	AI 518P

A.8 Pressure Transducer

Positive pressure

Make	:	Omicron
Model	:	P8741 – 6 – 100BG
Range	:	0 to 100 absolute
Accuracy	:	±0.1% of full scale

Vacuum

Make	:	HIND HIVAC (Pirani)
Model	:	HPS – 2
Range	:	0.999 to 10^{-3} mbar (Digital)
Accuracy	:	±0.5% of full scale

A.9 Differential Pressure Transducer

Make	:	Omicron
Model	:	D9821 – 6 – 005BD
Range	:	0 to 5 bar
Accuracy	:	±0.1% of full scale

A.10 Thermocouple (*Metal sheathed K – type*)

Range	:	-200 to 1360°C
Sensitivity	:	±0.1°C
Accuracy	:	±0.5°C

A.11 Vacuum Pumping System

Type	:	Rotary vacuum pump
Make	:	HIND HIVAC
Model	:	ED – 30
Pumping speed	:	500 1/min
Vacuum level	:	1×10^{-3} mbar

A.12 Hydrogen Valves

Make	:	Swagelok
Type	:	SS Bellows-Sealed valve
Model	:	SS – 4H and SS – 1RS4
Pressure range	:	0 to 80 bar and 0 to 344 bar
End connection	:	¼ ” tube fitting

Appendix B

Calibration Details

B.1 Thermocouples

Mineral insulated inconel sheathed "K" type thermocouples were used for measuring the metal hydride bed temperature and gas temperature at different locations in PCI and kinetics measurement experiments. The thermocouple wires used were of 0.56 mm (24 SWG). Grounded lead was carefully silver brazed to the end of metal – sheathed tube. The tube was drawn into SS 316 tube of ¼" diameter, which was filled with magnesium oxide (MgO) insulation.

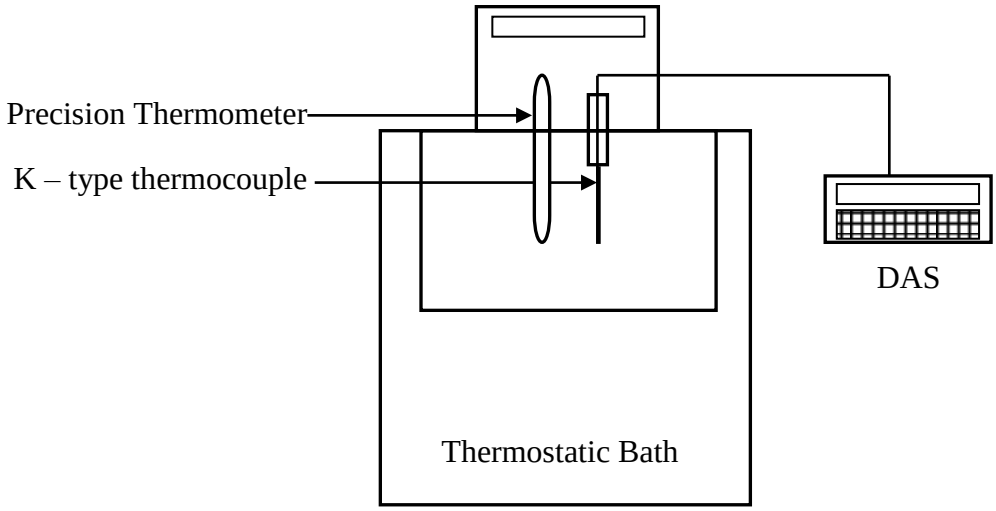

Fig. B.1 Schematic of calibration of thermocouples

Mercury-in-glass type standard reference thermometers and thermostatic bath of temperature accuracy ± 0.1°C were used for calibrating thermocouples. The temperature of the thermostatic bath can be varied between -50 to 200°C. Measuring ends of the thermocouple and reference thermometer were inserted in the thermostatic bath to the same depth. The thermocouple terminals were connected to the data logger, which was having a built in cold junction compensation circuit. The values of precision thermometer and the data logger were noted for different temperatures at steady state. The actual temperature as indicated by the precision thermometer T_a and the measured temperature T_m, were plotted as shown in Fig. B.2.

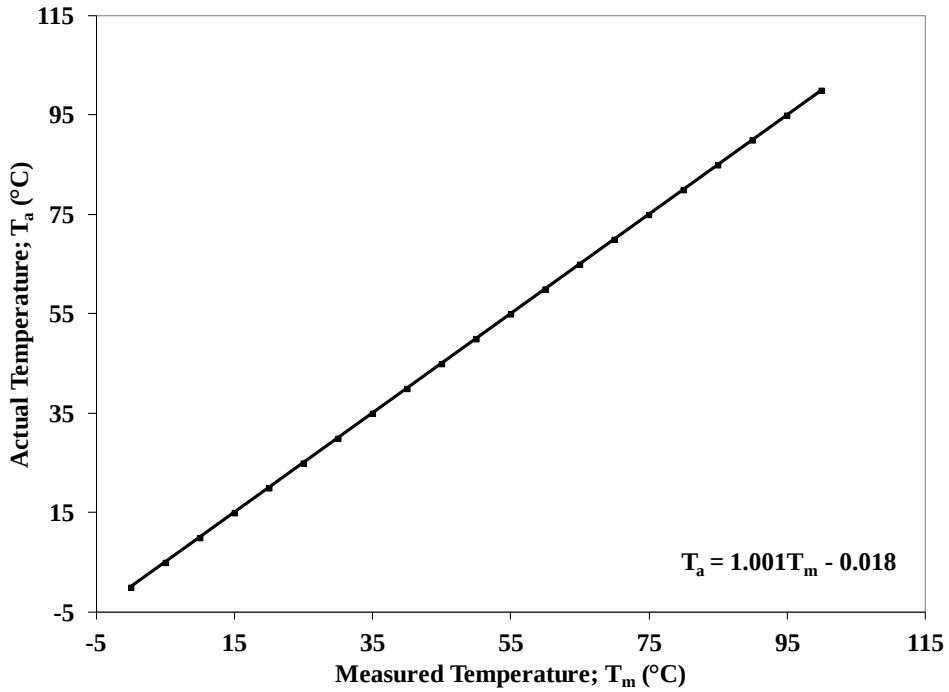

Fig. B.2 Relation between actual and measured temperatures

B.2 Pressure Transducers

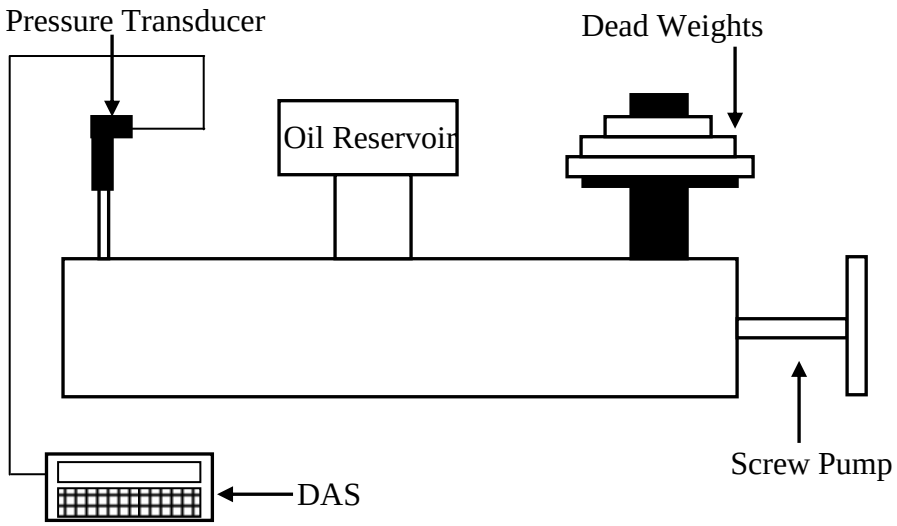

Fig. B.3 Schematic of calibration of pressure transducers

Hydrogen gas pressure in PCI and kinetic measurement setups are measured using piezoresistive pressure transducers with range from 0 – 100 bar and an accuracy of 0.1% of full scale. Dead weight tester as shown in Fig. B.3 was used

to calibrate the pressure transducers. Predetermined pressure was developed in the tester by adding dead weight and the corresponding pressure transducer output was recorded. The pressures were varied in steps by adding and removing dead weights to cover the complete pressure range of pressure transducer to be calibrated. Calibration was started from zero applied pressure to the maximum capacity of the pressure transducer. The same procedure was repeated backwards from the maximum applied pressure to zero value. The results are presented in Table B.1.

Table B.1 Calibration results for pressure transducers

Pressure Transducer **Range:** 0-100 bar **Condition during calibration:** 25±3 ºC, 40 to 60% RH			
Sl. No.	**Standard Average Reading; bar**	**Measured Reading; bar**	**Correction; bar**
1	5	5.05	-0.05
2	10	9.99	0.01
3	20	19.89	0.11
4	30	29.89	0.11
5	40	39.84	0.16
6	50	49.81	0.19
7	60	59.8	0.2
8	70	69.8	0.2
9	80	79.8	0.2
10	90	89.8	0.2

Appendix C

Error Analysis

The uncertainty in the estimated or calculated quantity was estimated based on the uncertainties in the primary measured quantities. If the estimated quantity R is a function of independent primary measurements x_1, x_2, x_3, …… x_n, which can be represented as

$$E = f(x_1, x_2, x_3, ...x_n) \tag{C.1}$$

If δR is the uncertainty in the estimated quantity R and δx_1, δx_2, δx_3, …….. δx_n are the uncertainties in the independent measured variables, then δ_E can be calculated as

$$\delta R = \sqrt{\left[\left(\frac{\partial R}{\partial x_1}\delta x_1\right) + \left(\frac{\partial R}{\partial x_2}\delta x_2\right) + \left(\frac{\partial R}{\partial x_3}\delta x_3\right) + ... + \left(\frac{\partial R}{\partial x_n}\delta x_n\right)\right]} \tag{C.2}$$

Temperature, pressure, mass of hydrogen absorbed/desorbed, hydrogen storage capacity and reacted fraction were measured/estimated during the PCI and kinetics measurements.

C.1 Measured Quantities

The mass of hydrogen was calculated by measuring the temperature, pressure and supply volume. The maximum possible uncertainty was estimated from the minimum value of the measured quantity and the accuracy of the measurement system. The uncertainty in different measurement quantities are listed in Table C.1.

Table C.1 Maximum uncertainty in the measured quantities

Sl. No.	Measurement	Device	Accuracy	Minimum quantity measured	Maximum uncertainty
1.	Hydrogen gas temperature in tubing and supply volumes	K-type thermocouple	± 0.5 K	293 K	±0.171%
2.	Hydrogen gas pressure on upstream of compact pressure regulator	Piezoresistive type transducer	± 0.000625 bar	1 bar	±0.0625%
3.	Hydrogen gas pressure on downstream of compact pressure regulator	Piezoresistive type transducer	± 0.01 bar	1 bar	±0.01%
4.	Temperature of MH Bed	K-type thermocouple	±0.5 K	293 K	±0.171%
5.	Hydrogen gas pressure in storage volume	Piezoresistive type transducer	± 0.0025 bar	1 bar	±0.25%
6.	Temperature of coolant	K-type thermocouple	± 0.5 K	293 K	±0.171%
7.	Mass of alloy	Digital weighing balance	±0.1g	25 g	±0.4%
8.	Mass of reactor	Digital weighing balance	±0.1g	1000 g	±0.01%
9.	Length	Digital vernier caliper	±0.1mm	5 mm	±2%

C.2 Estimated Quantities

C.2.1 Effective thermal conductivity measurements

Estimated quantity in effective thermal conductivity measurement is temperature gradient across the metal hydride bed.

Uncertainty in calculation of temperature gradient across the metal hydride bed

$$\delta\frac{dT}{d(\ln r)}=\sqrt{\left[\frac{\delta(\Delta T)}{\ln(\Delta r)}\right]^2+\left[-\frac{\Delta T}{(\ln(\Delta r))^2}\times\frac{1}{\Delta r}\times\delta(\Delta r)\right]^2}=1.43 \qquad \text{(C.3)}$$

$$\delta k_e=\sqrt{\left(\frac{\partial k_e}{\partial\left(\frac{dT}{d(\ln r)}\right)}\delta\left(\frac{dT}{d(\ln r)}\right)\right)^2}=0.049 \qquad \text{(C.4)}$$

The maximum uncertainty in the estimation of ETC values was found to be ± 5.1%.

C.2.2 Hydrogen absorption (Quantity) measurements

Estimated quantities are mass and weight percent of hydrogen. As mentioned in section 3.2.4, the volumes V_1 to V_7 were calculated during the fabrication of the experimental setup, and the uncertainty associated with these estimations remained constant throughout all of the experiments. The uncertainty associated with the supply volume (V_s) was 2.22 ml. The volume V_8 was calculated each time the sample was loaded, and the maximum uncertainty was calculated to be 1.33 ml. The mass of hydrogen absorbed by the metal alloy was calculated using equations C.1 to C.4, and the uncertainty in each quantity was calculated as follows:

The total amount of hydrogen transferred ($m_{T,H2,a}$) from the supply volume to the reactor was calculated using equation (C.1) based on the ideal gas law and compressibility factor Z(p,T).

$$m_{T,H_2,a} = \frac{\Delta p V_s}{Z(p_1,T_2)R_H T_2} \qquad \text{(C.5)}$$

Where

$$Z = f(p,T) = 1 + (B_0 + B_1 T + B_2 T^2)p \times 10^{-6} + (C_0 + C_1 T + C_2 T^2)p^2 \times 10^{-12}$$

$B_0 = 0.0096$, $B_1 = -15.45E^{-9}$, $B_2 = 82.314E^{-13}$,

$C_0 = 18.167E^{-8}$, $C_1 = -83.222E^{-11}$, $C_2 = 9.327E^{-13}$,

p – supply pressure in MPa, T – Temperature in K

The amount of free gas present in the reactor was calculated as follows:

$$m_{f,R,a} = \frac{p_{Raa} V_R}{Z(p_3,T_3)R_H T_3} - \frac{p_{Rba} V_R}{Z(p_3,T_3)R_H T_3} \qquad \text{(C.6)}$$

The amount of hydrogen absorbed in the metal hydride can be calculated using the following equation.

$$m_{MH,a} = m_{T,H_2,a} - m_{f,R,a} \qquad \text{(C.7)}$$

Hence, the hydrogen storage capacity of the metal hydride is given by

$$W_{H_2,a}(wt\%) = \frac{m_{MH,a}}{m_{alloy}} \times 100 \qquad \text{(C.8)}$$

Uncertainty in the calculation of amount of hydrogen transferred to the reactor

$$\delta m_{T,H_2,a} = \sqrt{\left(\frac{\partial m_{T,H_2,a}}{\partial \Delta p}\delta \Delta p\right)^2 + \left(\frac{\partial m_{T,H_2,a}}{\partial V_s}\delta V_s\right)^2 + \left(\frac{\partial m_{T,H_2,a}}{\partial T}\delta T\right)^2 + \left(\frac{\partial m_{T,H_2,a}}{\partial Z}\delta Z\right)^2} \qquad \text{(C.9)}$$

As Z is a function of pressure and temperature (Eq. C.5), the uncertainty associated with Z is estimated by:

$$\delta Z = \sqrt{\left(\frac{\partial Z}{\partial p}\delta p\right)^2 + \left(\frac{\partial Z}{\partial T}\delta T\right)^2} \qquad \text{(C.10)}$$

$$\frac{\partial Z}{\partial p} = 9.62\times10^{-3}; \frac{\partial Z}{\partial T} = -1.04\times10^{-8}$$

The estimated uncertainty associated with Z is $9.616E^{-5}$.

The quantities in equation C.5 were calculated using the real gas equation m=pV/ZRT, and the calculated values were as follows:

$$\frac{\partial m_{T,H_2,a}}{\partial \Delta p} = 3.04\times10^{-7}; \frac{\partial m_{T,H_2,a}}{\partial V_S} = 16.192; \frac{\partial m_{T,H_2,a}}{\partial T} = -2.028\times10^{-5};$$
$$\frac{\partial m_{T,H_2,a}}{\partial Z} = -0.00604$$

By using equation C.1, the uncertainty in the calculation of the mass transferred was calculated as $\delta m_{T,H2,a} = 3.6E^{-5}$ g.

Similarly, the uncertainty in the calculation of the free gas present in the reactor was calculated as $\delta m_{f,R,a} = 2.1E^{-5}$ g.

The uncertainty in the mass of hydrogen absorbed by the metal hydride is

$$\delta m_{MH,a} = \sqrt{\left(\delta m_{T,H_2,a}\right)^2 + \left(\delta m_{f,R,a}\right)^2} = 4.172\times10^{-5} g \qquad \text{(C.11)}$$

The uncertainty in the wt% calculation is

$$\delta wt\% = wt\% \times \sqrt{\left(\frac{\delta m_{MH,a}}{m_{MH,a}}\right)^2 + \left(\frac{\delta m_{alloy}}{m_{alloy}}\right)^2} = 2.16\times10^{-4} \qquad \text{(C.12)}$$

$$\frac{\delta wt\%}{wt\%}\times100 = 0.701\% \qquad \text{(C.13)}$$

The uncertainty in the storage capacity was calculated from the cumulative uncertainties of individual steps. The maximum cumulative uncertainty in total wt% was calculated to be 1.63% for Mg + 50 wt% $LaNi_{4.6}Al_{0.4}$ hydride.

The maximum cumulative uncertainty in total wt% was calculated at 2.1% for the $La_{0.8}Ce_{0.2}Ni_5$ hydride.

C.2.3 Error in sorption kinetics measurements

The mass of hydrogen absorbed/desorbed by MH are functions of pressure, temperature, storage volumes, etc. as given in Eqs. (4.1) to (4.7). The error in estimation of amount of mass absorbed by MH can be determined as given in Eq. (C.12).

$$\delta m_{s,i} = \sqrt{\left(\sum_{j=1}^{5}\frac{\partial m_{s,i}}{\partial P}\delta P\right)^2 + \left(\sum_{j=1}^{5}\frac{\partial m_{s,i}}{\partial V}\delta V\right)^2 + \left(\sum_{j=1}^{5}\frac{\partial m_{s,i}}{\partial Z}\delta Z\right)^2 + \left(\sum_{j=1}^{5}\frac{\partial m_{s,i}}{\partial T}\delta T\right)^2} \qquad \text{(C.14)}$$

Here, Z is the compressibility factor for hydrogen and is given by Eq. (2). Z is a function of pressure and temperature. The error in calculation of Z is given by Eq. (C.3)

$$\delta Z = \sqrt{\left(\frac{\partial Z}{\partial P}\delta P\right)^2 + \left(\frac{\partial Z}{\partial T}\delta T\right)^2} = 9.616\times10^{-5} \qquad \text{(C.15)}$$

The values of δP, δV and δT are given in Table C. 1.

$$\sum_{j=1}^{5}\frac{\partial m_{s,i}}{\partial P}\delta P = 9.145\times10^{-7},\ \sum_{j=1}^{5}\frac{\partial m_{s,i}}{\partial V}\delta V = 8.907\times10^{-3},\ \sum_{j=1}^{5}\frac{\partial m_{s,i}}{\partial Z}\delta Z = 9.097\times10^{-4}$$

and $\sum_{j=1}^{5}\frac{\partial m_{s,i}}{\partial T}\delta T = 0.0158$

$\therefore \delta m_{s,i} = 0.01785\,\text{g}.$

Similarly,

$$\delta m_{s,f} = \sqrt{\left(\sum_{j=1}^{5}\frac{\partial m_{s,f}}{\partial P}\delta P\right)^2 + \left(\sum_{j=1}^{5}\frac{\partial m_{s,f}}{\partial V}\delta V\right)^2 + \left(\sum_{j=1}^{5}\frac{\partial m_{s,f}}{\partial Z}\delta Z\right)^2 + \left(\sum_{j=1}^{5}\frac{\partial m_{s,f}}{\partial T}\delta T\right)^2} \qquad \text{(C.16)}$$

The values of different components of R.H.S of Eq. (A.9) are found to be:

$$\sum_{j=1}^{5}\frac{\partial m_{s,f}}{\partial P}\delta P = 7.3162\times10^{-7}\,,\ \sum_{j=1}^{5}\frac{\partial m_{s,f}}{\partial V}\delta V = 8.266\times10^{-4}\,,\ \sum_{j=1}^{5}\frac{\partial m_{s,f}}{\partial Z}\delta Z = 8.4423\times10^{-4}$$

and $\sum_{j=1}^{5}\frac{\partial m_{s,f}}{\partial T}\delta T = 0.01467$

$\therefore \delta m_{s,f} = 0.01686$ g.

And hence, $\delta m_s = \sqrt{\left(\delta m_{s,i}\right)^2 + \left(\delta m_{s,f}\right)^2} = 0.02455$

Now,

$$\delta m_v = \sqrt{\left(\sum_{j=6}^{7}\frac{\partial m_v}{\partial P}\delta P\right)^2 + \left(\sum_{j=6}^{7}\frac{\partial m_v}{\partial V}\delta V\right)^2 + \left(\sum_{j=6}^{7}\frac{\partial m_v}{\partial Z}\delta Z\right)^2 + \left(\sum_{j=6}^{7}\frac{\partial m_v}{\partial T}\delta T\right)^2} = 3.367\times10^{-4} \qquad \text{(C.17)}$$

$\delta m_a = \sqrt{\left(\delta m_s\right)^2 + \left(\delta m_v\right)^2} = 0.0245$ g.

Similarly, error in estimation of mass of hydrogen desorbed is obtained as $\delta m_d = 4.411\times10^{-3}$ g.

For mass of hydrogen absorbed / desorbed, cumulative error was determined. Maximum percentage errors in weight percent were 3.95% for absorption and 4.6% in the case of desorption.

REFERENCES

[1] Groll M. Reaction beds for dry sorption machines, Heat Recovery and CHP 1993; 13: 341-346.

[2] Murthy SS, Anil Kumar E. Advanced materials for solid state hydrogen storage: “Thermal engineering issues”, Applied Thermal Engineering 2014; 72: 176-189.

[3] Ram Gopal M, Murthy SS. Prediction of metal hydride refrigerator performance based on reactor heat and mass transfer, International Journal of Hydrogen Energy 1995; 20 (7): 607-614.

[4] Ram Gopal M, Murthy SS. Studies on heat and mass transfer in metal hydride beds, International Journal of Hydrogen Energy 1995; 20(11): 911-917.

[5] Muthukumar P, Maiya MP, Murthy SS. Performance tests on a thermally operated hydrogen compressor, International Journal of Hydrogen Energy 2008; 33(1): 463-469.

[6] Mohan G, Maiya MP, Murthy SS. Performance simulation of metal hydride hydrogen storage device with embedded filters and heat exchanger tubes, International Journal of Hydrogen Energy 2007; 32(18): 4978-4987.

[7] Murthy SS. Heat and mass transfer in solid state hydrogen storage: A review, Journal of Heat Transfer 2012; 134: 031020-1 – 031020-11.

[8] Anil Kumar E, Maiya MP, Murthy SS, Measurement and analysis of effective thermal conductivity of $MmNi_{4.5}Al_{0.5}$ hydride bed, Industrial and Engineering Chemistry Research 2011; 50: 12990-12999.

[9] Sun DW, Deng SJ, Theoretical descriptions and experimental measurements on the effective thermal conductivity of metal

hydride powder beds, Journal of Less Common Metals 1990; 160: 387-395.

[10] Matsushita M, Monde M, Mitsutake Y. Predictive calculation of the effective thermal conductivity in a metal hydride packed bed, International Journal of Hydrogen Energy 2014; 39: 9718-9725.

[11] Mayer U, Groll M, Supper W. Heat and mass transfer in metal hydride reaction beds: Experimental and theoretical results, Journal of Less Common Metals 1987; 131: 235-244.

[12] Klein HP, Groll M. Heat transfer characteristics of expanded graphite matrices in metal hydride beds, International Journal of Hydrogen Energy 2004; 29: 1503-1511.

[13] Muthukumar P, Groll M. Metal hydride based heating and cooling systems: A review, International Journal of Hydrogen Energy 2010; 35: 3817-3831.

[14] Willers E, Groll M. The two-stage metal hydride heat transformer, International Journal of Hydrogen Energy 1999; 24: 269-276.

[15] Isselhorst A, Groll M. Two-stage metal hydride heat transformer laboratory model, Journal of Alloys and Compounds 1995; 231: 888-894.

[16] Werner R, Groll M. Two-stage metal hydride heat transformer laboratory model: Results of reaction bed tests, Journal of Less-Common Metals 1991; 172-174: 1122-1129.

[17] Matsushita M, Monde M, Mitsutake Y. Experimental formula for estimating porosity in a metal hydride packed bed, International Journal of Hydrogen Energy 2013; 38: 7056-7064.

[18] Kempf A, Martin W. Measurement of the effective thermal properties of $TiFe_{0.85}Mn_{0.15}$ and its hydrides, International Journal of Hydrogen Energy 1986; 11: 107-116.

[19] Kapischke J, Hapke J. Measurement of the effective thermal conductivity of a metal hydride bed with chemical reaction, Experimental Thermal and Fluid Science 1994; 9: 337-344.

[20] Suda S, Kobayashi N, Yoshida K, Ishido Y, Ono S. Experimental measurements of thermal conductivity, Journal of Less Common Meals 1980; 74: 127-136.

[21] Kapischke J, Hapke J. Measurement of effective thermal conductivity of a Mg-MgH_2 packed bed with oscillating heating, Experimental Thermal and Fluid Science 1998; 17: 347-355.

[22] William AW, Assael MJ. Thermal Conductivity Measurements, The Measurement, Instrumentation and Sensors Handbook on CD-ROM, CRC Press, USA, 1999, 33-1 – 33-12.

[23] Suissa E, Jacob I, Hadari Z. Experimental measurements and general conclusions on the effective thermal conductivity of powdered metal hydrides, Journal of Less Common Metals 1984; 104: 287-295.

[24] Misiorek H, Sorokina N, Mucha J, Jezowski A. Thermal conductivity of Niobium hydrides in the temperature range 4.2 to 420 K, Journal of Alloys and Compounds 1991; 176: 233-240.

[25] Lloyd G, Kim JK, Razani A. Thermal conductivity measurement of metal hydride compacts developed for high power reactors, Journal of Thermophysics and Heat Transfer 1998; 12: 132-137.

[26] Ishido Y, Kawamura M, Ono S. Thermal conductivity of magnesium-nickel hydride powder beds in a hydrogen atmosphere, International Journal of Hydrogen Energy 1982; 7: 173-182.

[27] Kallweit J, Hahne E. Effective thermal conductivity of metal hydride powders: Measurement and theoretical modelling, 10th International Heat Transfer Conference, Brighton, UK 1994.

[28] Hahne E, Kallweit J. Thermal conductivity of metal hydride materials for storage of hydrogen: Experimental investigation, International Journal of Hydrogen Energy 1998; 23: 107-114.

[29] Christopher MD. Application of the transient hot wire technique for measurement of effective thermal conductivity of catalysed sodium alanate for hydrogen storage, M. S. Thesis, Virginia Polytechnic Institute, 2006.

[30] Mercks B, Dudoignon P, Garnier J, Marchand D. Simplified transient hot wire method for effective thermal conductivity measurement in geo materials: Microstructure and saturation effect, Advances in Civil Engineering 2012; 02: 1-10.

[31] Dedrick DE, Kanouff MP, Replogle BC, Gross KJ. Thermal properties characterization of sodium alanates, Journal of Alloys and Compounds 2005; 389: 299-305.

[32] Gustafsson SE. Transient plane source techniques for thermal conductivity and thermal diffusivity measurements of solid materials, Rev. Sci. Instrum 1991; 62: 797-804.

[33] Flueckiger SVT, Pourpoint T, Fisher TS, Zheng Y. In situ characterization of metal hydride thermal transport properties, International Journal of Hydrogen Energy 2010; 35: 614-621.

[34] Beattie SD, Harris A, Levchenko A, Rudolph J, Willson CD, McGrady GS. Thermal conductivity and specific heat measurements of metal hydrides, URL: http://btinnovations.org/shanebeattie/Papers/Thermal_Conductivity_Measurement_of_Metal_Hydrides_Aug_21.pdf.

[35] Goodell P. Thermal conductivity of hydriding alloy powders and comparisons of reactor systems, Journal of the Less Common Metals 1980; 74: 175-184.

[36] Pons M, Dantzer P, Guilleminot JJ. A measurement technique and a new model for the wall heat transfer coefficient of packed bed (reactive) of powder without gas flow, International Journal of Heat and Mass Transfer 1993; 36: 2635-2646.

[37] Pons M, Dantzer P. Determination of thermal conductivity and wall heat transfer coefficient of hydrogen storage materials, International Journal of Hydrogen Energy 1994; 19: 611-616.

[38] Isayev K, Schur D. Study of thermophysical properties of a metal-hydrogen system, International Journal of Hydrogen Energy 1996; 21: 1129-1132.

[39] Luikov AV, Shashkov AG, Vasiliev LL, Fraiman YE. Thermal conductivity of porous systems, International Journal of Heat and Mass Transfer 1968; 11: 117-140.

[40] Masamune S, Smith JM. Thermal conductivity of beds of spherical particles, Industrial and Engineering Chemistry Fundamentals 1963; 2(2): 136-143.

[41] Sun DW, Deng SJ. A theoretical model predicting the effective thermal conductivity in powdered metal hydride beds, International Journal of Hydrogen Energy 1990; 15: 331-336.

[42] Kuznetsov S. Homogenization methods for problems with multiphysics, temporal and spatial coupling, PhD Thesis, Columbia University 2012; 1-4, http://academiccommons.columbia.edu/catalog/ac:148608.

[43] Asakuma Y, Miyauchi S, Yamamoto T, Aoki H, Muira T. Homogenization method for effective thermal conductivity of

metal hydride bed, International Journal of Hydrogen Energy 2004; 29: 209-216.

[44] Ueoka K, Miyauchi S, Asakuma Y, Hirosawa T, Morozumi Y, Aoki H, Miura T. An application of a homogenization method to the estimation of effective thermal conductivity of a hydrogen storage alloy bed considering variation of contact conditions between alloy particles, International Journal of Hydrogen Energy 2007; 32: 4225-4232.

[45] Melnichuk M, Silin N, Peretti H. Optimized heat transfer fin design for a metal hydride hydrogen storage container, International Journal of Hydrogen Energy 2009; 34: 3417-3424.

[46] Veerraju Ch, Ram Gopal M. Heat and mass transfer studies on plate fin-and-elliptical tube type metal hydride reactors, Applied Thermal Engineering 2010; 30: 673-682.

[47] Freni A, Cipiti F, Cacciola G. Finite element-based simulation of a metal hydride-based hydrogen storage tank, International Journal of Hydrogen Energy 2009; 34: 8574-8582.

[48] Muthukumar P, Singhal A, Bansal GK. Thermal modeling and performance analysis of industrial-scale metal hydride based hydrogen storage container, International Journal of Hydrogen Energy 2012; 37: 14351-14364.

[49] Ghafir MFA, Batcha MFM, Raghavan VR. Prediction of the thermal conductivity of metal hydrides- The inverse problem, International Journal of Hydrogen Energy 2009; 34: 7125-7130.

[50] Raghavan VR, Martin H. Modeling of two phase thermal conductivity, Chemical Engineering and Processing 1995; 34: 439-446.

[51] Suda S, Kobayashi N, Yoshida K. Thermal conductivity in metal hydride beds, International Journal of Hydrogen Energy 1981; 6: 521-528.

[52] Nagel M, Komazaki Y, Suda S. Effective thermal conductivity of a metal hydride bed augmented with a copper wire matrix, Journal of the Less Common Metals 1986; 12: 35-43.

[53] Dieterich M, Pohlmann C, Bürger I, Linder M, Röntzsch L. Long-term cycle stability of metal hydride-graphite composites, International Journal of Hydrogen Energy 2015; 40(46): 16375-16382.

[54] Pons M, Dantzer P. Effective thermal conductivity in hydride packed beds I: study of basic mechanisms with the help of the Bauer and Schlunder model, Journal of the Less Common Metals 1991; 172-174: 1147-1156.

[55] Zhang J, Fisher TS, Ramachandran PV, Gore JP, Mudawar I. A review of heat transfer issues in hydrogen storage technologies, Journal of Heat Transfer 2005; 127: 1391-1398.

[56] Suda S, Komazaki Y, Kobayashi N. Effecive thermal conductivity of metal hydride beds, Journal of the Less Common Metals 1983; 89: 317-324.

[57] Suda S, Komazaki Y. The effective thermal conductivity of a metal hydride bed packed in a multiple waved sheet metal structure, Journal of the Less Common Metals 1991; 172-174: 1130-1137.

[58] Wang H, Prasad AK, Advani SG. Hydrogen storage systems based on hydride materials with enhanced thermal conductivity, International Journal of Hydrogen Energy 2012; 37: 290-298.

[59] Wang H, Prasad AK, Advani SG. Hydrogen storage systems based on hydride materials incorporating a helical coil heat

exchanger, International Journal of Hydrogen Energy 2012; 37: 14292-14299.

[60] Muthukumar P, Maiya MP, Murthy SS. Experiments on a metal hydride based hydrogen compressor, International Journal of Hydrogen Energy 2005; 30: 879-892.

[61] Bershadsky E, Josephy Y, Ron M. Permeability and themal conductivity of porous metallic matrix hydride compacts, Journal of the Less Common Metals 1989; 153: 65-78.

[62] Ron M, Bershadsky E, Josephy Y. Thermal conductivity of PMH compacts, measurements and evaluation, International Journal of Hydrogen Energy 1992; 17: 623-630.

[63] Ron M, Bershadsky E, Josephy Y. The thermal conductivity of porous metal matrix hydride compacts, Journal of the Less Common Metals 1991; 172-174: 1138-1146.

[64] Kim KJ, Montoya B, Razani A, Lee K. Metal hydride compacts of improved thermal conductivity, International Journal of Hydrogen Energy 2001; 26: 609-613.

[65] Kim K, Lloyd G, Feldman Jr. K, Razani A. Thermal analysis of the $Ca_{0.4}Mm_{0.6}Ni_5$ metal hydride reactor, Applied Thermal Engineering 1998; 18: 1325-1336.

[66] Kim JK, Park IS, Kim KJ, Gawlik K. A hydrogen-compression system using porous metal hydride pellets of $LaNi_{5-x}Al_x$, International Journal of Hydrogen Energy 2008; 33: 870-877.

[67] Shim JH, Park M, Lee YH, Kim S, Im YH, Suh JY, Cho YW. Effective thermal conductivity of MgH_2 compacts containing expanded natural graphite under a hydrogen atmosphere, International Journal of Hydrogen Energy 2014; 39: 349-355.

[68] Sanchez RA, Klein HP, Groll M. Expanded graphite as heat transfer matrix in metal hydride beds, International Journal of Hydrogen Energy 2003; 28: 515-527.

[69] Yasuda N, Tsuchiya T, Okinaka N, Akiyama T. Thermal conductiviy and cycle characteristic of metal hydride sheet formed using aamid pulp and carbon fiber, Intenational Journal of Hydrogen Energy 2013; 38: 1657-1661.

[70] Inoue S, Iba Y, Matsumura Y. Drastic enhancement of effective thermal conductivity of a metal hydride packed bed by direct synthesis of single walled carbon nanotubes, International Journal of Hydrogen Energy 2012; 37: 1836-1841.

[71] Yagi S, Kunii D. Studies on Effective Thermal Conductivities in Packed Beds, American Institute of Chemical Engineers 1957; 3: 373-381.

[72] Zehner P, Schlunder EU. Thermal Conductivity of Granular Materials at Moderate Temperatures, Chemie Ingenieur Technik 1970; 42: 993-941.

[73] Dietz PW. Effective Thermal Conductivity of Packed Beds, Industrial and Engineering Chemistry Fundamentals 1979; 18(3): 283-286.

[74] Da Silva EP. Industrial prototype of a hydrogen compressor based on metallic hydride technology. International Journal of Hydrogen Energy 1993; 18(4): 307-311.

[75] Lototskyy MV, Yartys VA, Pollet BG, Bowman Jr RC. Metal hydride hydrogen compressors: A review. International Journal of Hydrogen Energy 2014; 39: 5818-5851.

[76] Muthukumar P, Maiya MP, Murthy SS. Parametric studies on a metal hydride based single stage hydrogen compressor. International Journal of Hydrogen Energy 2002; 27: 1083-1092.

[77] Mayer U, Groll M, Supper W. Heat and mass transfer in metal hydride reaction beds: experimental and theoretical results. Journal of the Less-Common Metals 1987; 131: 235-244.

[78] Sun D, Deng S. Study of the heat and mass transfer characteristics of metal hydride beds. Journal of the Less-Common Metals 1988; 141: 37-43.

[79] El-Osery IA. A comparative study of in-out and out-in hydrogen reaction alternatives for metal hydride beds using RET1 computer code. International Journal of Hydrogen Energy 1984; 9: 412-424.

[80] Nakagawa T, Inomata A, Aoki H, Miura T. Numerical analysis of heat and mass transfer characteristics in the metal hydride bed. International Journal of Hydrogen Energy 2000; 25: 339-350.

[81] Dogan A, Kaplan Y, Veziroglu TN. Numerical investigation of heat and mass transfer in a metal hydride bed. Applied Mathematics and Computation 2004; 150: 169-180.

[82] Muthukumar P, Maiya MP, Murthy SS. Experiments on a metal hydride based hydrogen compressor. International Journal of Hydrogen Energy 2005; 30: 879-892.

[83] Laurencelle F, Dehouche Z, Goyette J, Bose TK. Integrated electrolyser-metal hydride compression system. International Journal of Hydrogen Energy 2006; 31: 762-768.

[84] Murthy SS. Heat and mass transfer in solid state hydrogen storage: A Review. Journal of Heat Transfer 2012; 134: 031020-1 – 031020-11.

[85] Mohan G, Maiya MP, Murthy SS. Performance simulation of metal hydride hydrogen storage device with embedded filters and heat exchanger tubes. International Journal of Hydrogen Energy 2007; 32: 4978-4987.

[86] Nomura K, Akiba E, Ono S. Development of a metal hydride compressor. Journal of Less Common Metals 1983; 89: 551-558.

[87] Kim JK, Park IS, Kim KJ, Gawlik K. A hydrogen-compression system using porous metal hydride pellets of $LaNi_{5-x}Al_x$. International Journal of Hydrogen Energy 2008; 33: 870-877.

[88] Hopkins RR, Kim KJ. Hydrogen compression characteristics of a dual stage thermal compressor system utilizing $LaNi_5$ and $Ca_{0.6}Mm_{0.4}Ni_5$ as the working metal hydrides. International Journal of Hydrogen Energy 2010; 35: 5693-5702.

[89] Odysseos M, De Rango P, Christodoulou CN, Hlil EK, Steriotis T, Karagiorgis G et al. The effect of compositional changes on the structural and hydrogen storage properties of (La-Ce)Ni_5 type intermetallics towards compounds suitable for metal hydride hydrogen compression. Journal of Alloys and Compounds 2013; 580: 5268-5270.

[90] Sharma VK, Anil Kumar E. Studies on La based intermetallic hydrides to determine their suitability in metal hydride based cooling systems. Intermetallics 2015; 57: 60-67.

[91] Mohan G, Maiya MP, Murthy SS. Performance simulation of metal hydride hydrogen storage device with embedded filters and heat exchanger tubes. International Journal of Hydrogen Energy 2007; 32: 4978-4987.

[92] Muthukumar P, Patel KS, Sachan P, Singhal PN. Computational study on a metal hydride based three-stage hydrogen compressor. International Journal of Hydrogen Energy 2012; 37: 3797-3806.

[93] Bayane C, Sciora E, Gerard N, Bouchdoug M. $LaNi_5$ hydride formation. The effect of the thermal conductivity of the holder on the kinetics. Thermochimica Acta 1993; 224: 193-202.

[94] Kawamura M, Ono S, Higano S. Experimental studies on the behaviours of hydride heat storage systems. Energy Conversion and Management 1982; 22: 92-105.

[95] Yonezu I, Nasako K, Honda N, Sakai T. Development of thermal energy storage technology using metal hydrides. Journal of the-Less Common Metals 1983; 89: 351-358.

[96] Ward PA, Corgnale C, Teprovich Jr JA, Motyka T, Hardy B, Peters B et al. High performance metal hydride based thermal

energy storage systems for concentrating solar power applications. Journal of Alloys and Compounds 2015; 645: S374-S378.

[97] Satya Sekhar B, Muthukumar P, Saikia R. Tests on a metal hydride thermal energy storage system. International Journal of Hydrogen Energy 2012; 37: 3818-3824.

[98] Reiser A, Bogdanovic B, Schlichte K. The application of Mg-based metal-hydrides as heat energy storage systems. International Journal of Hydrogen Energy 2000; 25: 425-430.

[99] Felderhoff M, Borislav Bogdanovic. High temperature metal hydrides as heat storage materials for solar and related applications. International Journal of Molecular Sciences 2009; 10: 325-344.

[100] Liang G, Boily S, Huot J, Van Neste A, Schulz R. Hydrogen absorption properties of a mechanically milled Mg–50 wt.% LaNi composite. Journal of Alloys and Compounds 1998; 268: 302-307.